TÉCNICO LISBOA

Solar still performance and enhancement techniques analysis using an alternative thermal model approach

André António Vieira Lisboa

Thesis to obtain the Master of Science Degree in

Mechanical Engineering

Supervisors: Prof. Miguel Abreu de Almeida Mendes
Dr. Raquel Inês Segurado Correia Lopes da Silva

Examination Committee

Chairperson: Prof. José Manuel da Silva Chaves Ribeiro Pereira
Supervisor: Prof. Miguel Abreu de Almeida Mendes
Member of the Committee: Prof. Pedro Jorge Martins Coelho

January 2021

To the start of a new chapter...

Acknowledgments

I would like to thank my supervisors Professor Miguel Abreu de Almeida Mendes and Raquel Segurado Silva for their availability and guidance over the past months. It was a challenging task full of obstacles that would have been difficult to overcome without help.

Finally, I would like to thank my family and friends for their support, which allowed me to stay motivated during these years.

Resumo

Em todo o mundo, o crescente stress hídrico e a escassez de água estão a tornar-se um problema que afeta principalmente regiões empobrecidas. A dessalinização é vista como uma solução viável, porém as principais técnicas para obter água dessalinizada, como a osmose inversa e os processos térmicos modernos, necessitam, além de recursos tecnológicos e energéticos, de infraestruturas. Estes recursos carecem nos países menos desenvolvidos, tornando impraticável o uso destas tecnologias de dessalinização. Devem ser por isso, fornecidas soluções de pequena escala e de baixo custo. Focando na dessalinização solar, uma opção é o simples, económico, e fácil de construir destilador solar.

O destilador solar é acessível, necessitando de materiais e conhecimentos técnicos simples para ser construído. No entanto, apresenta uma reduzida produção de água. Ao longo dos últimos anos o destilador solar tem sido cada vez mais estudado, teórica e experimentalmente, de forma a melhorar o seu desempenho. Existe, no entanto, pouco rigor. Por um lado, as melhorias experimentais são feitas em diferentes condições atmosféricas, localizações, e designs de destilador solar, não dando noções claras ao construtor. Por outro lado, o modelo termodinâmico mais utilizado é conhecido por sobrestimar a produção de água, mas, tem sido utilizado pela sua simplicidade. É importante prever com precisão a produção de água do destilador solar, para minimizar o recurso a ensaios experimentais.

Neste trabalho, é desenvolvido um modelo termodinâmico para aumentar a precisão da simulação do destilador solar, para diferentes designs, locais e condições atmosféricas. O modelo é capaz de capturar a física do destilador solar, conseguido seguir a evolução da temperatura de água e prever a produção de água, com um desvio máximo de 6% para as experiências avaliadas. Adicionalmente, numa experiência escolhida da literatura, é realizado um estudo paramétrico para compreender melhor como aumentar a produção de água. Os parâmetros que devem ser optimizados são, a profundidade da água, altura das paredes, o escalar da estrutura, isolamento, radiação solar incidente e diferença de temperatura entre base do distilador solar e o seu vidro. Finalmente, com base no estudo paramétrico e nas soluções existentes na literatura, são apresentadas, modeladas e avaliadas, opções reais que podem ser implementadas. Opções como por exemplo, modificação do design do destilador solar (até 19% e 70% num dia de Verão e Inverno, respectivamente), instalar reflectores externos/internos (até 21%/7% e 73%/79% num dia de Verão e Inverno, respectivamente), melhor isolamento (até 20%), e arrefecimento do vidro (até 29% para grandes quantidades de água, pouco efeito em mais pequenas). Também foram feitos estudos preliminares em outras soluções, como a separação da evaporação/condensação (até 80%), utilização de uma ventoinha no interior para promover a convecção (até 22%), ou utilização de um meio poroso (até 10% e 20%, não isolado e isolado, respectivamente).

Palavras-chave: Dessalinização, Pequena escala, Baixo Custo, Destilador solar, Análise/Modelação termodinâmica, Aumento da produção de água

Abstract

Around the globe, increasing water stress and scarcity are becoming a problem that particularly affects poor regions. Desalination is seen as a viable solution, however, the main techniques for obtaining fresh water, such as reverse osmosis and modern thermal processes, require technological and energy resources as well as infrastructures that are lacking in less developed countries. Unfeasible the use of these technologies, small scale and low cost solutions must be provided. Focusing on solar desalination, one option is the simple, accessible and easy to construct solar still.

The solar still is an economical device, which relies on simple materials and technical knowledge, however, it presents a low production. Enhancing the performance of the solar still has been increasingly studied theoretically and experimentally in recent years. On the one hand, the experimental improvements are carried out under different ambient conditions, locations, and solar still designs, not giving clear insight to the constructor. On the other hand, it is known that the most commonly used thermal model overestimates the water production, yet it has been used because of its simplicity. It is important to accurately predict the yield of a solar still so that resources do not have to be spent on experiments.

In this thesis, a thermal model is elaborated to increase the accuracy and precision for different designs, locations and ambient conditions. The model is able to capture the physical evolution of the solar still, following the water temperature quite well, and predicts the water yield with a maximum deviation around 6% for the evaluated experiments. Moreover, in a selected experiment from the literature, a parametric analysis is performed to further understand how to improve the water yield. The parameters that must be optimized are water depth, walls height, scaling of the structure, insulation, incident solar radiation and basin-glass temperature difference. Finally, based on the parametric study and on the identified improvement solutions from the literature, feasible real options are analysed, such as modification of the solar still design (up to 19% and 70% on a summer and winter day, respectively), adding external/internal reflectors (up to 21%/7% and 73%/79% on a summer and winter day, respectively), better insulation (up to 20%) and glass cooling cover (up to 29% for large water quantities, low/none effect on smaller ones). Moreover, preliminary studies on evaporation and condensation separation (up to 80%), use of a fan inside to promote convection (up to 22%), or use of a porous medium (up to 10% and 20%, not insulated and insulated, respectively).

Keywords: Desalination, Small-scale, Low-cost, Solar still, Thermal modelling, Water yield enhancement

Contents

List of Tables

List of Figures

Nomenclature

Greek symbols

α	Absorption coefficient ; Thermal diffusivity (m^2/s)
α_n	Normal incidence absorption coefficient
α_{sun}	Solar altitude $(^o)$
β	Surface inclination angle $(^o)$; Thermal expansion coefficient (K^{-1})
ΔH_{H_2O}	Latent heat of vaporization (J/kg)
δ	Solar declination
ϵ	Emissivity coefficient
γ	Surface azimuth angle $(^o)$
γ_{sun}	Solar azimuth angle $(^o)$
λ	Longitude $(^o)$
ϕ	Latitude $(^o)$
Φ_{foam}	Foam porosity
ρ	Density (kg/m^3); Reflectivity
σ	Stefan–Boltzmann constant $(\approx 5.67 \times 10^8\ W/m^2K^{-4})$
τ	Transmissivity
θ	Angle of incidence of beam radiation for a surface $(^o)$
θ_z	Solar zenith angle $(^o)$
υ	Kinematic viscosity (m^2/s)
φ	Relative humidity

Roman symbols

$\dot{m}$	Mass flow (kg/s)

A Area (m^2)

C Solar still length (m)

c_p Heat capacity at constant pressure $(J/(kgK))$

c_v Vapour concentration $(kmol/m^3)$

e, f, g, h, x, y Variables used to compute shadows and reflected area (m); x as porous fraction

F View factor

g Gravitational acceleration constant ($\approx 9.8\ m/s$)

H Height (m)

$h_{c,a-g}$ Convective heat transfer coefficient from solar still air to glass cover (W/m^2K)

$h_{c,b-w}$ Convective heat transfer coefficient from basin to water (W/m^2K)

$h_{c,g-out}$ Convective heat transfer coefficient from glass cover to outside (W/m^2K)

$h_{c,w-a}$ Convective heat transfer coefficient from water to solar still air (W/m^2K)

$h_{c,wall-a}$ Convective heat transfer coefficient from wall to solar still air (W/m^2K)

$h_{r,g-sky}$ Radiative heat transfer coefficient from glass cover to sky (W/m^2K)

$h_{r,w-g}$ Radiative heat transfer coefficient from water to glass cover (W/m^2K)

$h_{r,w-wall}$ Radiative heat transfer coefficient from water to wall (W/m^2K)

$h_{r,wall-g}$ Radiative heat transfer coefficient from wall to glass cover (W/m^2K)

I Incident solar radiation (W/m^2)

J_M, J_H Chilton–Colburn J-factors for mass and heat transfer, respectively

K_i Insulation thermal conductivity $(W/(mK))$

k_t Sky clearness index

L Solar still width (m)

L_i Insulation thickness (m)

Le Lewis number

m Mass (kg)

N Molar flow $(kmol/s)$

Nu Nusselt number

P Perimeter (m)

Pr Prandtl number

$Q_{c,a-g}$ Heat transfer due to convection between air within the still and glass cover (W)

$Q_{c,a-wall}$ Heat transfer due to convection between wall and air within the still (W)

$Q_{c,b-w}$ Heat transfer due to convection between basin and water (W)

$Q_{c,g-out}$ Heat transfer due to convection between glass cover and outside air (W)

$Q_{c,w-a}$ Heat transfer due to convection between water cover and air within the still (W)

Q_{cond} Heat transfer due to condensation (W)

Q_{evap} Heat transfer due to evaporation (W)

$Q_{lost,b}$ Heat lost from the basin to outside (W)

$Q_{lost,wall}$ Heat lost from the wall to outside (W)

$Q_{r,g-sky}$ Heat transfer due to radiation from glass to sky (W)

$Q_{r,g}$ Total heat transfer due to radiation from glass (W)

$Q_{r,w-glass}$ Heat transfer due to radiation between water and glass (W)

$Q_{r,w-wall}$ Heat transfer due to radiation between water and wall (W)

$Q_{r,wall-g}$ Heat transfer due to radiation between wall and glass cover (W)

$Q_{r,w}$ Total heat transfer due to radiation from water (W)

$Q_{sun,b}$ Heat transfer due to solar radiation incident on the basin (W)

$Q_{sun,g}$ Heat transfer due to solar radiation incident on the glass cover (W)

$Q_{sun,wall}$ Heat transfer due to solar radiation incident on the walls (W)

$Q_{sun,w}$ Heat transfer due to solar radiation incident on the water (W)

R Universal gas constant (≈ 8314 J/kmol.K);Ratio of beam radiation on the tilted surface to that on a horizontal surface

Ra Rayleigh number

Re Reynolds number

Ri Richardson number

Sc Schmidt number

Sh Sherwood number

T Temperature (K)

w Humidity ratio

p Pressure (N/m^2)

v Wind velocity (m/s)

Subscripts

a Air inside the solar still

b Basin

$back$ Back wall

c Convection

$cond$ Condensation

dif Diffuse radiation

dr Direct/Beam radiation

$evap$ Evaporation

exp Exposed area to direct solar radiation

$film$ Film over the glass cover

$front$ Front wall

G Global horizontal irradiance

g Glass

$horizontal$ Horizontal surface

$lateral$ Lateral/Side wall

$lost$ Lost heat

out Outside ambient air

ref Mirror/Reflector

$Reflected$ Reflected area

$shad$ Imposed shadow area

sky Sky

$tilted$ Tilted surface

$total$ Back wall with external reflector/mirror

w Water

$wall$ Wall, it is specified if it is $front$, $lateral$ or $back$

x Characteristic length

Chapter 1

Introduction

In this chapter the motivation for this thesis is presented. It is emphasized the fact that water is a core element of human society, yet many developing countries still lack adequate access to usable water sources. Desalination is seen as a viable solution for the provision of fresh water, therefore a thorough analysis of this issue is carried out. Finally, contributions on the state of the art and the outline of the thesis are described.

1.1 Motivation

Water is one of the most vital and yet finite resources in the world. Only 3% of all water in the world is fresh water and only about a third of it is easily accessible [1]. Furthermore, this natural resource is not evenly distributed around the globe, leading to social disparities between villages, cities, and even countries that lack access to potable or at least usable water.

Over the past years, the growing consumption of water, together with increasing pollution, global warming, and poor management of water resources, has been depleting the world water reserves. These actions are causing higher water stress globally, as it is possible to observe in Fig.1.1. According to *Mekonnen and Hoekstra* [2], *" two-thirds of the global population live under conditions of severe water scarcity at least 1 month of the year "*. Countries that were already short in water reserves now face a worse situation, and even more developed countries are encountering problems, such as, South Africa, who recently experienced a severe water shortage.

Water is crucial to ensure quality of life, basic health security, and economic prosperity. On this matter the United Nations (UN) have elaborated an agenda, the 2030 Agenda for Sustainable Development [4], to resolve major existing problems in the world. A list composed of 17 goals, aims to find solutions to eradicate poverty, focus on sustainability, and fulfill people's lives economically and socially, as well as provide technological progress. Goal 6 stands to ensure access to clean water and sanitation for all, which is widely considered as a basic need but is currently still lacking in the majority of developing countries.

Technologies and techniques to collect, desalinate, and recover wastewater, must be developed

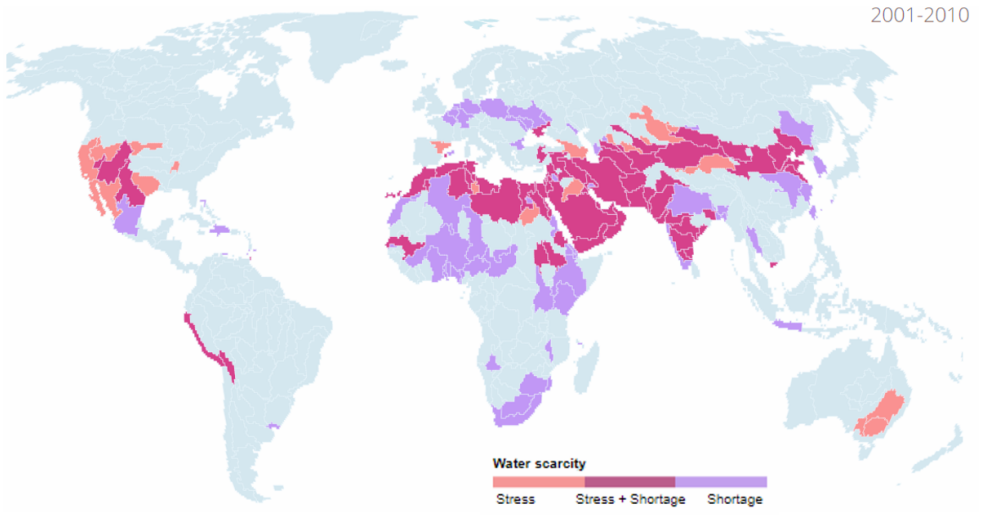

Figure 1.1: Water scarcity around the globe, data collected from 2001 to 2010; adapted from [3].

to guarantee fresh water for these countries. As an example, many warm arid regions in Africa are under severe climatic conditions and therefore suffer severe water shortages almost all year round. The inhabitants of such locations, whose farming systems and basic needs are highly dependent on rainfall, need a reliable alternative to access water so that they can maintain their sustainability, food and health security. In that matter, coastal rural areas may have a sustainable and accessible solution through seawater desalination. The aim of this work is to focus on small-scale and low-cost devices, and investigate reliable solutions that can give ”water stability” to developing countries and therefore help to achieve the goals promoted by the UN.

Various techniques for water desalination have existed for a long time and their objective is to remove impurities/salts of contaminated water or seawater and convert it into potable or at least usable water. As schematically represented in Fig.1.2, desalination technologies can be divided into two main groups [5], membrane, and thermal desalination.

Membrane technologies for desalination rely on removing salts and other particles from seawater by using water porous membranes which are impermeable to ions. The three main membrane processes are electrodialysis, nanofiltration and reverse osmosis (RO). Common to all these processes is that the feed water must be pre-treated to remove unwanted species, as well as the cost of membrane maintenance and replacement.

Nanofiltration is a more recent technology that can process large volumes of water and continuously produce streams of products, however, it cannot remove dissolved components due to its membrane porosity. Electrodialysis is the process of transporting ions from seawater to another solution when using an electric field. This process is mainly used for ion removal therefore it is not suitable to withdraw suspended solids and other contaminants. The main advantage of this technique is the use of low-pressure which diminishes maintenance complexity, however, its high cost still makes it a less favoured approach. The most well-known process is RO, which consists of pumping seawater at very high pressure through membranes with very small pores removing most solids and contaminants. The main disadvantages are

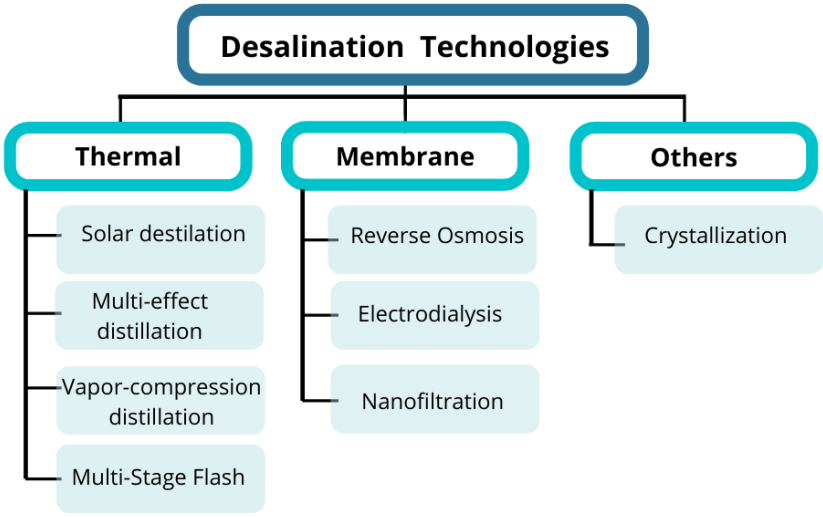

Figure 1.2: Overview of desalination technologies.

the initial cost of the RO unit and the amount of water needed to produce fresh water, which is around three times as much water as they treat. RO membranes remove important minerals in the water, thus needing a post-mineralization process. Of all processes involved in water desalination, RO is responsible for most of the membrane desalinated water produced worldwide (main countries being: United Arab Emirates, Saudi Arabia, and the United States) and it is being increasingly implemented all over the world. This because it can produce fresh water at a higher rate and more economically than the remaining solutions when on large scale. [6, 7].

A RO small-scale seawater desalination plant is not feasible to implement in most of the coastal rural areas mentioned. This is due to the following three principle obstacles: energy resources, infrastructures, and technical knowledge. Even though it consumes less energy, when on large scale, than other desalination methods, a reliable electrical grid system is needed to run the RO plant. Countries that are abundant in energy resources and lack of fresh water, normally rely on reverse osmosis or thermal desalination technologies, to desalinate water. Moreover, a high initial investment is needed to build a RO plant, together with costly maintenance and technical expertise, which is essential to keep it running.

Thermal desalination covers all processes where energy is supplied to a mass of water to facilitate the evaporation process of water vapor into the air and later condense the moisture present in the humid air on a designed surface. This approach is efficient at removing unwanted particles, however, collecting the condensed water is an inefficient process.

Thermal desalination plants are commonly equipped with the following technologies: Multi-Effect Distillation (MED), Vapor-Compression Distillation (VCD), or Multi-Stage Flash (MSF). It is important to highlight that thermal desalination processes would not be able to compete with membrane processes if energy was used to heat the water. To reduce energy costs, waste water from energy production (power or cooling) is used. Explaining each process briefly, MED (Fig. 1.3) consists of sequential stages with reduced pressure which contain water. It is supplied energy to promote the evaporation in the first

stage, and consequent steam transport in a tube to heat the next stage (with lower pressure). The steam inside the tube releases heat on to the next stage, and condenses, therefore producing fresh water. In this new stage, water absorbs the released heat, its temperature increases and it evaporates, allowing the process to continue to occur in the successive stages.

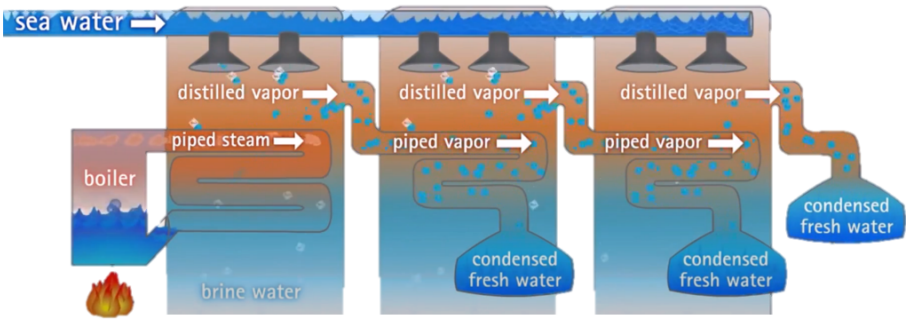

Figure 1.3: Representation of Multi-Effect Distillation (MED); adapted from [8].

MSF (Fig. 1.4) has stages in series, each containing a heat exchanger and a condensation collector. Adding to this, there is a tube carrying the inlet water in counterflow with the stages (represented by stream B). Similarly to MED, the pressure for each stage drops to promote water boiling. In each stage, the water boils and condenses when in contact with the tube carrying the cold water for the system inlet. The condensate is collected in each stage, and the brine water which did not boil and reached an equilibrium temperature goes to the next lower pressure stage and repeats the process. In VCD (Fig. 1.5), warm feed water is heated in the evaporator tubes until it boils. The vapor is removed from the evaporator and compressed. This process will increase vapor pressure and temperature. The vapor will pass through the evaporator tubes and condense, releasing latent heat to the water inside the evaporator producing even more vapor.

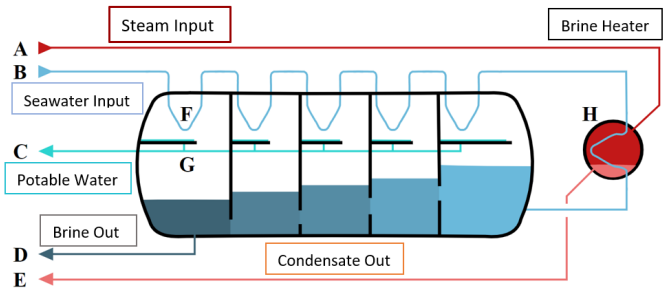

Figure 1.4: Representation of Multi-Stage Flash (MSF); adapted from [9].

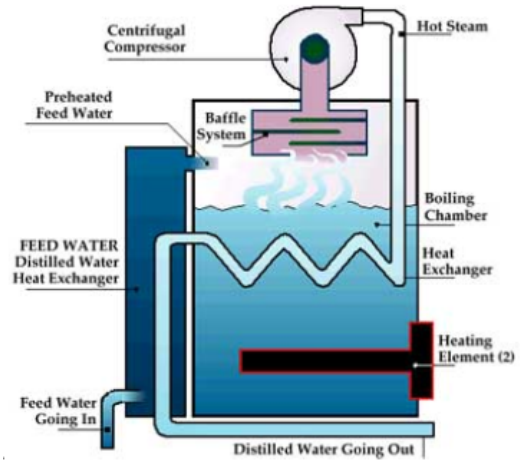

Figure 1.5: Representation of Vapor-Compression Distillation (VCD) adapted from [10].

Compared with other technologies, MED is fairly simple, it is easily adaptable to any energy source,

it is easy to operate and to maintain, and it has a low energy consumption. Its main disadvantage is scaling problems and it's incompatibility with higher temperature heat sources. MSF is one of the leading technologies of thermal desalination since it copes with higher temperatures than MED, however, it needs a huge amount of space (larger than RO), periodic maintenance, it has a high-energy consumption and, a large quantity of water is needed for production and cooling. VCD has high reliability, a long lifetime, and flexible operation, however, it requires highly skilled operators to do the maintenance.

Solar desalination is also a process of thermal desalination which, as the name suggests, relies on predictable and globally available solar energy. Typically, this type of desalination is associated with a device known as a solar still, schematically represented in Fig. 1.6, which will be thoroughly analyzed in the following sections. The solar still has an affordable construction as well as low technical maintenance, which makes it an interesting device for small-scale use. The major drawback of this device is its low productivity. The solar still exists for a long time, being the first reported situation of use in 1872 in the northern deserts of Chile to provide drinking water for animals used in nitrate mining [11]. It is important to make clear that the water obtained from the solar still, as with other methods, lacks minerals, so it is not recommended to consume it. Nevertheless, it can go through a simple post-mineralization treatment so that it can be drinkable, or it can be used for agriculture without the need for post-processing.

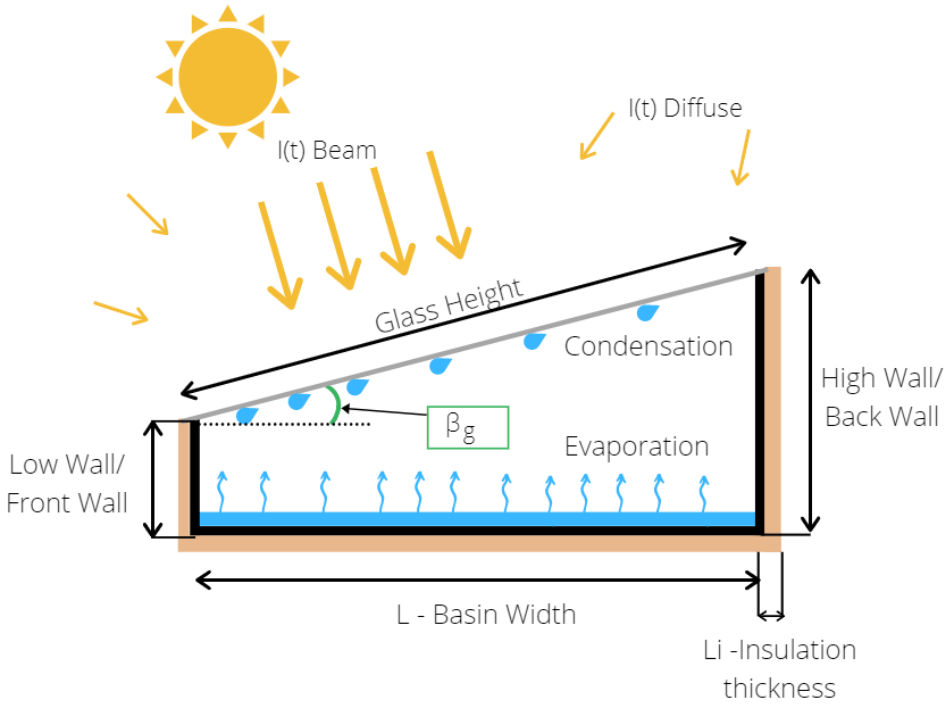

Figure 1.6: Solar still components schematic view. Legend: Black - Basin/Wall, Blue - Seawater, Brown - Insulation.

This document will focus on solar desalination, more specifically in the solar still, and the feasibility of implementing this option in developing regions. An analysis is provided on the processes taking place inside the solar still, how to predict water productivity for a given site and how to improve the performance of the device.

1.2 Overview of the Solar Still

This simple device can be easily manufactured with inexpensive materials to produce fresh water, thus making it a plausible small scale solution. For this reason it is important to understand its operation and limitations in order to maximize water yield.

1.2.1 Solar Still Structure and Operation

The conventional single basin and slope solar still consists of an enclosure with a right triangle or trapezoidal cavity, as represented in Fig. 1.6. Structure wise, the device basin and walls are commonly made of materials with low specific heat capacity and high thermal conductivity, such as aluminum, steel or iron, and painted black to maximize absorption of incident radiation. The basin is continuously fed and covered with seawater. On the top there is an inclined glass cover with high transmissivity to allow maximum radiation to reach the inside of the still. At the bottom of the inclined glass there is a tube to collect the condensed water. The solar still is sealed to prevent air exchange with the environment and well insulated, with glass wool, sawdust or foam, so that as little heat as possible is lost. The conventional solar still is described as having an average daily production of around 2-3 liters per square meter, depending on the location [5].

The processes that occur inside the solar still are quite simple. Solar radiation, which is neither absorbed nor reflected by the glass cover, reaches the basin and walls where it is absorbed. The basin rises temperature and consequently heats the seawater on it. The water temperature rises, which promotes water evaporation to the enclosure air. This evaporation is not due to boiling, but to the fact that there is a water vapor pressure gradient between the seawater (covering the basin) surface and the enclosure's air directly above. Moist hot air near the basin has a lower density and rises by natural convection until it reaches the glass. When the glass surface is colder than the air dew point, condensation occurs in the form of water droplets which will flow into the tube at the bottom of the glass cover. The air in contact with the glass decreases the temperature and increases density, causing it to descend to the water surface. This cycle will repeat along the day. The solar still is affected by external factors that vary throughout the day, such as solar radiation, wind speed and ambient temperature changes. The external factors disturb the solar still and have a direct impact on its performance.

Solar desalination systems may be characterized as passive or active. Active systems control some parameters of the solar still such as inner convection, glass temperature or solar still pressure by adding devices. Examples of possible changes are a small water heater, that facilitates the rise of water temperature, or a fan that promotes mass transfer and consequently water yield, however, these changes require energy from an external source [12]. Passive systems do not require additional energy input and are strongly influenced by environmental conditions. For this reason, it is essential that the passive solar still parameters, for example, structure design, water depth or insulation, are optimized to achieve maximum water productivity throughout the year.

1.2.2 Performance Improvement

Enhancing water production of the solar still has been thoroughly researched and numerous experiments have been conducted to improve the active and passive solar still performance. The following parameters are the most researched and considered relevant in the literature:

- **Increasing solar radiation:** To increase radiation intensity reaching the basin, Lei Mu et al. [13] used a Fresnel lens to enhance the single basin still performance and compared it with the conventional one. The Fresnel lens increased the water yield by 467.4%, however, the lens had to be constantly adjusted to the position of the sun to achieve this performance. Omara et al. [14, 15] investigated the advantage of using reflectors/mirrors on the back inner wall of a stepped solar still (Fig. 1.7) improving yield by 75%, and both inner reflectors and exterior reflectors resulting in 125% improvement when comparing to the conventional solar still. Tanaka [16] with a conventional solar still investigated the advantage of both internal and external reflectors improving yield by 70%.

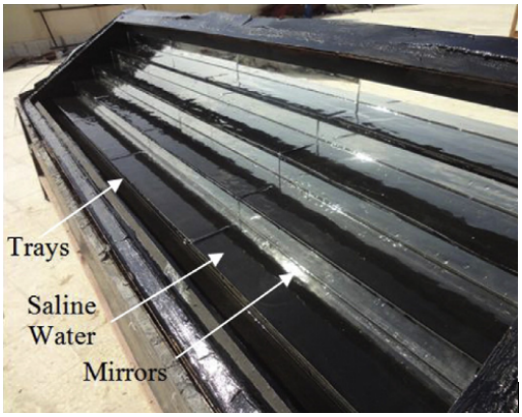

Figure 1.7: Single slope solar still with stepped basin and mirrors (figure by Omara et al. [14]).

- **Cover angle inclination and material:** Countless studies have been carried out on this matter, reporting that the optimum angle of inclination of the cover (β_g represented in Fig. 1.6) is equal to the latitude angle of the solar still location [17]. Adjustments may be done for the winter (increasing the glass angle by 15º) and summer season (decreasing the glass angle by 15º) to reduce the reflected radiation. It must be taken into account that a very low glass angle can cause water droplets to fall back onto the basin water and thus not be collected. The choice of the cover material must also be considered, as materials such as acrylic glass or glass have different surface tensions, which can reduce the water yield by limiting condensation. [18]

- **Basin water depth and renewal:** The influence of water depth is also frequently seen in the literature. Tiwari and Sahota [5], as well as many other researchers concluded that decreasing water depth increases the solar still performance. A recent study was conducted by El-Maghlany et al. [19] on the effect of discrete water renewal compared to continuous water supply. It showed that the discrete water supply slightly increases the productivity of the solar still, because the reservoir supplying the water had more time to raise temperature.

- **Solar still design:** Many designs have been tested, from single slope glass cover, to double slope (Fig. 1.9), pyramid shape, or even hemispherical glass cover [20]. There is agreement in the literature that an increase in the glass cover area promotes condensation [21]. The use of solar stills with a double (Fig. 1.8) or even triple basin has a higher productivity due to the reuse of latent heat and the increased condensation surface, however, it has a more complex construction. Another approach is to use a stepped solar still [22], which is represented in (Fig. 1.7). This design resulted in an improvement of about 50% due to a smaller volume of enclosure, less heat loss from the side walls, as well as decreasing shaded area of the basin over the day.

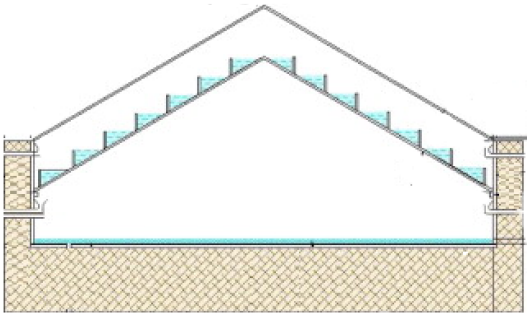

Figure 1.8: Representation of a double slope and basin solar still (figure by Elango et al. [23]).

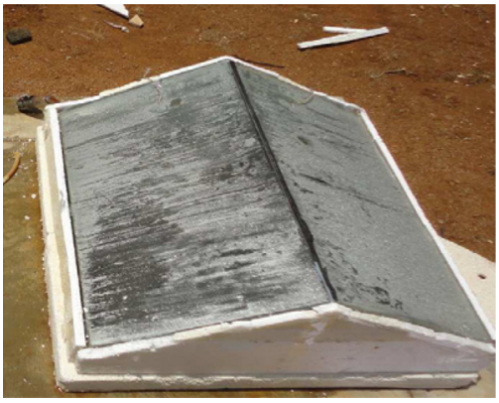

Figure 1.9: Double slope solar still (figure by Elango et al. [23]).

- **Use of a heat reservoir under the basin:** After the sun sets, a small amount of water is produced because there is no energy source to promote heat and mass transfer processes. The water production is maintained up to a certain moment by the thermal inertia of the components. The use of a thermal storage medium has shown a good effect in increasing the water yield at night, as described by Tabrizi and Sharak [24], who studied the effect of a sand reservoir under the basin (Fig. 1.10). Other materials were used to perform a similar task as analyzed by Kabeel et al. [25] who used a phase change material as a heat storage resulting in improvement as well.

Figure 1.10: Single slope solar still with overall structure made of glass, and a sandy reservoir under the basin (figure by Tabrizi and Sharak [24]).

- **Promoting convection inside the enclosure:** Kianifar and Mahian [26] theoretically and experimentally, evaluated the performance of a pyramid solar still with a small low velocity fan inside to increase convection. The results showed that the low-cost fan can be an effective method to increase fresh water production.

- **Wick/Porous Materials on the basin:** Covering the basin with porous materials has the advantage that it combines the properties of water and porous medium, as well as increasing basin surface and radiation absorbed. Murugavel and Sritharb [27] used different wick materials, such as light black cotton cloth (Fig. 1.11), light jute cloth, sponge sheet, coir mat and waste cotton pieces. Abdallah et al.[28] tried three absorbing materials, coated and uncoated metallic wiry sponges and volcanic rocks. Volcanic rocks increased the performance by around 50%. Bilal and Jamil [29] made a relevant experiment by covering the basin with a pumice stone (Fig. 1.12). In contrast to other experiments, his work showed a lower water productivity when using the porous materials. The main causes pointed out by the researcher for this lower water production were low thermal conductivity of the pumice stone and lack of water exposure to the enclosure air. These are important constraints to take into account when trying to use new materials in the solar still.

Figure 1.11: Solar still basin covered with a black cloth (figure by Murugavel and Sritharb [27]).

Figure 1.12: Solar still basin covered with pumice stones (figure by Bilal and Jamil [29]).

- **Reducing glass temperature:** Reducing glass temperature can be done in two ways, namely by pouring water over the glass cover or by blowing air with a fan onto the glass cover. The result of these measures is an increase in the temperature difference between glass and water, which induces heat and mass transfer [21]. Badran [30] installed a sprinkler above the glass cover, which increased the water yield by 20%. The utilization of a fan in experiments has not a clear agreement in the literature. Although some studies show that a high wind velocity over the cover increases the water yield [31], other studies have shown that an increasing wind speed on the glass cover might decrease water production [32]. When choosing to implement this technique, a detailed analysis must be done on the external conditions and the solar still design.

More recently, innovative studies have been done with multistage solar stills. These reuse the latent heat of water from condensation and transfer it to successive evaporators and condenser groups.

Chiavazzo et al. [33] and his colleagues not only analyzed theoretically, but also tested a prototype experimentally (Fig. 1.13) and achieved impressive results with around 3 $L/(m^2h)$ in laboratory conditions. Following the same line of thought, Zhenyuan et al. [34] succeeded in further improving the multi-stage solar still, by optimizing parameters such as materials and the gap distance between evaporator and condenser, which enabled him to perform 5.78 $L/(m^2h)$ in laboratory conditions, and estimates a $10-20$ L/m^2 production depending on the final design and the weather conditions. These units seem promising for the future, however more research has to be done. Simpler materials, design and maintenance must be provided, so that it is easy and accessible to reproduce.

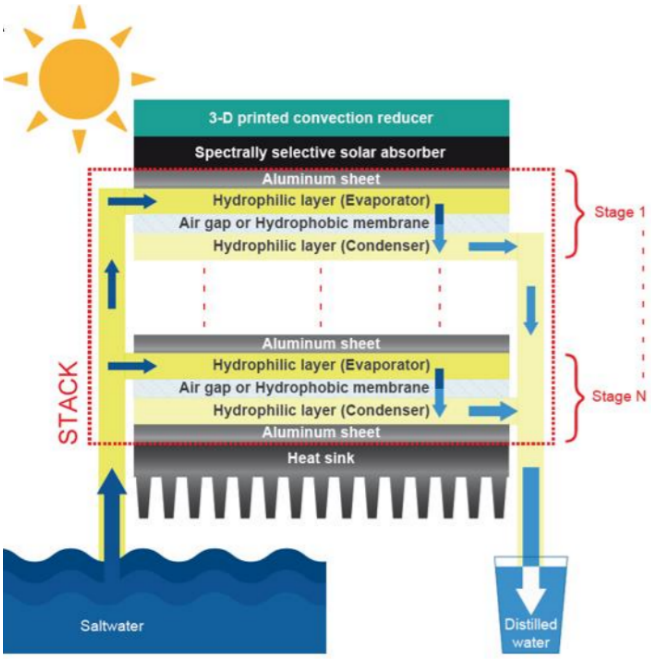

Figure 1.13: Representation of the experimental setup of modular passive solar still. (figure by Chiavazzo et al.[33])

Even though the solar still presents a low production capacity, multiple efforts have been done to make it into a more attractive solution. As it is important to experiment and create new solutions to improve the solar still performance, theoretical modeling has also an important role.

1.2.3 Theoretical Model

Predicting with precision and simplicity the water production of solar stills with different designs, characteristics and situated in different locations is an important task that avoids time-consuming experimental work.

In the existing literature, the majority of the models consist of a macroscopic energy balance to the basin (Eq. 1.1), water (Eq. 1.2), and glass (Eq. 1.3).

$$(mc_p)_b \frac{\partial T_b}{\partial t} = \alpha_b I(t) A_b - Q_{c,b-w} - Q_{lost,b} \tag{1.1}$$

$$(mc_p)_w \frac{\partial T_w}{\partial t} = \alpha_w I(t) A_b - Q_{evap} - Q_{r,w-g} - Q_{c,w-g} + Q_{c,b-w} \tag{1.2}$$

$$(mc_p)_g \frac{\partial T_g}{\partial t} = \alpha_g I(t) A_g + Q_{evap} + Q_{r,w-g} + Q_{c,w-g} - Q_{r,g-sky} - Q_{c,g-out} \tag{1.3}$$

It can be seen in Fig. 1.14 a representation of the heat transfer processes considered by these models approach [35].

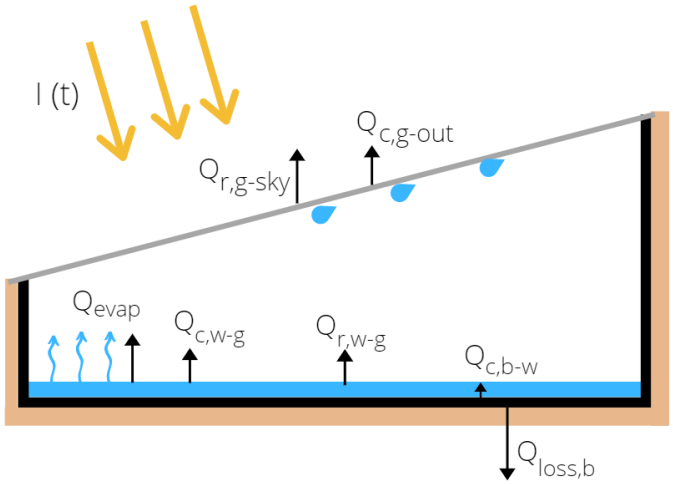

Figure 1.14: Schematic view of the solar still, presenting the heat transfer exchanges of the basin, water and glass considered by the standard model approach.

Firstly, if we look at the basin balance equation, the first term on the right side of the equation, $\alpha_b I(t) A_b$, refers to the incident solar radiation absorbed by the basin. The basin has two terms of heat loss, one refers to the heat exchanged by convection with water, $Q_{c,b-w}$, and the other to the heat lost through the basin insulation, $Q_{lost,b}$. Secondly, in the water energy balance, heat is gained from the absorbed incident solar radiation and the heat given off by the basin. The water energy balance equation includes the energy lost through evaporation, Q_{evap}, convection between water and glass, $Q_{c,w-g}$, and radiation heat exchange between water and glass, $Q_{r,w-g}$. Finally, the glass gains heat due to a similar absorption of incident radiation, and heat from radiation and convection exchange with water. It is assumed that the evaporated water condenses immediately. Therefore, it is considered a heat gain in the energy balance of the glass. The glass loses energy due to radiation and convection exchange with the outside, $Q_{r,g-sky}$ and $Q_{c,g-out}$, respectively.

The thermal models seen in the literature use the same general equations and differ in the correlations for convective and evaporative heat transfer between water and glass. Dunkle [36] proposed a thermal model with widely accepted empirical correlations to predict the performance of a double slope and single basin solar still. To calculate the heat transfer coefficient due to natural convection caused by the temperature difference between the basin and the glass, Dunkle used the empirical correlation of Jacob [37] for the free convection of air between parallel plates. Dunkle selected the correlation constants according to an average operating temperature range of 50°C. Moreover, a modified Grashof was

also used, resulting in the following,

$$h_c = 0.884 \left(T_w - T_g + \frac{(p_w - p_g)T_w}{(268.9 \times 10^3 - p_w)} \right)^{\frac{1}{3}} \tag{1.4}$$

Dunkle further obtained the relation between the evaporation and the convective heat transfer coefficient by experiment,

$$h_{evap} = 16.273 \times 10^{-3} h_c \left(\frac{p_w - p_g}{T_w - T_g} \right) \tag{1.5}$$

It has been mentioned in the literature [5, 35, 38] that the Dunkle's model can present large deviation in practical application, especially when the solar still operates at temperatures higher than 55° C, or at low temperatures. This model was thought to be applied in a double slope solar still, however it is commonly used for all types of structures, leading to errors. Other limitations of this thermal model are that the thermophysical properties of humid air are assumed for an average operating temperature at 50° C, it is considered a 17° C of temperature difference between evaporation and condensation surfaces, the role of the walls and cover inclination are neglected as well as the characteristic length of the solar still.

Other thermal models have been provided to compute heat transfer coefficients of convection and evaporation and, more importantly, to improve the accuracy of predicting water production. Clark [39] pointed out that an additional factor to account for saturation must be introduced into the expression of the evaporative heat transfer coefficient. Clark conducted an indoor experiment to validate his model, however, did not perform the experiment in real conditions. Adhikari [40] questioned the fact that Dunkle's correlation is valid for a specific range of Grashof numbers and needs to be modified for higher values, thus performed simulation experiments and proposed a relationship to estimate the hourly distillate yield. Kumar and Tiwari model [41] proposed a correlations for the convective mass transfer, based on a regression analysis for their method. The researchers performed experiments on a single slope solar still under actual field conditions and took into account the effects of the still cavity, the operating temperature range, and the orientation of the condenser cover. Tsilingiris model [42], is based on similar correlations of Dunkle's model, and takes into account the role of the thermophysical properties of a binary mixture of dry air and water–vapor humid air instead of dry air properties alone.

Dunkle's model has been acknowledged by most of the researchers and is adopted in the majority of the literature due to its simplicity and easy computation. However, due to the referred simplifications is commonly reported that it overestimates the water yield values. As a result of being one of the most accepted in the literature, it will be used as a comparison in the following work.

1.3 Contributions to the State-of-the-art

The motivation of this thesis is to contribute to two major points: (1) the improvement of the solar still theoretical analysis and (2) assess possible approaches to increase fresh water output of solar stills.

In the first part of this work, it is provided a thermal model that differs from others since it acknowl-

edges energy balances for all solar still components and the air within. Adding to this, a detailed analysis about the pre-processing done on the solar radiation data, the choice of different properties, and the description of the correlations used, which have a major influence on the solar still performance. All these variables add new constraints and complexity to give a more reliable yield prediction. For the second part, a detailed analysis of the solar still operation and limitations are done, to find the parameters that can be optimized. Based on the parametric study, realistic approaches that can be implemented are evaluated.

To summarize, the work presented and the objectives aimed to reach are the following:

- To develop a thermal model, taking into account all the components role, to increase accuracy in the prediction of the solar still performance.
- To perform a parametric study to further understand how can water production be enhanced.
- Suggestion of structural improvements and analysis of the literature contributions, along with comparisons with the conventional solar still.

1.4 Thesis Outline

This document first of all addressed the motivation behind this thesis, which highlighted the fact that there are still regions in the world today that do not have access to an essential element such as water. The UN recognized that this is a major problem that needs to be solved and thus has been prioritized a one of the objectives to be achieved by 2030. Taking into account the importance of providing low cost and small-scale solutions that can be implemented in developing countries, the various existing desalination processes were examined. Of all existing techniques, the one that can be a possible solution is desalination by using a solar still. A brief overview of the solar still was presented, as well as the improvements analysed experimentally and the theoretical model approaches, that resulted from previous research.

In **Chapter 2**, a thermal model to predict the solar still performance is proposed. It is given a description in detail of all assumptions, correlations, analogies as well as energy balances used.

Chapter 3 focuses on implementing the model, which includes validating, verifying, so that it can be analyzed the uncertainty of the constraints and assumptions made. At the end of this chapter, a comparison between the water yield prediction of the proposed model, Dunkle's model, and various experimental data is done.

Chapter 4 presents a parametric analysis made to the different solar still variables in order to optimize the structure and achieve higher productivity. The analysis is followed by realistic construction suggestions to improve the device.

At last, in **Chapter 5**, the proposed thermal model and the performance improvement studies are evaluated. Suggestions for future work are given for further development and improvement of the solar still.

Chapter 2

Thermal Model

The proposed thermal model consists of an analysis to all the components of the solar still. In this chapter the governing equations, the energy balance equations, the calculations of the heat transfer coefficients, the analogies of heat and mass transfer, and the constants used in this work are examined in detail.

A set of governing equations must be solved and design variable must be defined. The design variables are the various design parameters chosen for the solar still, for example, the height of the walls, width and length of the basin, water quantity and others. The relevant governing equations are the energy and mass equations. Momentum equations are not required to be solved because the pressure in the enclosure is considered constant.

2.1 Energy Balance Equations

Firstly it is going to be described and analyzed the energy balance for each component of a conventional single basin single slope solar still. Figure 2.1 presents the heat exchanges for this thermal model approach.

The assumptions made for these balances are: (1) No vapor leakage in the solar still; (2) Water mass over the basin is constant, since it is assumed that evaporated water is renewed every time step; (3) The temperature gradient along water, glass and basin is negligible due to its small thickness.

Even though the terms used are explained in detail in the following chapters, a preliminary explanation of the nomenclature must be provided. Starting by addressing the subscripts for each component, glass (g), water (w), basin (b), walls ($wall$) and air (a). The walls subscript is followed by the designation of the wall, if $Front$, $Back$ or $Lateral$. For general heat transfer, Q is used, and the subscript indicates the type of heat exchange, incident solar radiation (sun), convection (c), radiation (r), evaporation ($evap$), condensation ($cond$) or heat loss ($lost$). Following the subscript, the surface to which it refers is given, e.g. $Q_{sun,g}$, refer to the incident radiation absorbed by the glass. In some cases, two bodies are referred meaning that there is heat exchange between them, e.g. $Q_{c,w-a}$, refers to the heat exchange due to convection between water and air in the solar still. The term h is the heat transfer coefficient and follows

the same subscript reasoning.

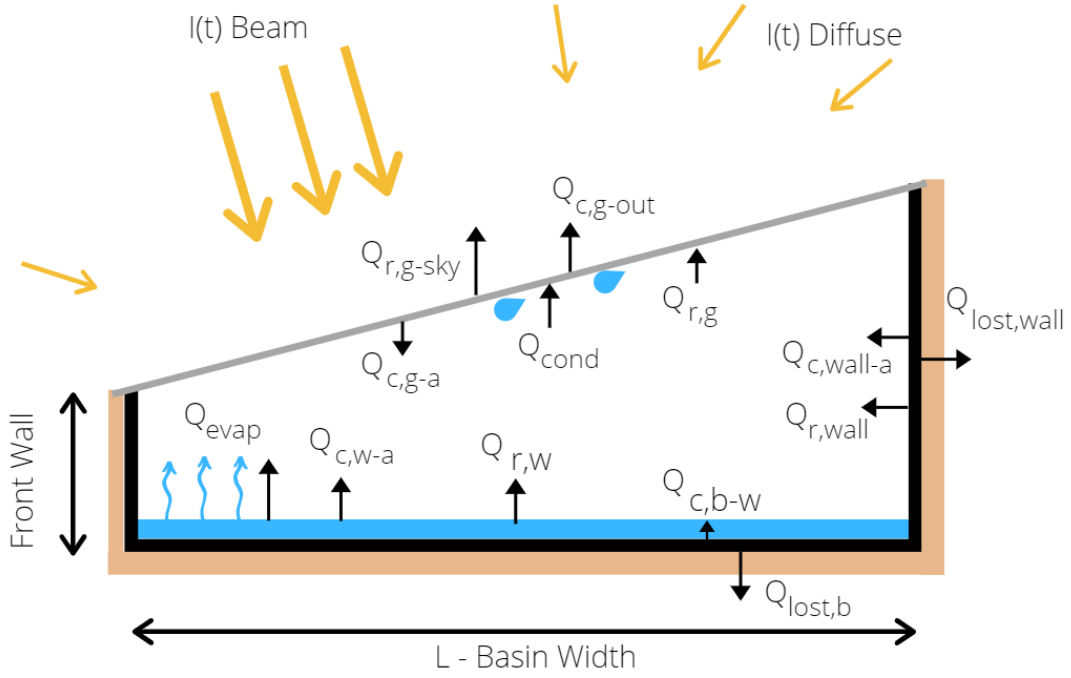

Figure 2.1: Solar still heat transfer processes schematic view. Remaining walls have similar heat exchanges as the one represented. Legend: Black - Basin/Wall, Blue - Seawater, Brown - Insulation.

1. **Glass Energy Balance**

   The energy balance equation for the glass cover is the following,

$$(mc_p)_g \frac{\partial T_g}{\partial t} = Q_{sun,g} + Q_{cond} + Q_{r,g} + Q_{c,a-g} - Q_{r,g-sky} - Q_{c,g-out} \tag{2.1}$$

   The input energy results from the absorbed solar radiation $Q_{sun,g}$, the radiation heat transfer between glass and the remaining surfaces $Q_{r,g}$, the latent heat of the condensed water Q_{cond}, and the convection heat transfer between air and glass $Q_{c,a-g}$. Although a film of water forms under the glass due to water vapour condensation, according to the simplified thermal models of the solar still [35] it is assumed as a first approach that the glass exchanges heat with the air by convection. The absorbed solar radiation is divided into direct I_{dr}, and diffuse radiation I_{dif}. The absorption coefficient of each surface is given by α and the correspondent surface subscript.

$$Q_{sun,g} = \alpha_g A_g (I_{dr,g} + I_{dif,g}) \tag{2.2}$$

$$Q_{c,a-g} = h_{c,a-g} A_g (T_a - T_g) \tag{2.3}$$

$$Q_{cond} = \dot{m}_{cond} \triangle H_{H_2O} \tag{2.4}$$

   The glass exchanges heat by radiation with water and walls. The summatory in Eq. 2.7 accounts for the radiation from front, back (indicated in Fig. 1.6), and lateral walls. The respective view

factor, F_{1-2}, must be computed for each radiation heat exchange (subscript $1-2$ represent the surfaces that interact). It was assumed that the humid air does not interfere with the radiative heat exchange between surfaces, and therefore this effect should be investigated in more detail in a future work.

$$Q_{r,g} = Q_{r,w-g} + Q_{r,walls-g} \tag{2.5}$$

$$Q_{r,w-g} = h_{r,w-g} A_w (T_w - T_g) F_{w-g} \tag{2.6}$$

$$Q_{r,walls-g} = \sum h_{r,wall-g} A_{wall} (T_{wall} - T_g) F_{wall-g} \tag{2.7}$$

The glass loses heat in the form of radiation to the atmosphere and because of the convective heat transfer caused by wind,

$$Q_{r,g-sky} = h_{r,g-sky} A_g (T_g - T_{sky}) \tag{2.8}$$

$$Q_{c,g-out} = h_{c,g-out} A_g (T_g - T_{out}) \tag{2.9}$$

2. **Water Energy Balance**

The energy balance equation for the water is the following,

$$(mc_p)_w \frac{\partial T_w}{\partial t} = Q_{sun,w} - Q_{evap} - Q_{r,w} - Q_{c,w-a} + Q_{c,b-w} - \dot{m}_{evap} (T_w - T_{out}) c_{p,w} \tag{2.10}$$

The water is heated due to the incident solar radiation, $Q_{sun,w}$, and convection heat from the basin, $Q_{c,b-w}$.

$$Q_{sun,w} = I_{dr,w} (\tau_g)_{dr} \alpha_w A_{exp,w} + I_{dif,w} (\tau_g)_{dif} \alpha_w A_w \tag{2.11}$$

$$Q_{c,b-w} = A_w h_{c,b-w} (T_b - T_w) \tag{2.12}$$

It loses heat by giving away energy for water evaporation, Q_{evap}, convection, $Q_{c,w-a}$, radiation, $Q_{r,w}$, and to heat the renewal water, $\dot{m}_{evap} (T_w - T_{out}) c_{p,w}$ (since the renewal water temperature is not known for the majority of the experimental works, it is set as being at outside temperature) .

$$Q_{evap} = \dot{m}_{evap} \triangle H_{H_2O} \tag{2.13}$$

$$Q_{c,w-a} = A_b h_{c,w-a}(T_w - T_a) \tag{2.14}$$

$$Q_{r,w} = Q_{r,w-g} + Q_{r,w-walls} \tag{2.15}$$

$$Q_{r,w-walls} = \sum h_{r,w-wall} A_w (T_w - T_{wall}) F_{w-wall} \tag{2.16}$$

3. **Basin Energy Balance**

   The energy balance equation for the basin is the following,

$$(mc_p)_b \frac{\partial T_b}{\partial t} = Q_{sun,b} - Q_{c,b-w} - Q_{lost,b} \tag{2.17}$$

   The basin gains heat by absorbing incident radiation, $Q_{sun,b}$, and loses heat to the water above it by convection, $Q_{c,b-w}$, and to the exterior, $Q_{lost,b}$.

$$Q_{sun,b} = I_{dr,b}(\tau_g \alpha_b)_{dr} \tau_w A_{exp,b} + I_{dif}(\tau_g \alpha_b)_{dif} \tau_w A_b \tag{2.18}$$

$$Q_{lost,b} = A_b U_b (T_b - T_{out}) \tag{2.19}$$

4. **Wall Energy Balance**

   The general wall heat balance is given by,

$$(mc_p)_{wall} \frac{\partial T_{wall}}{\partial t} = Q_{sun,wall} + Q_{r,w-wall} - Q_{r,wall-g} - Q_{c,a-wall} - Q_{lost,wall} \tag{2.20}$$

   The walls absorb incident solar radiation, $Q_{sun,wall}$, and lose heat by convection due to interaction with the enclosure's air. They also lose heat by radiation exchange with other surfaces, and to the exterior by conduction.

$$Q_{sun,wall} = I_{dr,wall}(\tau_g \alpha_{wall})_{dr} A_{exp,wall} + I_{dif_{wall}}(\tau_g \alpha_{wall})_{dif} A_{wall} \tag{2.21}$$

$$Q_{lost,wall} = A_{wall} U_{wall} (T_{wall} - T_{out}) \tag{2.22}$$

5. **Solar Still Air Energy Balance**

   The energy balance equation for the air inside the still is the following,

$$(mc_p)_a \frac{\partial T_a}{\partial t} = Q_{c,w-a} + Q_{c,wall-a} - Q_{c,a-g} \tag{2.23}$$

The air's heat gain or loss is due to the heat transfer convection mechanisms when it interacts with water, walls, and glass.

2.2 Incoming Radiation

2.2.1 Beam and Diffuse Radiation

Commonly from the available solar radiation data, which is obtained by pyranometers, it is possible to get the global solar radiation I_G, on a horizontal surface. In a simplified and conservative approach, it can be assumed that this global irradiance is the sum of two components, the direct/beam radiation, I_{dr}, and the diffuse, I_{dif}, thus they must be split. It is more realistic to compute both components to perform the simulation than considering all as one. On the one hand, the absorbed direct radiation will only reach non-shaded areas and should not be account for in the entire solar still basin and walls. On the other hand, the diffusive radiation absorbed by each component depends on the view factor, which will be described later. Moreover, based on the literature, different transmissivities and absorption estimates are given for the materials depending on the type of solar radiation component [11]. According to a simplified isotropic sky model given in the same literature,

$$I_G = I_{dr} + I_{dif} \tag{2.24}$$

Diffuse radiation will depend on the sky clearness. The radiation may or may not be highly scattered, which influences the solar still performance. Once again, refining the calculation of these components allows a more accurate representation of realistic conditions and thus the prediction of water yield. One of the widely used correlations that is used to compute I_{dif}, is the Orgill and Hollands correlation [11],

$$\frac{I_{dif}}{I_G} = \begin{cases} 1 - 0.249k_t & \text{for } 0 \leq k_t \leq 0.35 \\ 1.5571.84k_t & \text{for } 0.35{<}k_t{<}0.75 \\ 0.177 & \text{for } k_t{>}0.75 \end{cases} \tag{2.25}$$

The clearness sky index, k_t, differs for each location and season as well as along the day and can be estimated from [11]. In the literature, the available information is relative to the average monthly sky clearness index for some locations (k_t of the closest location of the experiments is taken), which is going to be used to calculate radiation values. This leads to a theoretical error, as monthly average value is being used for every time step, however, it allows a more realistic approach. By computing the I_{dif}, consequently it is possible to obtain I_{dr}.

The simplified isotropic sky diffuse model states that the diffuse radiation is evenly distributed across the sky. The solar still glass is inclined, with the surface angle β_g, and it will not view the entire sky, so the diffuse radiation must be corrected with the appropriate view factor

$$I_{dif,g} = I_{dif}\left(\frac{1+\cos\beta_g}{2}\right) \tag{2.26}$$

The diffuse radiation absorbed by basin and walls depends on the view factor to the glass. It is important to note that the vertical surfaces only see half of the sky ($\beta_{wall} = 90°$), so the walls can only receive half of the diffuse radiation transmitted by the glass.

$$I_{dif,wall} = I_{dif,g} F_{wall-g} \tag{2.27}$$

$$I_{dif,b} = I_{dif,g} F_{b-g} \tag{2.28}$$

The absorbed beam radiation, I_{dr}, must be calculated according to the position of the sun and the surface inclination. The beam solar radiation will be given for a horizontal surface ($I_{dr,horizontal}$) when computing with Eq. 2.24, thus it must be corrected for the vertical walls ($I_{dr,wall}$) and inclined glass cover ($I_{dr,g}$). The geometric factor, R, is the ratio of beam radiation on the inclined surface to that on a horizontal surface [11].

$$R = \frac{I_{dr,tilted}}{I_{dr,horizontal}} = \frac{\cos\theta}{\cos\theta_z} \tag{2.29}$$

These equation carry new variables, such as θ, which is the angle of incident radiation on a surface, and θ_z, which is the zenith angle. It is possible to obtain them, by using the following correlations,

$$\begin{aligned}\cos\theta = {} & \sin\delta\sin\phi\cos\beta - \sin\delta\cos\phi\sin\beta\cos\gamma + \cos\delta\cos\phi\cos\beta\cos\omega \\ & + \cos\delta\sin\phi\sin\beta\cos\gamma\cos\omega + \cos\delta\sin\beta\sin\gamma\sin\omega\end{aligned} \tag{2.30}$$

$$\cos\theta_z = \cos\delta\cos\phi\cos\omega + \sin\phi\sin\delta \tag{2.31}$$

where, it is used the surface azimuth angle γ, the hour angle ω, the sun declination angle δ, and the latitude ϕ. It is necessary to compute ω and δ,

$$\omega = 15(t_{solar} - 12) \tag{2.32}$$

$$\delta = 23.45\sin\left(360(284+n)/365\right) \tag{2.33}$$

The term t_{solar} corresponds to local solar time, and n to the day number. To compute t_{solar},

$$t_{solar} = t + \frac{4(\lambda - LSTM) + EoT}{60} \tag{2.34}$$

where t represents the local time of the time step, λ the longitude, $LSTM$ is the Local Standard Time Meridian, and EoT is the equation of time to refine the solar hour. All these values can be computed with,

$$LSTM = 15 \times \Delta T_{UTC} \tag{2.35}$$

$$EoT = 9.87 \sin(2B) - 7.53 \cos(B) - 1.5 \sin B \tag{2.36}$$

$$B = \frac{360}{365}(n - 81) \tag{2.37}$$

where, ΔT_{UTC} is the difference of the Local Time from Universal Coordinated Time in hours. If there is daylight saving time, it should be taken 1h from t.

2.2.2 Materials Radiative Properties

The incident radiation plays an important role in the performance of solar stills, since it triggers the water production cycle. Direct and diffuse solar radiation reaching the glass cover are transmitted to the inside of the solar still, however, a small percentage is reflected and other absorbed. Water, like glass, will reflect and absorb some of the radiation allowing the remaining to reach the basin. Inside the solar still, there will be multi-reflection between all components, similar to the multi-effect sheet [11, 43].

In this work, detailed attention is given to the calculation of the radiation properties of glass and basin/wall, more precisely the transmissivity and absorption, respectively. The first approach consists of computing a glass transmissivity and a basin/wall absorption value which will be considered constant throughout the day. The second approach consists of a glass transmissivity value depending on the cover angle and angle of incidence of the solar radiation. In addition, an absorption coefficient of the walls and the basin, also depending on the angle of incidence of the solar radiation.

Analysing each component in more depth:

1. The glass cover will have different radiation attributes according to its physical properties, such as thickness, refractive index, and incidence angle of incoming radiation.

   As a first approach, it was decided to compute an average and conservative constant value for the glass transmissivity to beam radiation. For the considered range of angles of incident radiation on the glass and the types of glass that may be used in the construction, it can be assumed that the properties are independent of the wavelength [11]. This assumption facilitates the calculation of the transmissivity. To calculate the transmissivity of glass to beam radiations, as given by Modest [43], the following correlation should be considered,

   $$\tau_g = \exp\left(\frac{-kd}{\cos\theta_2}\right) \tag{2.38}$$

   For the variety of glasses that might be applied, the absorption coefficient, k, is in an acceptable range from $4m^{-1}$ to $32m^{-1}$, and the glass thickness, d, between $2.5mm$ and $5mm$. The angle of incidence is represented by θ. An average value of approximately $kd = 0.04$, might be considered [11]. The following reasoning is thought for an specific experimental work carried out by Kabeel

et al.[22], which will be analyzed in the next chapters. By analyzing Fig. 2.2 with the previous assumptions, and considering one sheet of glass, and an average incidence angle of 40º, the transmissivity will be close to 85%. This value will thus be assumed as an average value throughout the day.

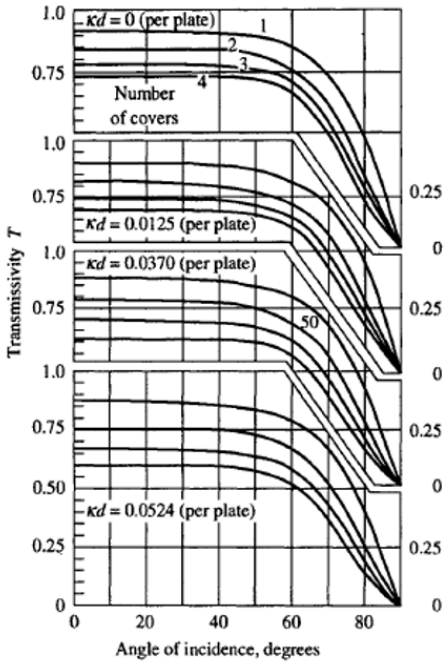

Figure 2.2: Transmittance (considering absorption and reflection) of one, two, three, and four covers for three types of glass; adapted from [11].

Following Beer's law, which states,

$$\tau + \alpha + \rho = 1 \tag{2.39}$$

it is possible to assume an absorption of 7% (value commonly seen in the literature, e.g. [22]), and a reflection of 8%. Later, in Chapter 3, a sensitivity analysis is presented to evaluate the impact of these initial assumptions. For the diffusive radiation transmitted, it is used Eq. 2.41.

Looking now at the second approach regarding glass transmissivity dependent of radiation incidence angle. Tanaka [44] gives a relation of glass transmissivity to direct beam radiation according to the incident angle of sun rays on the glass cover (θ, computed with Eq. 2.30).

$$(\tau_g)_{dr}(\theta) = 2.642\cos\theta - 2.163\cos^2\theta - 0.320\cos^3\theta + 0.719\cos^4\theta \qquad (glass\ 3mm\ thick) \tag{2.40}$$

Moreover, Tanaka [16] also gives the transmissivity to diffuse radiation dependent on the glass cover angle, by integrating transmissivity for diffuse radiation from all directions.

$$(\tau_g)_{dif} = -2.03 \times 10^{-5} \times \beta_g^2 - 2.05 \times 10^{-3} \times \beta_g + 0.667 \tag{2.41}$$

Transmissivity as a function of the angle of incidence of solar radiation was implemented in the

thermal model because it better represents reality. This topic is further analyzed in section 3.2.2.

2. Looking now at the water properties, water depth normally is chosen to be as small as possible. Assuming the depth around 2 cm, and analyzing the water absorption spectrum, it is possible to conclude that the majority of the radiation that reaches the water, predominantly visible light, is not absorbed by it. It was assumed a transmissivity value around 93%, absorption around 5%, and a reflection of 2%, which will be later validated. The value of absorption chosen is commonly seen in the literature [13, 22], and the transmissivity is also in agreement [23].

3. Two approaches were also used for the basin and wall absorption. These surfaces are usually painted black as stated before, thus they will be very close to a black body. It can be assumed a normal absorption of 95% [11]. It is reported in the same literature that the beam radiation absorption will also vary with incidence radiation angle, as shown in Fig. 2.3. The ratio of absorption to normal absorption, is given by,

$$\begin{aligned}\frac{\alpha}{(\alpha)_n} &= 1 - 1.5879 \times 10^{-3}\theta + 2.7314 \times 10^{-4}\theta^2 - 2.3026 \times 10^{-5}\theta^3 + 9.0244 \times 10^{-7}\theta^4 \\ &\quad - 1.8 \times 10^{-8}\theta^5 + 1.7734 \times 10^{-10}\theta^6 - 6.9937 \times 10^{-13}\theta^7\end{aligned} \tag{2.42}$$

where, θ for the basin and walls, can be computed with Eq. 2.30. To compute the absorption of solar diffuse radiation α_{dif}, a mean effective angle of incidence on the inclined surface under consideration must first be determined from Fig. 2.4 and then introduced into Eq. 2.30 [35].

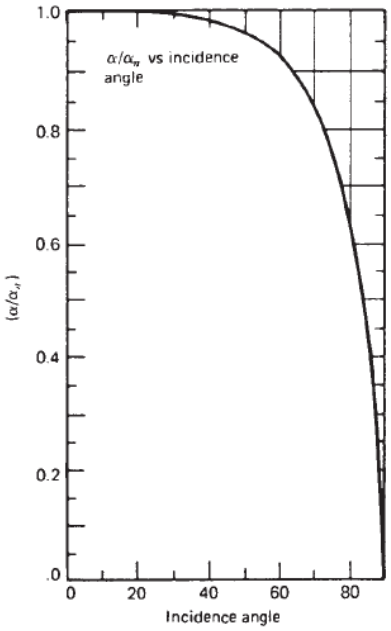

Figure 2.3: Ratio of solar absorptance and solar absorptance at normal incidence for a flat black surface; adapted from [11].

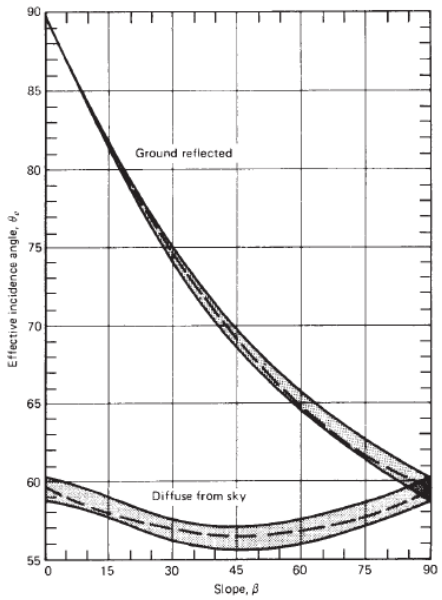

Figure 2.4: Effective incidence angle of isotropic diffuse radiation and isotropic ground-reflected radiation on sloped surfaces; adapted from [11].

For the beam radiation, considering an average incidence angle around 65° , a ratio of 90% seems

a good approximation. Thus, for a first conservative and simple approach the assumed constant value assumed for absorbed direct radiation is around, $\alpha_{b,dr} = 0.95 \times 0.9 \approx 0.87$. For the absorption of diffuse radiation by basin $\alpha_{b,dif}$ (horizontal surface) and walls $\alpha_{wall,dif}$(vertical surfaces), the effective incidence angle will be close to 60° , as represented in Fig. 2.4, corresponding to $\approx 90\%$ radiation absorption.

For the second approach, at each time step, basin and wall absorption of direct solar radiation will be computed with Eq. 2.42. To note that the diffuse radiation absorption is set constant ($\approx 90\%$) since an effective incidence angle is assumed constant throughout the day.

Inside the solar still, a multi-effect of reflections will exist, since radiation reflects on the water and the basin, and is reflected by the glass cover. This event will lead to a small increase in radiation absorption by the components.

Performing a similar radiation study as shown in Fig. 2.5, it can be understood that the basin will directly absorb radiation transmitted by glass and water, and will also absorb the multiple radiations reflected inside the solar still. This will lead to the following expression,

$$(\tau_G \tau_W \alpha_B) = \frac{\tau_G \tau_W \alpha_B}{1 - (\rho_G (1 - \alpha_B) \tau_W^2 + \rho_W)} \tag{2.43}$$

substituting the variables assumed before, $(\tau_G \tau_W \alpha_B) \approx 0.71$.

It is mentioned in [11] that a simpler approximation can be done to take into account in the multi effect radiation.

$$(\tau_G \tau_W \alpha_B) \approx 1.01 \tau_G \tau_W \alpha_B \tag{2.44}$$

In this case it would lead to $(\tau_G \tau_W \alpha_B) \approx 0.7$, which is practically the same value obtained from Eq. 2.43. Since the effect of multiple reflection has a small influence, it was neglected in the thermal model.

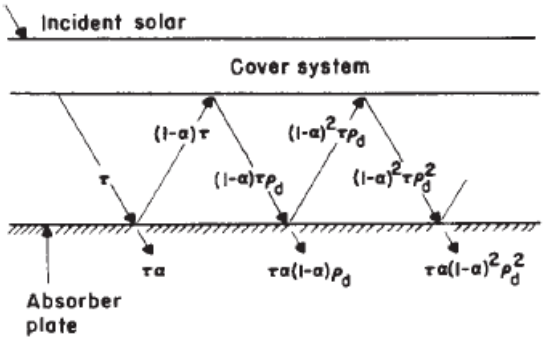

Figure 2.5: Representation of the multi-effect radiation reflection. (figure adapted from [11])

2.2.3 Shadows

Throughout the year the solar altitude (α_{sun}) and azimuth (γ_{sun}) vary, which affects the incident radiation components on the basin and the walls, as well as its exposition to the solar radiation (Fig. 2.6). In

addition, there are shadows, which can be caused by clouds or by objects like trees or buildings, that may shadow the solar still. In winter, the basin is shaded longer than in summer because of the lower sun altitude. The azimuth also plays an important role. The longer the sun is behind or laterally to the solar still, the more shadow there will be, because of the back and lateral walls.

Shadows have a direct impact on the performance of the solar still, so they must be considered and modeled to accurately predict water yield. A model is presented to compute the area that shades the basin and the walls.

The shaded area of the basin receives no beam radiation but absorbs the diffuse radiation. Not taking shading into account in the model leads to overestimations and errors.

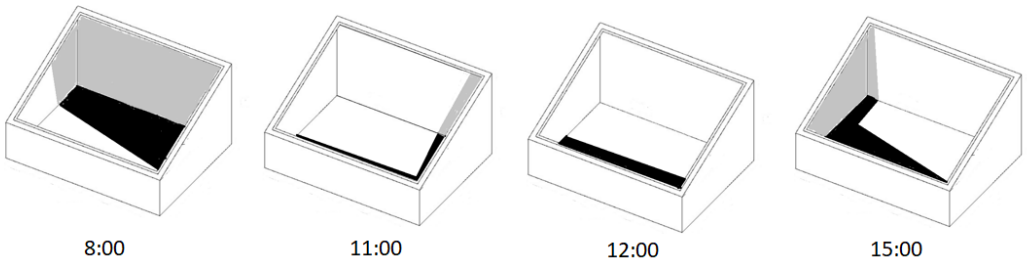

Figure 2.6: Representation of shaded area throughout a day for different hours.

A detailed and a simplified approach were carried out to calculate the basin exposed to the beam radiation. Considering the conventional solar still enclosure facing south, the following shadows are computed:

1. Front and one side wall shadow, when the solar azimuth angle is between -90° and 90° (Fig. 2.7);

2. Back and one side wall shadow, when the solar azimuth angle is greater than 90° and smaller than -90° (Fig. 2.8);

3. Front wall shadow, when the solar azimuth angle is equal to -90° .

First it is analysed the detailed shadow computation. The following calculations were made for cases where the sun is in front of the still ($|\gamma_{sun}| < 90°$) represented in Fig. 2.7. Points A and B represent the shadow of the low wall corner and the shadow of the high wall corner, respectively. The terms e and g represent the distance of the points A and B, from the lateral wall, f the distance of A from the front wall, and h the distance of B from the back wall. The darker grey area represents the shadow imposed by the lateral/ sidewall and the lighter grey area represents the shadow of the front wall. It is possible to get the coordinates of point A and point B, which enables the shadow calculation.

First, for each time step, it is necessary to compute the solar altitude α_{sun}, and the azimuth γ_{sun}, to get an approximate shadow length.

$$\sin \alpha_{sun} = \sin \phi \sin \delta + \cos \phi \cos \delta \cos h \tag{2.45}$$

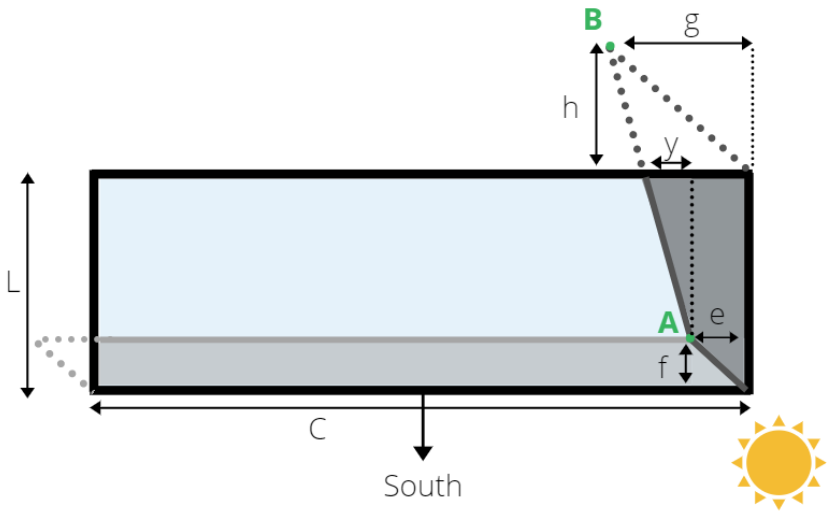

Figure 2.7: Top view of the solar still basin, covered by the shadow of front and lateral walls (when $|\gamma_{sun}| < 90°$).

$$\sin \gamma_{sun} = \frac{-\sin h \cos \delta}{\sin (90° - \alpha_{sun})} \tag{2.46}$$

It is possible to get e and g, using the front an back wall height, respectively.

$$e/g = \frac{H_{wall,front/back}}{\tan(\alpha_{sun})} \sin(90° - \gamma_{sun}) \tag{2.47}$$

By performing the following equation, the values f and h, can be computed, using the front an back wall height, respectively,

$$f/h = \frac{H_{wall,front/back}}{\tan(\alpha_{sun})} \sin(\gamma_{sun}) \tag{2.48}$$

and finally, the shadow imposed on the basin by the front wall can be computed as,

$$A_{shad,(wall,front)} = \frac{C + (C - e)}{2} \times C \tag{2.49}$$

The calculation of the shadow imposed by the lateral wall (darker grey area) is divided into two figures, a trapezium and a triangle, represented by the dotted line in Fig. 2.7. Using a straight line connecting A and B,

$$y = ax \tag{2.50}$$

and by calculating the appropriate slope,

$$a = \frac{g - e}{h + (l - f)} \tag{2.51}$$

it is possible to get y seen in Fig. 2.7

By knowing the base of the triangle for each time step, which is given by $l - f$, it is possible to find y.

$$y = a \times (l - f) \tag{2.52}$$

The computation of the shadow of the lateral wall on the basin, is the sum of the trapezoidal and triangular areas,

$$A_{shad,(wall,lateral)} = \frac{L + (L - f)}{2} \times e + \frac{L - f}{2} \times y \tag{2.53}$$

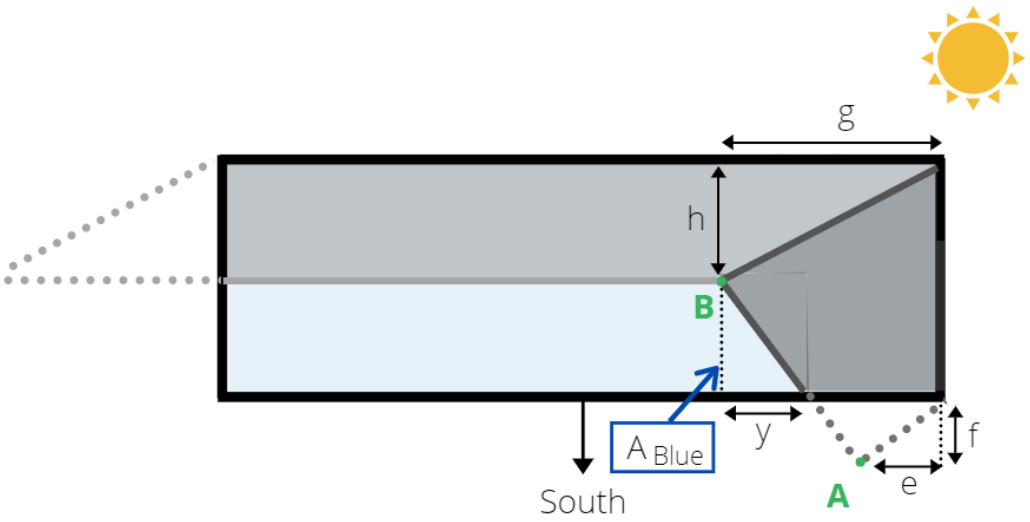

Figure 2.8: Top view of the solar still basin, covered by the shadow of the back and lateral wall (when $|\gamma_{sun}| > 90°$).

If the sun is behind the solar still ($|\gamma_{sun}| > 90°$), as represented in Fig. 2.8, a similar computation can be done. The dimensions e, f, g, and h are taken as stated in Eq. 2.47 and 2.48. The area shaded due to the back wall (lighter grey) is computed as,

$$A_{shad,(wall,back)} = \frac{C + (C - g)}{2} \times h \tag{2.54}$$

The lateral shadow (darker grey), for simplicity, can be computed as a sum of the light grey are and blue area (the small triangle until the dashed line, represented as A_{Blue}), which is later subtracted.

$$A_{shad,(wall,lateral)} + A_{Blue} = \frac{L + (L - h)}{2} \times g \tag{2.55}$$

To obtain y, shown in Fig. 2.8, we have to repeat the process of Eq. 2.50 and Eq. 2.51. Firstly, the slope between point A and B has to be computed, and then it is possible to obtain y, since it is known the distance between B and the front wall. The following values are computed,

$$a = \frac{g - e}{f + (L - h)} \tag{2.56}$$

$$y = a \times (L - h) \tag{2.57}$$

The area of the blue triangular area (see Fig. 2.8), which needs to be subtracted in Eq. 2.55, is

$$A_{Blue} = \frac{y \times (L - h)}{2} \tag{2.58}$$

Let us now look at the simplified shadow model. Instead of computing in detail the dimensions of the shadow, it is computed an average shadow height. For the case represented in Fig. 2.7, the area imposed by the front wall and lateral wall are respectively computed as,

$$A_{shad,(wall,front)} = f \times C \tag{2.59}$$

$$A_{shad,(wall,lateral)} = \frac{e + g}{2} \times L \tag{2.60}$$

For the case represented in Fig. 2.8, the area imposed by the back wall and lateral wall are respectively computed as,

$$A_{shad,(wall,back)} = h \times C \tag{2.61}$$

$$A_{shad,(wall,lateral)} = \frac{e + g}{2} \times C \tag{2.62}$$

For both simplified and detailed shadow model, the area exposed to $I_{dr,b}$, depending on γ_{sun}, will be,

$$A_{exp,b} = A_b - (A_{shad,(wall,back/front)} + A_{shad,(wall,lateral)}) \tag{2.63}$$

The simplified shadow model, as the name suggests is quite simple, existing some overlap when performing the sum of the shadows. Nonetheless, it is possible to see in Fig. 2.9 that there is little deviation between shadow models for the representative summer day. The winter day presents a larger deviation, however, this will not have a great impact on the water yield. A study was conducted to check how both shadow models affect the water yield and it was found that the deviation is about 3%.

To model shadow on the walls a simplified approach was chosen and the following considerations were taken into account:

1. All walls shaded, when $\gamma_{sun} > 90^\circ$ and smaller $\gamma_{sun} > -90^\circ$, since the sun is behind the solar still and generally at low altitude.

2. Front and one lateral wall shaded (right, if $\gamma_{sun} > 0^\circ$ or left, $\gamma_{sun} < 0^\circ$), when $90^\circ > \gamma_{sun} > -90^\circ$. Back wall partly shaded by lateral wall, and remaining lateral wall partly shaded by front wall.

The shadow on the back wall when $-90^\circ < \gamma_{sun} < 90^\circ$, is computed by using and average shadow height of the lateral walls, and the height of the back wall,

$$A_{shad,(wall,lateral)} = \frac{e + g}{2} \times H_{wall,back} \tag{2.64}$$

$$A_{exp,(wall,back)} = A_{wall,back} - A_{shad,(wall,lateral)} \tag{2.65}$$

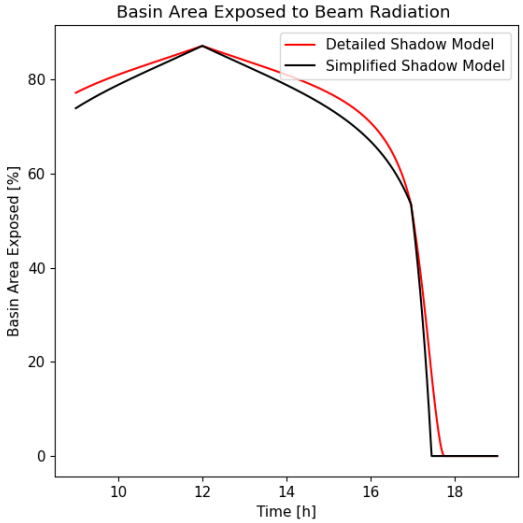

(a) Shading on the basin for the experimental work data (representative of a summer day).

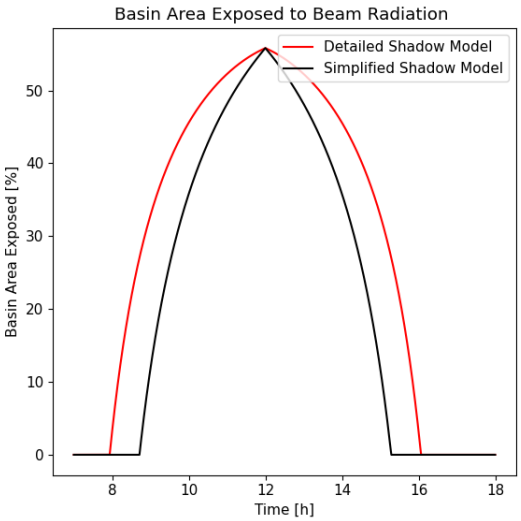

(b) Shading on the basin, for a representative winter day

Figure 2.9: Comparison between detailed and simplified shadow model,by presenting the basin area exposed to the sun throughout the day. The study was done on the experiment carried out by Kabeel et al. [22]

For the shaded area on the lateral walls, when $-90° < \gamma_{sun} < 90°$, by using the shadow height of the front wall and the lower wall height, an approximate shaded area caused by the front wall, and consequently the exposed lateral area can be computed as,

$$A_{shad,(wall,front)} = e \times H_{wall,front} \tag{2.66}$$

$$A_{exp,(wall,lateral)} = A_{wall,lateral} - A_{shad,(wall,front)} \tag{2.67}$$

2.3 Convection Heat transfer

In this and the following chapters, some dimensionless numbers are needed to compute heat transfer convection coefficient and the mass transfer coefficients. The Grashof number, *Gr*, measures the ratio of buoyancy forces to viscous forces.

$$Gr_x = \frac{g\beta(T_{hot} - T_{cold})x^3}{\upsilon^2} \tag{2.68}$$

The Prandtl number, *Pr*, is the ratio of the momentum to thermal diffusivity.

$$Pr = \frac{\upsilon}{\alpha} \tag{2.69}$$

The Rayleigh number, *Ra*, which is the product of Grashof and Prandtl numbers, allows the characterization of natural convection flow.

$$Ra_x = \frac{g\beta(T_{hot} - T_{cold})x^3}{\upsilon\alpha} \tag{2.70}$$

The Nusselt number, *Nu*, is the ratio between heat transfer by convection and heat transfer by conduction. It provides a measure of the convective heat transfer occurring on a considered surface, and thus allows the heat transfer coefficient to be calculated.

$$Nu_x = \frac{hx}{k_f} \tag{2.71}$$

All these dimensionless numbers need a generic characteristic length x that can be well defined based on some specific dimension of the solar still cavity.

In a conventional solar still, natural convection promotes not only heat transfer between the air inside the device, the walls, the basin and the glass cover, but also the evaporation of water from the seawater covering the basin and the condensation of water vapour on the glass cover.

The proposed approach in this thesis differs from other thermal models because it includes the analysis of walls and air inside the solar still. The air is modeled fairly simple being it considered a homogeneous body, meaning that water content, temperature, and relative humidity are assumed evenly distributed all over the mass of air for each time step. This leads to new energy balances and the need for computation of new heat transfer coefficients, more specifically between water/air, glass/air, and walls/air. Fig. 2.10 represents the natural convection between each surface and the air.

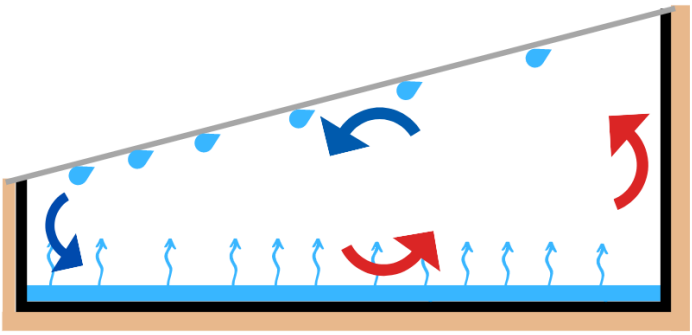

Figure 2.10: Representation of natural convection interactions between air and water, walls and glass

The following Nusselt numbers correlations are taken from the same literature reference [45]. To compute the heat transfer coefficient for the walls, $h_{c,wall-a}$, the following correlation is used,

$$Nu_L = \left(0.825 + \frac{0.387Ra_L^{1/6}}{(1 + (0.492/Pr)^{9/16})^{8/27}}\right) \qquad L = H_{wall} \qquad (10^4 < Ra_L < 10^{13}) \tag{2.72}$$

Assuming the basin temperature to be higher than water, and water at a higher temperature than air, it is possible to compute heat transfer coefficient between basin and water, $h_{c,b-w}$, and water and air, $h_{c,w-a}$, with Eq. 2.73 and 2.74, respectively.

$$Nu_L = 0.54 Ra_L^{1/4} \qquad (10^4 < Ra_L < 10^7) \tag{2.73}$$

$$Nu_L = 0.15 Ra_L^{1/3} \qquad (10^7 < Ra_L < 10^{11}) \tag{2.74}$$

To compute the characteristic length for these correlations it is necessary the area and perimeter of the considered surface,

$$L = \frac{A}{P} \tag{2.75}$$

The glass is a downward inclined cold surface, and for these cases, there is less agreement in the literature. There are references for the upward inclined hot surface, being the main referenced studies from Fuji [46] and Vliet [47]. The correlations of these researches are experimental and may incur an error. Furthermore, a similarity relationship has been assumed between convection on upward inclined hot surfaces and downward inclined cold surfaces. The experimental correlations mentioned presented below are used for the bottom part of the glass (facing the solar still).

$$Nu_L = 0.13((GrPr)^{1/3} - (Ra_c)^{1/3}) + 0.56(Gr_c Pr \cos\beta_g)^{1/4} \qquad (Fuji) \tag{2.76}$$

$$Nu_L = 0.6(GrPr \sin\beta_g)^{1/5} \qquad (Ra < Ra_c) \qquad (Vliet) \tag{2.77}$$

$$Nu_L = 0.3 Ra^{0.24} \qquad (Ra > Ra_c) \qquad (Vliet) \tag{2.78}$$

For both correlations the characteristic length is the glass height. The transition Rayleigh, from laminar to turbulent is given by Vliet,

$$Ra_c = 0.3 \times 10^7 \exp(0.18\beta_g) \qquad (Vliet) \tag{2.79}$$

2.4 Evaporation and Condensation

As mentioned at the beginning of this chapter, besides the energy equation, the conservation of the mass equation is required. It is assumed that the water evaporating from the basin is immediately renewed and thus the seawater mass on the basin remains constant. It is also assumed that the water condensing on the glass is collected immediately.

The evaporation of water and the resulting condensation on the glass cover is the main objective of the solar still. Understanding this fundamental phenomenon allows an improvement in water production.

Water evaporation in the solar still, is not caused by boiling, but by the water vapor pressure/concentration gradient between the water surface, $p_{v,w}/c_{v,w}$, and the enclosure air, $p_{v,a}/c_{v,a}$, inside the solar still. This gradient induces the mass transport of water molecules into the air. According to the Örvös et al. [48], the molecular evaporation rate is given by

$$\dot{N}_{mol} = A_b k_G (p_{v,w} - p_{v,a}) = k_c (c_{v,w} - c_{v,a}) \tag{2.80}$$

where k_G and k_c, are the mass transfer coefficient due to the pressure and molar concentration difference, respectively, and A is the area. By manipulating the equation by changing the concentrations into humidity ratio w and evaporation coefficient σ, it is possible to obtain the evaporated water mass rate,

$$\dot{m}_{evap} = A_b k_c M_{H_2O} (c_{v,w} - c_{v,a}) \frac{\rho_a}{\rho_w} = A_b \sigma (w_w - w_a) \tag{2.81}$$

where,

$$w = \frac{c_v M_{H_2O}}{\rho_a} \tag{2.82}$$

and,

$$\sigma = k_c \rho_a \tag{2.83}$$

Most commonly, w is given as,

$$w = \frac{M_{H_2O}}{M_a} \frac{\varphi p_{v,sat}}{P - p_{v,sat}} \tag{2.84}$$

and from [33],

$$p_{v,sat} = \exp\left(\frac{25.317 - 5144}{T}\right) \tag{2.85}$$

where P is the total air pressure, φ the relative humidity, and subscript sat represents the saturated state for the correspondent temperature.

Applying the Chilton-Colburn analogy, it is possible to obtain σ. For air-water systems, the assumption that the Lewis number is 1 is often made. By applying the similarity between heat transfer and mass transfer it is possible to obtain the evaporated water.

$$J_H = \frac{Nu}{RePr} Pr^z = \frac{Sh}{ReSc} Sc^z = J_M \tag{2.86}$$

Manipulating the equation,

$$\frac{h_c}{k_c \rho c_{p,a}} = \left(\frac{Sc}{Pr}\right)^z = Le^z = 1 \tag{2.87}$$

The heat transfer due to convection, h_c, and the heat capacity of the air, $c_{p,a}$, allows to get,

$$\sigma = \frac{h_c}{c_{p,a}} \tag{2.88}$$

To conclude, for each time step the evaporated mass rate can be computed as,

$$\dot{m}_{evap} = A_b \frac{h_{c,w-a}}{c_{p,a}} (w_w - w_a) \tag{2.89}$$

As mentioned before, the air inside the still is modeled and restrictions on evaporation and condensation are specified. A strict restriction is applied, which does not allow evaporation if the φ reaches

saturation in the time step under consideration.

Condensation is done similarly to evaporation, being the only difference that the mass transfer now is from the moist warm air to the cold glass.

$$\dot{m}_{cond} = A_g \frac{h_{c,a-g}}{c_{p,a}}(w_a - w_g) \tag{2.90}$$

where w_g is computed with 2.84 using glass temperature.

The restriction is set that condensation only occurs when the glass is below the dew point of the air. A study was carried out to verify the effects of all these strict restrictions and is presented in section 3.2.3.

At the end of each time step, it is needed to compute φ, so that the evaporated and condensed water from the following time step can be calculated. First, it is necessary to calculate the sum of the water existing in the air, $m_{v,a_{t-1}}$, with the difference between evaporated and condensed water in that time step, $(\dot{m}_{evap} - \dot{m}_{cond})\Delta t$.

$$m_{v,a} = m_{v,a_{t-1}} + (\dot{m}_{evap} - \dot{m}_{cond})\Delta t \tag{2.91}$$

The vapour pressure is given by,

$$p_{v,a} = \frac{m_{v,a} R T_a}{M_{H_2O} V} \tag{2.92}$$

and finally,

$$\varphi = \frac{p_{v,a}}{p_{v,sat}} \tag{2.93}$$

2.5 Inner Radiation Heat transfer

Radiation heat transfer takes place within the solar still between the water mass with the glass cover and the walls and between the walls and the glass cover.

All the analyzed components were considered as gray surfaces. However, taking into account that the emissivities of these surfaces are close to 1, reflectivity of the radiation is very small and therefore negligible. This said, the reflection of radiation between surfaces was not considered. With these simplified considerations, instead of applying the original radiosity equations [43, 45], the radiative heat exchange between all surfaces was rather calculated with the reasoning presented below.

Since all components are modeled, it is important to determine the appropriate view factors (F_{1-2}) to obtain an accurate simulation. The subscript indices 1 and 2 represent the considered surfaces. The radiation heat transfer coefficient is computed as,

$$h_{r,1-2} = \epsilon \sigma (T_1^2 + T_2^2)(T_1 + T_2) \tag{2.94}$$

where σ represents the Stefan–Boltzmann constant and ϵ the effective emissivity between surfaces.

$$\epsilon = \left(\frac{1}{\epsilon_1} + \frac{1}{\epsilon_2} - 1 \right)^{-1} \tag{2.95}$$

It is important to stress the necessity to choose the appropriate view factors between surfaces, so that the correct heat exchanged by radiation is computed.

$$Q_{r,1-2} = h_{r,1-2} A_1 (T_1 - T_2) F_{1-2} \tag{2.96}$$

2.6 Heat Losses

The glass cover, walls, and basin are sources of heat loss. Usually, the walls and the basin of the solar still are well insulated and have low heat losses. Glass heat losses are caused by radiation exchange with the environment and by external convection because of the wind over the glass.

Radiation lost by the glass to the environment is given by the known radiation exchange formula in Eq. 2.94, more specifically,

$$h_{r,g-sky} = \epsilon\sigma(T_g^2 + T_{sky}^2)(T_g + T_{sky}) \tag{2.97}$$

The sky temperature, which accounts for a nonuniform temperature of the atmosphere and the radiation exchange only in certain wavelength ranges [5, 11], can be calculated with the following equation,

$$T_{sky} = 0.0552 T_{out}^{1.5} \tag{2.98}$$

One of the most used correlation for external losses because of the wind, is given by Watmuff and Charters [49],

$$h_{c,g-out} = 2.8 + 3v \qquad (0 < v < 7m/s) \tag{2.99}$$

Performing an analogy between heat transfer and electric current, basin and walls lose heat due to thermal conduction through the insulating material and external convection. The overall heat transfer coefficient can be computed as follows,

$$U = \left(\frac{L_i}{K_i} + \frac{1}{h_{c,g-out}} \right)^{-1} \tag{2.100}$$

where, L_i represents the insulation thickness, and K_i its thermal conductivity.

Chapter 3

Implementation of the Thermal Model

During the development of the thermal model, numerous literature references, various restrictions and approaches, as well as the other existing thermal models were taken into account. The model presented in Chapter 2 includes several parameters and assumptions that are going to be analyzed. It will be followed by an evaluation of these parameters impact on the prediction of the overall performance of the solar still. Moreover, the proposed model will be applied to experiments in the literature and comparisons will be made between the thermal model, Dunkle's model (see section 1.2.3), and experimental data from the literature.

3.1 Overview of Thermal Model Outputs

For each time step, the model calculates the temperatures of basins, walls, air, water and glass as well as the water yield, as described in the previous chapter. The temperatures and the cumulative water are computed and plotted, for the experimental work carried out by Kabeel et al. [22]. The experimental data can be compared (dashed line) with the theoretical estimate (thick line), shown in Fig. 3.1.

The simulation follows the physical evolution of the different parameters evaluated with an accuracy considered reasonable. Larger discrepancies are found between the estimated and the experimental glass temperature. This is due to the fact that in the experiments the thermocouple is normally located on the outside of the glass and is therefore influenced by the external conditions. Nevertheless, the water temperature, which is considered the most reliable measured temperature, presents acceptable deviations.

Other relevant information can be obtained for further analysis, such as the basin area exposed to solar radiation (calculation is explained in detail in subsection 2.1.2) and the evaporation/condensation rate over the day, as shown in Fig. 3.2. Understanding these parameters will later allow to optimize the solar still and improve the water production.

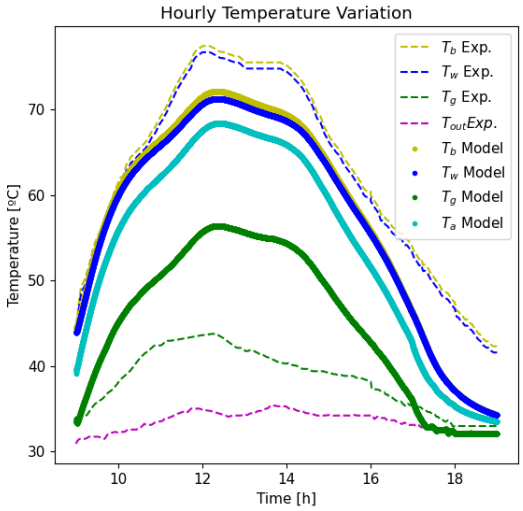

(a) Hourly temperature variation for the proposed model, as well as the experimental data

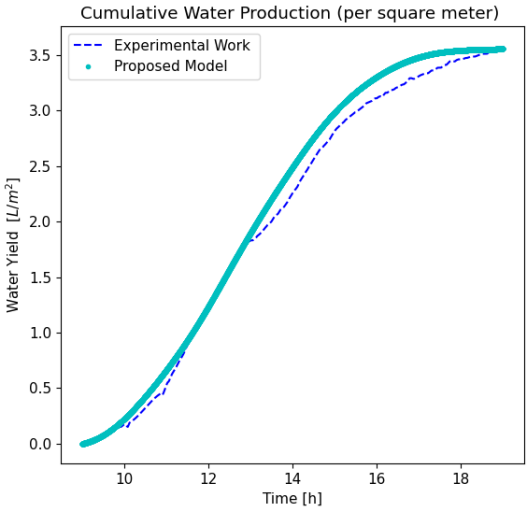

(b) Cumulative water yield for the proposed model, as well as the experimental data

Figure 3.1: Main outputs of the thermal model applied to the data from the experiment carried out by Kabeel [22]

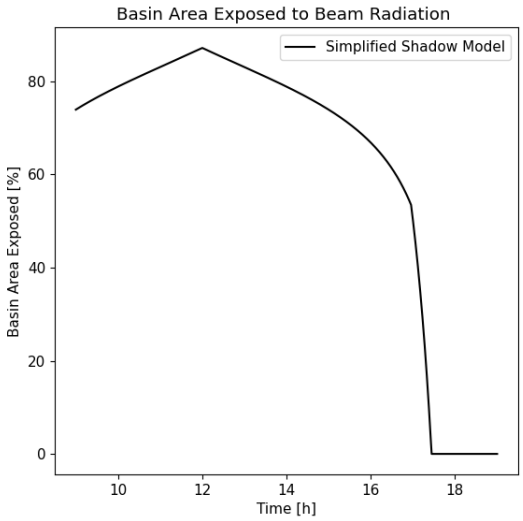

(a) Exposed basin area to direct beam radiation, computed by the proposed thermal model

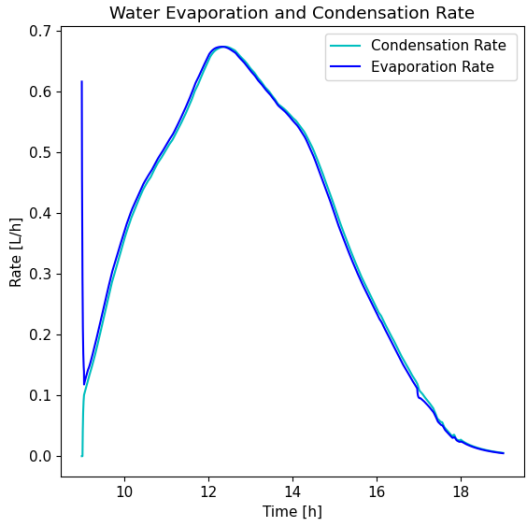

(b) Evaporation and condensation rate, computed by the proposed thermal model

Figure 3.2: Additional outputs of the thermal model applied to the data from the experiment carried out by Kabeel et al. [22]

3.2 Verification and Validation of the Thermal model

Verification has been described by Roache [50] as ”solving the equations right”.A well-performed verification allows the thermal model to solve the required equations, and the simulation routine to be completed and converge. The model may not follow the experimental results well due to the correlations used or the constants/assumptions chosen, which are analyzed in the validation.

Validation aims to determine *"the degree to which a model (and its associated data) is an accurate representation of the real world"*. In other words, quantify the uncertainty of the thermal model assumptions. A well performed validation allows the thermal model to follow with precision the evolution of the real system, in this case the water yield and temperatures of basin, water and glass.

The data from the experimental work conducted by Kabeel et al. [22] is used to perform the verification and validation procedure. The data used from this experiment are listed in Appendix A.0.1.

3.2.1 Time Step

It is very important to choose the appropriate time step for the simulation. If it is set too large, the simulation will destabilize and diverge, however, if it is set too small, it will be time-consuming. It is also important to point out that there are errors due to the time discretization, strict restrictions, and approximations made over each time step. A study of the experimental data has been carried out, where 0.5s is the smallest time step used and 13s is the largest time step since a larger time step led the simulation not to be completed.

Figure 3.3 presents the absolute water yield deviation between the water yield for 0.5s and for increasingly larger time steps. It is possible to infer that for these time steps, the deviation is very small, around 0.5%, meaning that the thermal model converges. The time step was chosen to be 5s to ensure the reliability of the results and to reduce the simulation time.

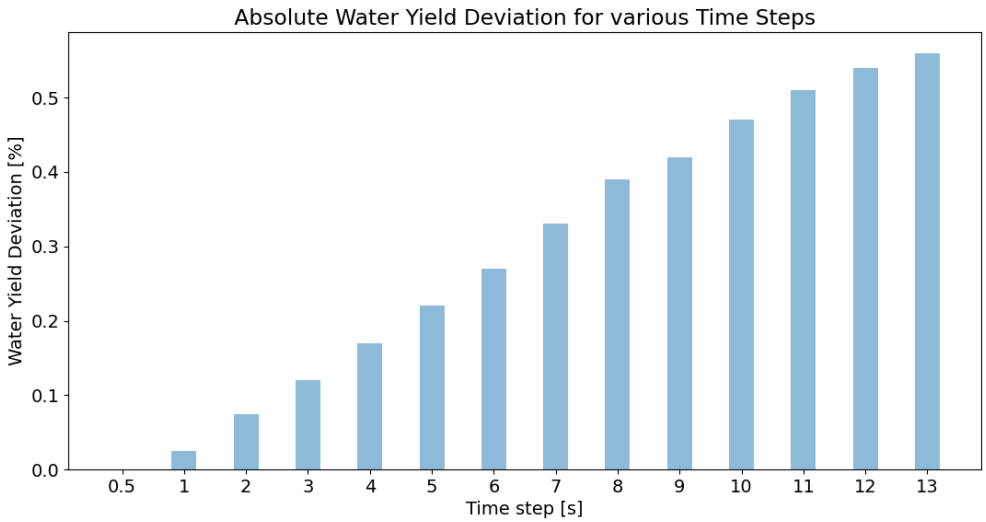

Figure 3.3: Absolute water yield deviation for different time steps. The reference case has a time step of 0.5s .

3.2.2 Materials Radiative Properties

As explained in Chapter 2, the radiative properties for the glass, water, basin, and walls are of great importance for the execution of the thermal model. Some values, such as basin/walls normal absorption

and radiative properties of the water, were attributed. Thus, it will be analyzed their impact on the overall yield. Moreover, two different approaches were used for the glass transmissivity and the absorption of basin and walls. The effect of setting transmissivity and absorption constant for the entire simulation or being incidence angle-dependent is studied, and it will be emphasized the importance of considering these parameters angle dependent.

Starting with an investigation of τ_g and $\alpha_{b/w}$ independent of incidence angle of beam radiation. As mentioned in subsection 2.2.2, the first approach assumed for the glass a constant value of $\tau_g = 0.85$ and $\alpha_g = 0.07$. It will be analyzed the impact of varying the absorption for a fixed $\tau_g = 0.85$, shown in Fig. 3.4, and varying the transmittance for constant $\alpha_g = 0.07$, shown in Fig. 3.5.

The value of τ_g was chosen accordingly to an average solar altitude of the experiment work day, and the α_g is a commonly used value for glass. It can be seen in Fig. 3.4 that α_g has little effect on the solar still performance. In contrast, the τ_g has a major influence in the water yield, as shown in Fig. 3.5 and evaluated in Table 3.1.

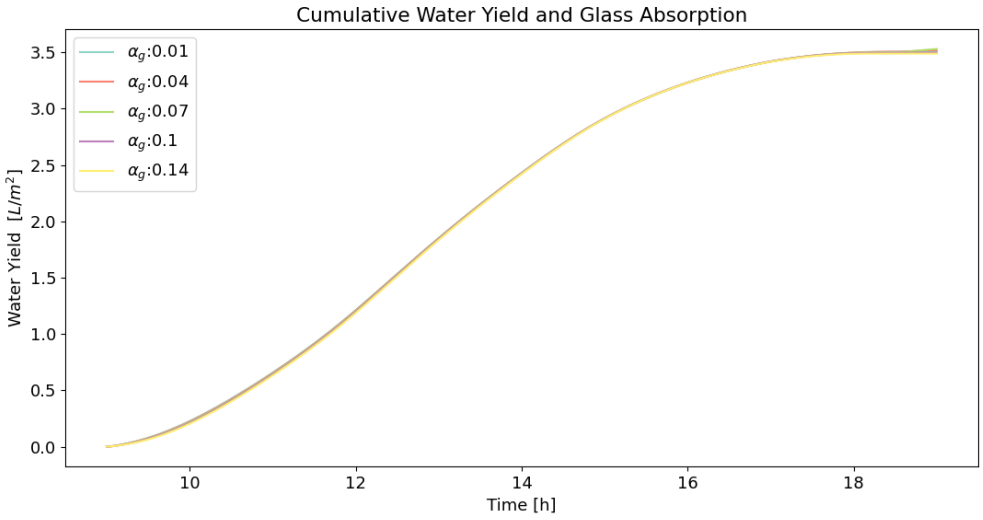

Figure 3.4: Sensitive analysis to α_g for fixed value of τ_g

τ_g	-5,9%	-2,9%	+2,9%	+5,9%
Water Yield Deviation	-5,9%	-2,9%	+2,9%	+5,9%

Table 3.1: Sensitive analysis to τ_g. Reference values are $\tau_g = 0.85$ and $Water\ Yield = 3.55\ L/m^2$.

To analyze the impact of taking a constant α_b throughout the day (α_b independent of solar radiation incidence angle) into account, the α_n (in Eq. 2.42) is varied. It was assumed in subsection 2.2.2, $\alpha_n = 95\%$ for the basin and the walls . The α was varied, however, the assumed average solar altitude of 65° was kept the same when applied Eq. 2.42. In Fig. 3.6 is presented the impact of varying α_n. The water yield is sensitive to α_n, which can be observed in Table 3.6. Varying this parameter has a bigger impact than the glass transmissivity because, it is affecting basin and wall solar radiation absorption.

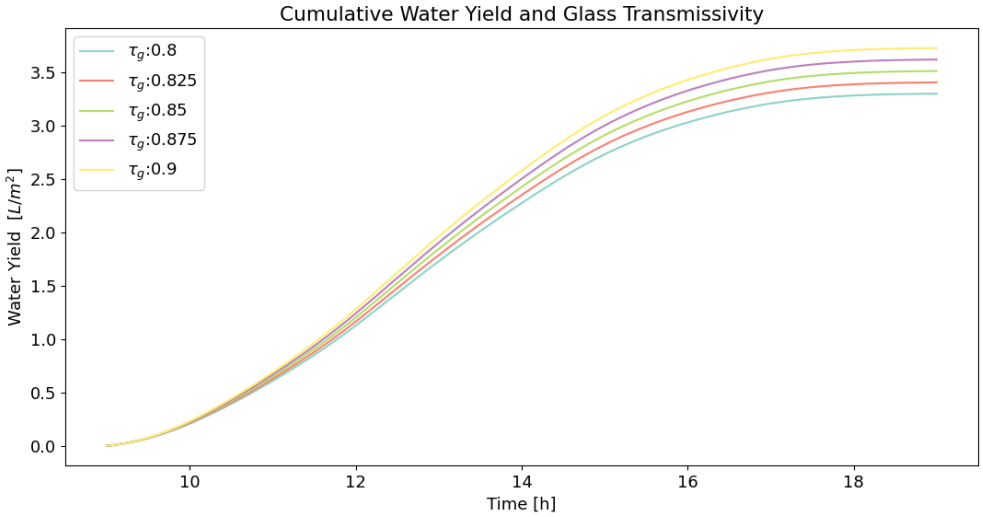

Figure 3.5: Sensitive analysis for different constant values of τ_g

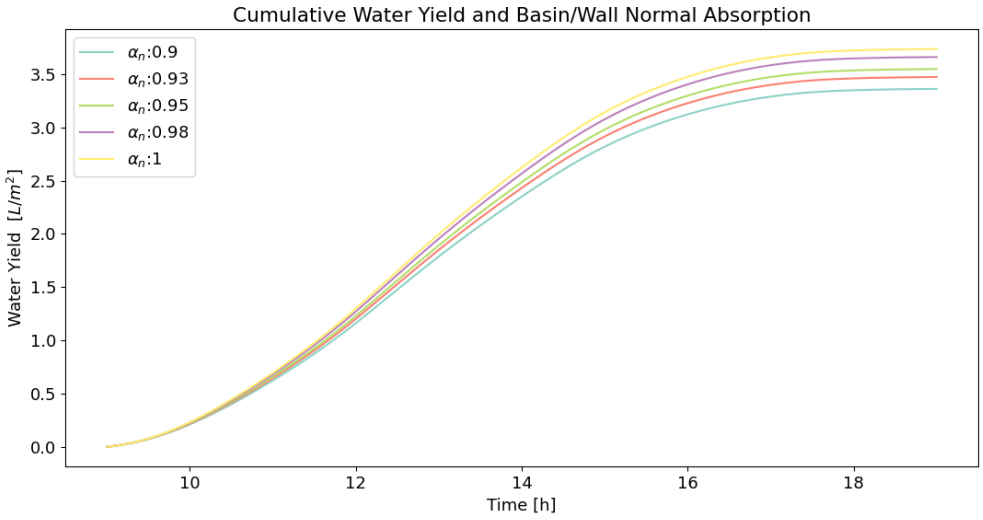

Figure 3.6: Sensitive analysis to $(\alpha)_n$

α_n	-1,4%	-0,6%	+0,8%	+1,4%
Water Yield Deviation	-5,3%	-2,1%	+3,1%	+5,3%

Table 3.2: Sensitive analysis to α_n. Reference values are $\alpha_n = 0.95$ and $Water\ Yield = 3.55\ L/m^2$.

With these studies it is highlighted that the choice of glass transmissivity and basin/walls absorption are relevant for the thermal model implementation. Reasonable values were chosen for the glass transmissivity and basin absorption, taking into account the day and the materials used in the experiment and thus the theoretical water yield is close to the experimental one. However, if a simulation for a whole year is desired, it is not practical to evaluate how these parameters vary for each day. Moreover, these parameters are not constant over a day. It is therefore important to perform a detailed angle-dependent

analysis, which is more appropriate than assuming constant parameters.

On the second approach, the radiative properties stated in Chapter 2 are incident angle-dependent. To compute glass transmissivity and basin absorption, Eq. 2.40 and 2.42 were used, respectively. Figure 3.7 shows how these properties vary throughout the day. In this case it can be observed that over a long period of time the absorption and transmissivity remain more or less constant. However, at the end of the day, absorption and transmissivity decrease due to the sun movement, resulting in more reflection for both surfaces. For this reason, angle-dependent properties are more suitable to use.

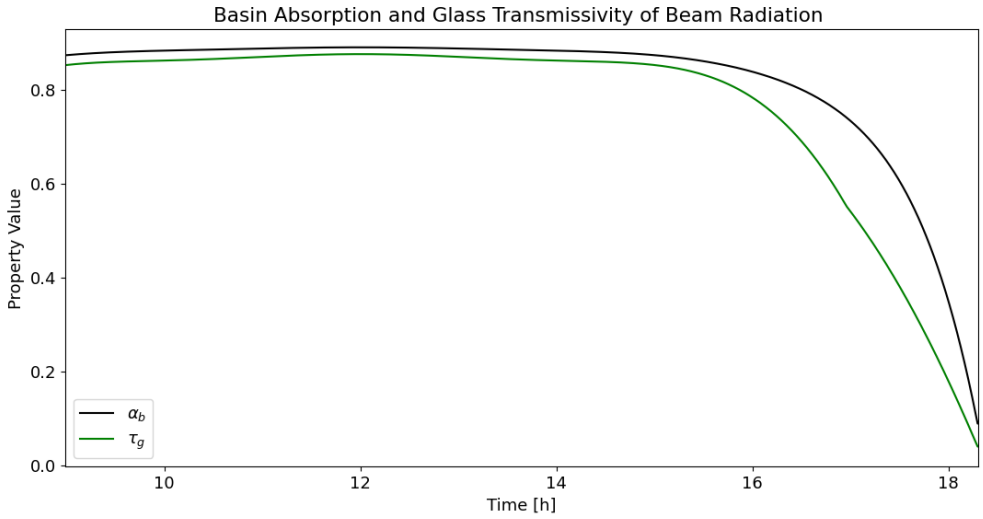

Figure 3.7: Analysis of α_b and τ_g of beam radiation throughout the day

Lastly, a study of water transmissivity, for an acceptable range of values, was also carried out. Table 3.3 shows the results of the sensitivity analysis for the transmissivity of water, with varying absorption and constant reflectivity (following Eq. 2.39). As it can be stated the effect of varying the absorption and transmissivity as almost no influence on the water yield.

τ_w	-5,2%	-2,6%	+2,6%	+5,2%
Water Yield Deviation	$\approx 0\%$	$\approx 0\%$	$\approx 0\%$	$\approx 0\%$

Table 3.3: Sensitive analysis to τ_w, with α_w varying and $\rho_w = 2\%$. Reference values are $\tau_w = 0.95$ and $Water\ Yield = 3.55\ L/m^2$.

In summary, it can be evidenced that properties, such as the transmissivity of glass and water, have a direct impact on the solar radiation reaching the basin and/or the walls, which influences the water yield prediction. Even though, reasonable and conservative values for the materials' radiative properties were chosen for the first approach (constant radiative properties), the study emphasized that some of these values are sensitive and that they must be computed as close to reality as possible. The angle-dependent approach was chosen for both τ_g and α_b since it is considered more realistic, and when applied for a whole year simulation values are automatically computed according to sun's position and do not have to be set manually for each specific day. Only the water radiative properties were considered

to be constant. With this analysis, it was possible to quantify the influence of the assumed radiation parameters on the prediction of the water yield.

3.2.3 Air model

As described in the previous chapter, to model the air inside the solar still several constraints were assumed. The following properties, which are represented in Table 3.4, are evaluated:

1. Use of stationary or transient equation for the air energy balance;
2. Restrictions regarding evaporation and condensation, which are relative humidity dependent;
3. Model evaporation and condensation heat included in the basin and glass energy balances equation respectively, or in the air energy balance.

For the first study (Option 1) it is found that the use of a stationary or transient equation for air gives the same results. Air has a very low thermal inertia, so it is not necessary to use a transient energy balance for air.

For the second study (Option 2), the restrictions on evaporation and condensation are removed, however, the relative humidity was still calculated for each time step. In the model, evaporation is allowed only until the air is saturated, while condensation occurs only when the glass temperature is below the dew point temperature of the air. Removing the restrictions does not affect the predicted yield. Since evaporation is controlled by Eq. 2.90, which depends on the relative humidity of the air, and the air is close to saturation, evaporation can only take place if the air is dehumidified by condensation. As presented in Fig. 3.2, evaporation is restricted by condensation rate.

The last study (Option 3) examined whether the heat involved in condensation and evaporation could be modeled in the air heat balance instead of the heat balance equations for glass and water. This led to a large deviation in the prediction of the water yield. Due to the low thermal inertia of air, heat gains and losses cause large deviations in the air temperature at each time step.

	Option 1	Option 2	Option 3
Water Yield Deviation	$\approx 0\%$	$\approx 0\%$	+203%

Table 3.4: Water yield deviation according to the studied option (enumerated at the beginning of section 3.2.3).

3.2.4 Modeling lateral walls

The thermal model presented differs from others because all components are modeled. In this section, how walls were modeled is analyzed, and its important role in the solar still performance is evaluated. Commonly, these surfaces are painted black to absorb the incident radiation, to limit condensation on the walls and to increase the air temperature. Two options for modeling the walls are given and compared:

1. All walls are modeled in detail. Each one with the corresponding energy balance equation, including its specific convection heat transfer coefficient, the absorption of incident radiation and heat loss.

2. All walls are modeled, however, no incident radiation is considered, neither beam nor diffuse radiation. Lateral walls interact with air and are a source of heat loss by conduction.

From Fig. 3.8 it can be concluded that an incorrect characterization of the variables acting in the walls (Option 2) leads to a significant deviation in the water yield prediction. Walls are not exclusively a source of heat loss and affect the performance of the solar still.

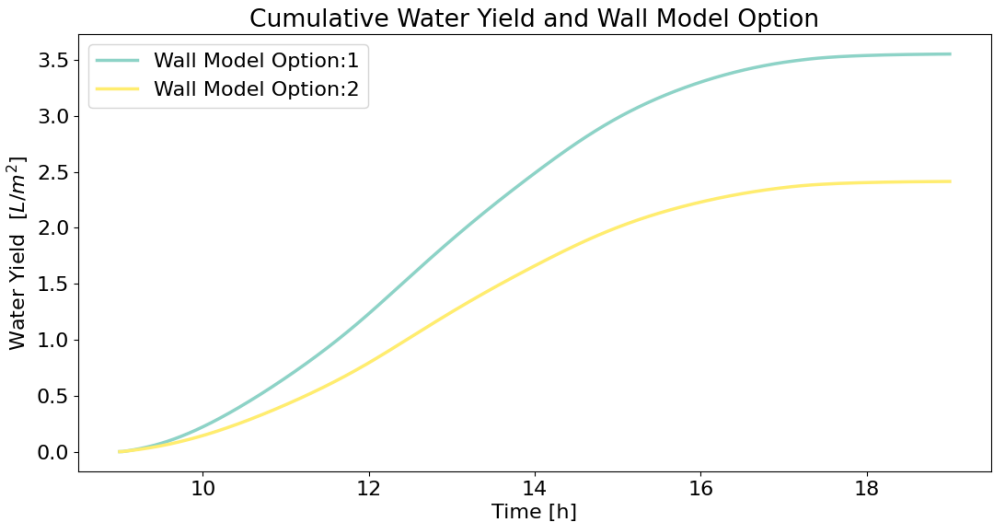

Figure 3.8: Analysis to wall model option effect on cumulative yield prediction. Option 1 - Walls absorb solar radiation; Option 2 - Walls do not absorb solar radiation

3.2.5 Glass Heat Losses

The glass cover loses heat to the outside by convection and radiation heat transfer. An analysis is done on the computation of the sky temperature and heat losses. In the literature, it is possible to find two main correlations for the sky temperature to compute radiation heat transfer.

One correlation is represented in Eq. 2.98 and the other is,

$$T_{sky} = T_{air} - 6 \tag{3.1}$$

In Wafmuf's report [49] it is possible to find two correlations for the cover heat losses. One correlation, which is the one used (Eq. 2.99, only calculates the convection heat transfer, needing therefore an additional equation for radiation heat transfer. The other correlation calculates both convection and radiation heat transfer together,

$$h_{wind} = 5.7 + 3.8 * v \qquad (0 < v < 5m/s) \tag{3.2}$$

Both changes had a similar water yield prediction with a minimal deviation of less than 1%.

3.2.6 Shadow Model

This analysis covers the importance of correcting the incident solar radiation absorbed by the basin. Using the correct incident solar radiation is very important since it is the water production cycle enhancer. Considering more radiation than it is will overestimate water yield, and considering less will underestimate it. Even though a simplified shadow model is computed, it allows the thermal model to follow the thermophysical processes inside the solar still with greater accuracy.

In Fig. 3.9, it can be examined the effect of using the shadow model (Option 1) and not using it (Option 2). As can be analyzed, the non-consideration of the shadow model leads to an overestimation of the water yield of about 30%, thus reinforcing the need to consider a shadow model.

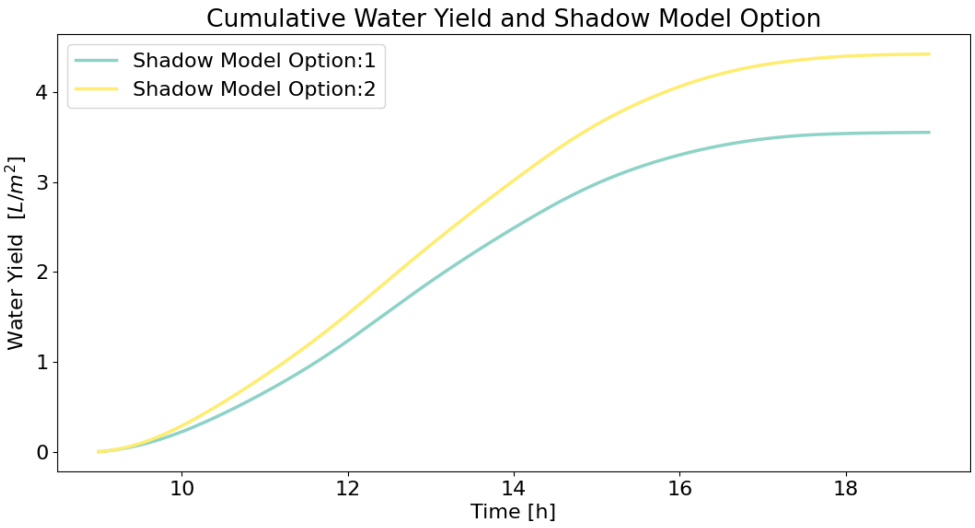

Figure 3.9: Analysis to shadow model option effect on cumulative yield prediction. Option 1 - Shadows are considered; Option 2 - Shadows are not considered

3.2.7 Heat Convection Coefficient

As already mentioned, this thermal model performs a heat balance for each modeled component. The most uncertain heat transfer coefficient correlation used is that of the glass cover.

In this section, two of the most frequently cited correlations in the literature, Vliet's (Eq. 2.77 and 2.78) and Fuji's (Eq. 2.76), are analyzed. Fig. 3.10 presents the error in water yield by using both correlations not only for the experiment analyzed so far but also for other experiments with single basin and slope solar stills (an experiment carried out by Omara [14] and two experiments performed by Kabeel [25], data in Appendix A). Implementing the thermal model in more experiments allows for a more robust verification.

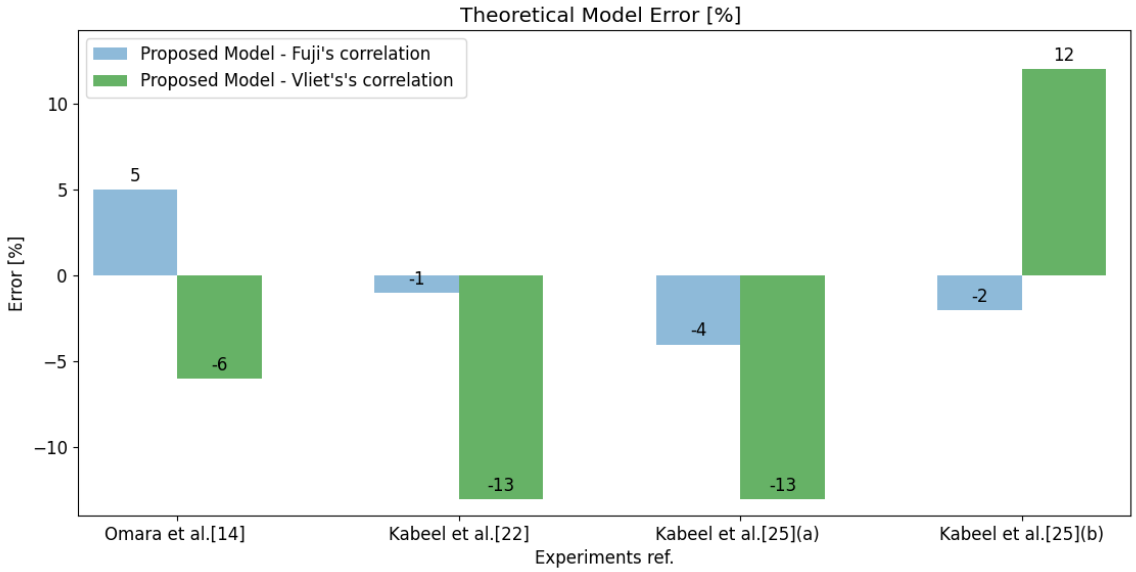

Figure 3.10: Theoretical error for various experiments, using Vliet and Fuji convection coefficient correlations for the glass cover

The overall results of all investigated experiments show that Fuji's correlation fits better by presenting the minor deviation from the experimental results. It should be noted that the temperatures simulated with Fuji also fit better than when using Vliet's correlation, which overestimates the temperatures. This said, it was assumed Fuji's correlation in this thermal model.

It is important to highlight that, for a specific solar still geometry, one could accurately obtain a heat convection correlation through a set of detailed Computational Fluid Dynamic (CFD) simulations. However, this would involve a non-negligible additional effort, which is outside the scope of the present work but could be useful to take up in a future study.

3.2.8 Insulation Thermal Conductivity

The choice of the correct input parameters is important because it has a direct effect on the results obtained. In this study, the thermal conductivity of the insulation was varied to observe its influence.

Insulation materials have tabled properties which may vary between a range of values because real materials have imperfections. In this particular case, the material use is sawdust, which is said to have a thermal conductivity of about $K_i = 0.08\ W/(mK)$.

In Table 3.5 the deviation of the water yield is analyzed as a function of the variation in thermal conductivity. As can be observed, the thermal conductivity can influence slightly the water yield. A study must be carried out in the range of thermal conductivity values for each experiment, to understand its impact on the overall water yield. In this work, an average value of the thermal conductivity is given to the experiments simulated.

K_i	-19%	-6%	6%	+19%
Water Yield Deviation	-3,4%	-1,8%	+1,8%	+3,4%

Table 3.5: Sensitive analysis to the thermal conductivity of the insulation and its effect on the prediction of the water yield. Reference value $K_i = 0.08\ W/(m)K$

3.3 Comparing with Dunkle's model

3.3.1 Dunkle's Model Refined

In Chapter 1 it was mentioned that the model most frequently used in the literature is Dunkle's model. In his work, Dunkle states that of the incident radiation, around 80% is absorbed by the basin, for usual used materials and exterior conditions. This model was thought to be used in a double slope type solar still, so it is not suitable to be used in a conventional single slope still. Moreover, there is no mention of how to determine the incident solar radiation on the basin if the total horizontal solar radiation is used or if a shadow model is needed.

Fig. 3.11 presents the Dunkle's model when implemented without any refinement. The mentioned radiation properties are used, and no pre-processing of solar radiation data or shadow model is considered. To perform the simulation, energy balances from Eq.1.1, 1.2 and 1.3 are solved for each time step, with the heat transfer coefficients from Eq.1.4 and 1.5. Dunkle does not consider walls, thus the heat loss of the walls to the outside is not considered.

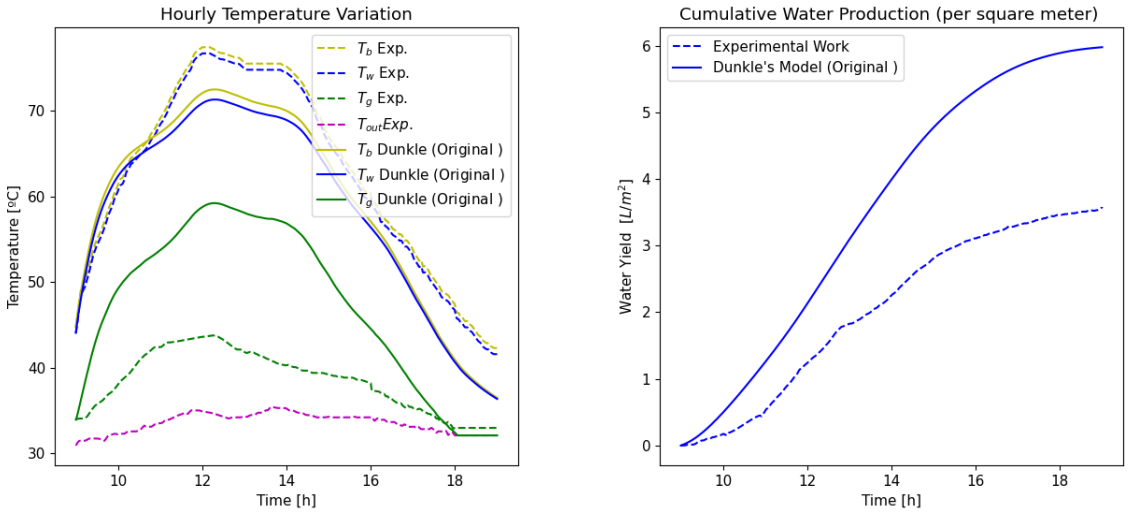

(a) Hourly temperature variation for the original Dunkle's model, as well as the experimental data

(b) Cumulative water yield for the original Dunkle's model, as well as the experimental data

Figure 3.11: Original Dunkle's model, without refinement, simulation results and comparison with experimental data from Kabeel et al. [22]

It can be observed in Fig. 3.11 that the theoretical water temperature follows reasonably well the experimental one, which, as said, is the most reliable temperature. However, the water yield shows a large deviation, which shows that a refinement is necessary.

Fig. 3.12 shows the refined Dunkle's model (thin line) with corrected solar radiation (includes radiation divided into beam and diffuse, and shadow model) and materials radiative properties, the proposed thermal model (thick line), and experimental results (dashed line). From this it can be inferred that Dunkle's model cannot follow as well the water and basin temperatures, however, presents the water yield with a smaller error than in Fig. 3.11. As can be seen, Dunkle's model can better follow the water yield output if the above changes are implemented.

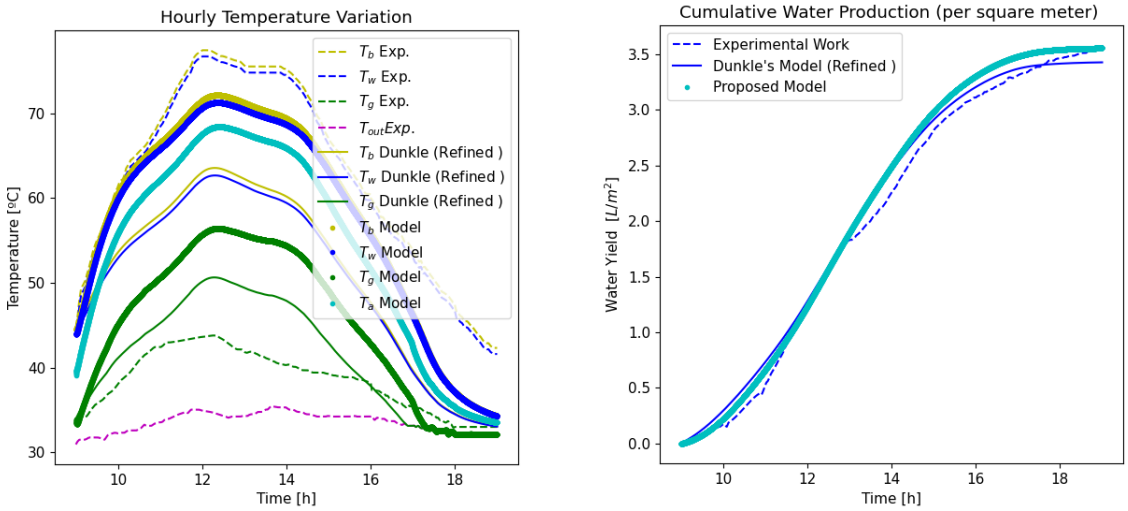

(a) Hourly temperature variation for the proposed and Dunkle's model, as well as the experimental data

(b) Cumulative water yield for the proposed and Dunkle's model, as well as the experimental data

Figure 3.12: Proposed thermal model and Dunkle's model,with refinement, simulation results and comparison with experimental data from Kabeel et al. [22].

3.3.2 Proposed Model and Dunke's Model Comparison

The models are implemented in four different experiments (data in the Appendix A) using the conventional single slope and a single basin solar still. Different locations, days, environmental conditions and solar still structures were investigated.

Experiments performed by Kabeel et al. [22] and Omara et al. [14], were done in the same location one year apart with the same solar still. The environmental conditions are slightly different, thus the water outcome is different.

Experiments conducted by Kabeel and Abdelgaied [25] (a and b) were executed with the same solar still in the same location, one month apart (June and July). Both have a similar incident solar radiation and outdoor temperature. In July, the sun altitude is higher, which leads to a larger exposed area because the shadows are smaller. Consequently, there is an increase in water production, which was achieved in the experiment and predicted by the proposed model.

The proposed thermal model is also applied to the other two designs: a conventional solar still with all walls made of glass with a sand reservoir under the basin (Fig. 1.10) carried out by Tabrizi et al. [24], and a double slope single basin solar still conducted by Elango et al. [23] (Fig. 1.9).

The use of Dunkle's model in Tabrizi et al. solar still is rather wrong, because the model was designed for a solar still influenced by horizontally disposed parallel surfaces. Being the lower one hot and the upper one cold, and neglecting the effect of the walls. In this particular still, vertical walls have an influence on the processes of heat and mass transfer that occur inside the still. Condensation takes place not only on the upper glass, as usual, but also on the vertical glass walls. Therefore, Dunkle's model was not used to simulate this experiment. The proposed model can predict the performance of this experiment by making small changes to the energy balance equations (data and equations in the Appendix A.0.4), since all components are modeled. On the double slope solar still both proposed and Dunkle's model, which was thought for these structures, can be used.

Looking at the results in Fig. 3.13, the refined Dunkle's model and the proposed thermal model present an acceptable small deviation from the experimental result. The proposed model is more complex since it takes into account all the different still components, however, it shows accuracy and precision in predicting the water produced. Moreover, it can follow quite well the water temperature, which is the most reliable temperature measured, in comparison with Dunkle's model (see e.g. Fig. 3.12).

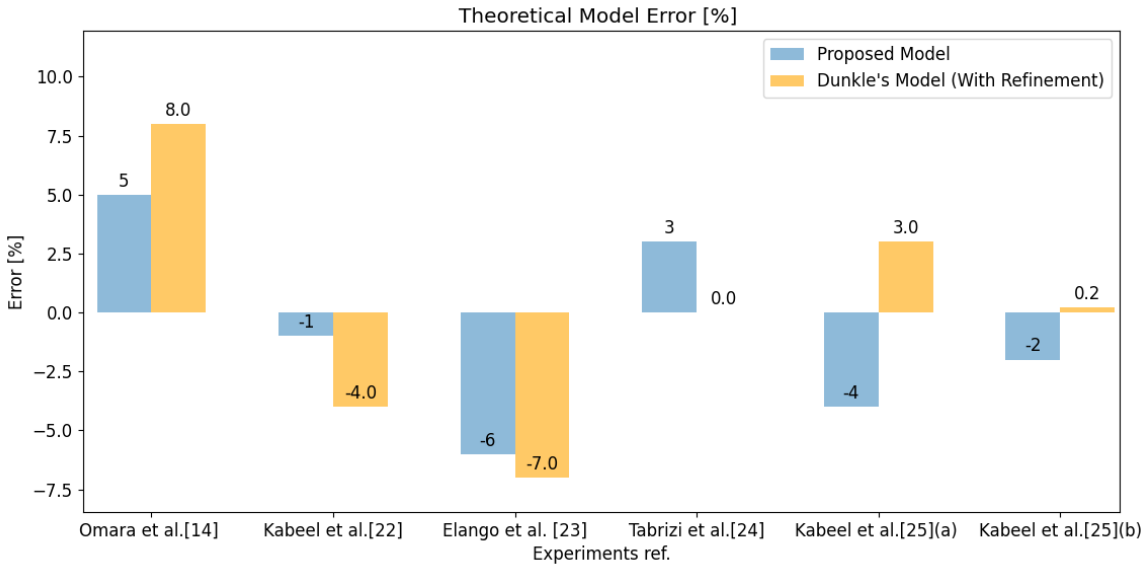

Figure 3.13: Water yield error in various experiments using the proposed thermal model and Dunkle's model with refinement. The experiment carried out by Tabrizi et al. [24] was not analyzed with Dunkle's model.

Chapter 4

Performance Improvement of the Solar Still

The following chapter contains a parametric study using the experimental data from Kabeel et al. [22]. Based on the parametric study, practical solutions are presented that can be implemented in the solar still to enhance water productivity. It is important to point out that even though this was the experiment chosen, an analysis must be carried out for the solar still structure and location chosen. No ambient conditions and solar still structures are the same, therefore an analysis should be done to ensure maximum yearly water production.

4.1 Parametric Study

To achieve the maximum water yield, a parametric study is carried out to characterize the variables that can optimize the solar still. All studies made in the following subsections examine the improvement or deterioration of the water production predicted. As a reference value, it is used the computed theoretical water yield for the experiment, which is $3.55\ L/m^2$. Some subsections provide the deviation of the water yield for a representative winter day (data in Appendix A.6) where the thermal model predicted $0.6\ L/m^2$.

The following parameters are going to be analyzed:(1) Scaling; (2) Increase of incident solar radiation; (3) Water depth; (4) Thermal inertia of basin/glass; (5) Insulation ; (6) Water renewal ; (7) Basin-glass temperature difference and its impact on condensation.

4.1.1 Scaling

It is important for the constructor to know the influence of scaling the solar still. Since the glass angle should correspond to the latitude of the location so that maximum incident radiation reaches the basin all year round, the most appropriate scaling option is to increase the length (C) of the solar still. If the width (L) of the solar still were to be increased, the cover glass would have to have a larger width as well, which is not a practical construction solution. This because it would be a very Walls and glass

height are kept the same.

Scaling the solar still has the advantage of minimizing wall shadowing on the basin, thus increasing incident solar radiation. As can be seen from Fig. 4.1 lower solar still lengths mean a decrease in water production, since the area exposed to radiation decreases. In the summer day, increasing the solar still length has little impact in increasing water production because the area exposed is already close to the maximum, shown in Fig. 2.9. The representative winter day benefits more from an increase in the length of the basin since the ratio between the exposed area and the shaded area increases much more than on a summer day.

Increasing the solar length by more than 20 m has a small effect on water production. This is because from this length on, the ratio between the exposed area and the shaded area does not vary significantly. Although the absorbed solar radiation increases due to a larger basin area, the size of the walls also increases, which increases heat losses.

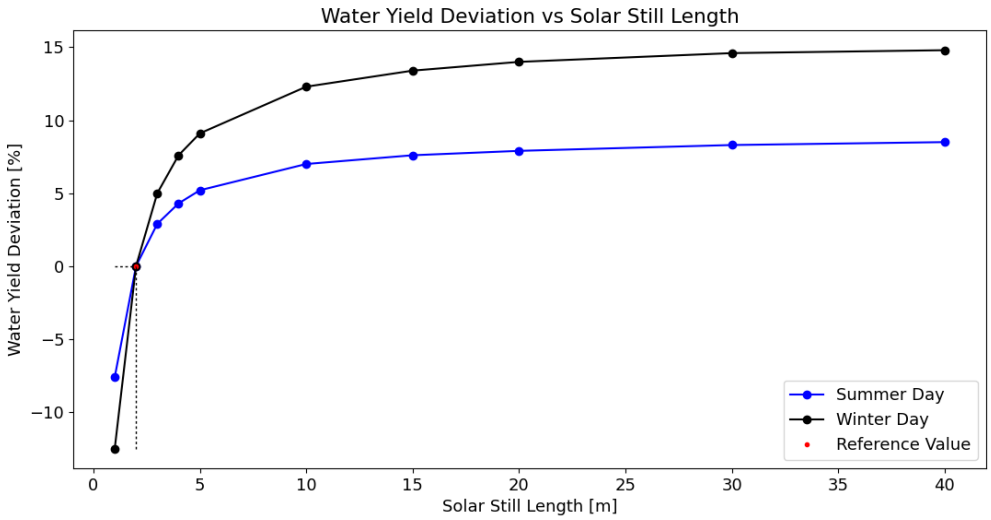

Figure 4.1: Water yield deviation as function of scaling the solar still, more specifically by changing the still length.

It is possible to conclude with this study that the construction of a larger solar still is preferred to various smaller devices, since water productivity increases.

4.1.2 Incident Radiation

An analysis is done on the incident radiation to determine the effect that it has on the performance of the solar still. If the solar radiation intensity is increased, the water yield logically also increases. It is shown in Fig. 4.2, that augmenting solar radiation by 65% leads to an almost 85 % enhancement of water yield. It was chosen not to further increase solar radiation because the water temperature would surpass 100^{o}C. This situation needs a new set of equations to model boiling, which were not taken into account in this model.

There are various options to increase the incident radiation, use of internal and/or external reflectors

[44] or a Fresnel lens [13]. It is also important to study the effect of increasing the area exposed to the sun by reducing shadows. This can be done by changing the structure of the still structure, for example by reducing the height of the walls. Another alternative to increase the absorption of radiation is by using a porous medium, as reported in the literature [28, 51], and further discussed in section 4.2.5.

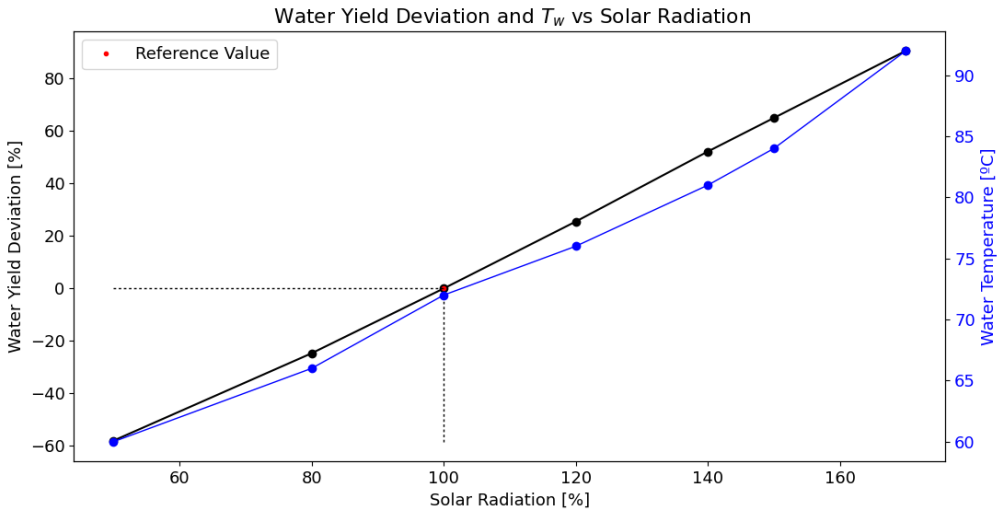

Figure 4.2: Water yield deviation and T_w as function of solar radiation input (100% represents the solar radiation data of the day considered).

4.1.3 Water Depth

One of the most studied parameters in the literature is water depth, which is related to the amount of water mass inside the still. In Fig. 4.3 it is presented a sensitive analysis to the water depth.

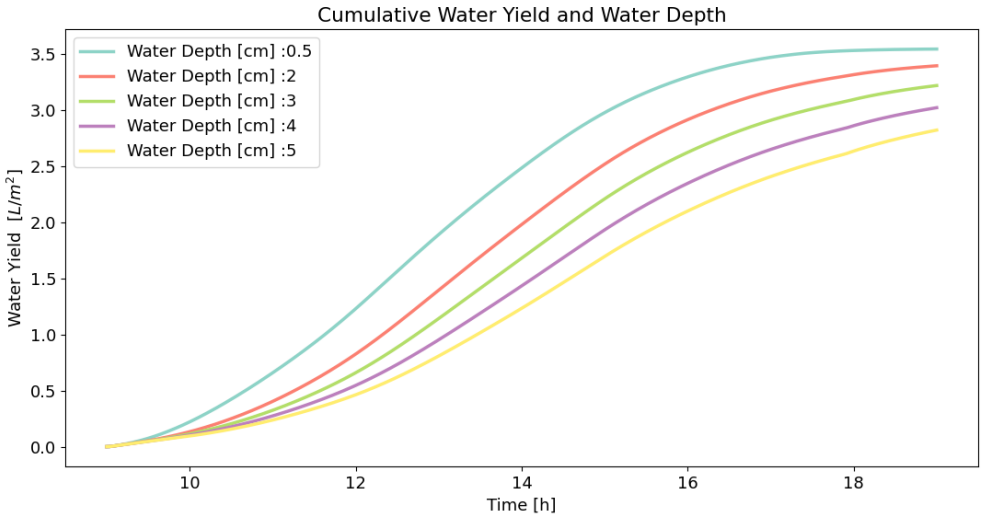

Figure 4.3: Sensitive analysis to water yield as function of water depth.

Water depth and therefore the amount of water in the solar still, has a great influence on the performance of the solar still. Less water mass and thus less thermal inertia means that the water temperature can be further increased, enhancing heat and mass transfer within the solar still.

From Fig. 4.3 it can be observed that the water yield becomes significantly lower with increasing depth. Minimum water depth is preferred in order to achieve maximum solar still performance (in this experiment, water depth was of 5 mm). For construction purposes, it may be complicated to maintain a very small water depth, thus some solutions will be later shown to increase water yield when larger water quantities are used (see sections 4.2.4 and 4.2.5).

4.1.4 Glass and Basin Thermal Inertia

Increasing thermal inertia by using materials with higher specific heat capacity or mass leads to a natural decrease in the solar still performance. This is because the bodies need more heat or time to react under the same irradiation conditions. The parameters chosen to be modified were the basin and glass thickness.

It can be seen in Fig. 4.4 that actually, both basin and glass presented almost no or little deviations in the water yield. The glass thickness parameter seemed to have no influence on the solar still yield.

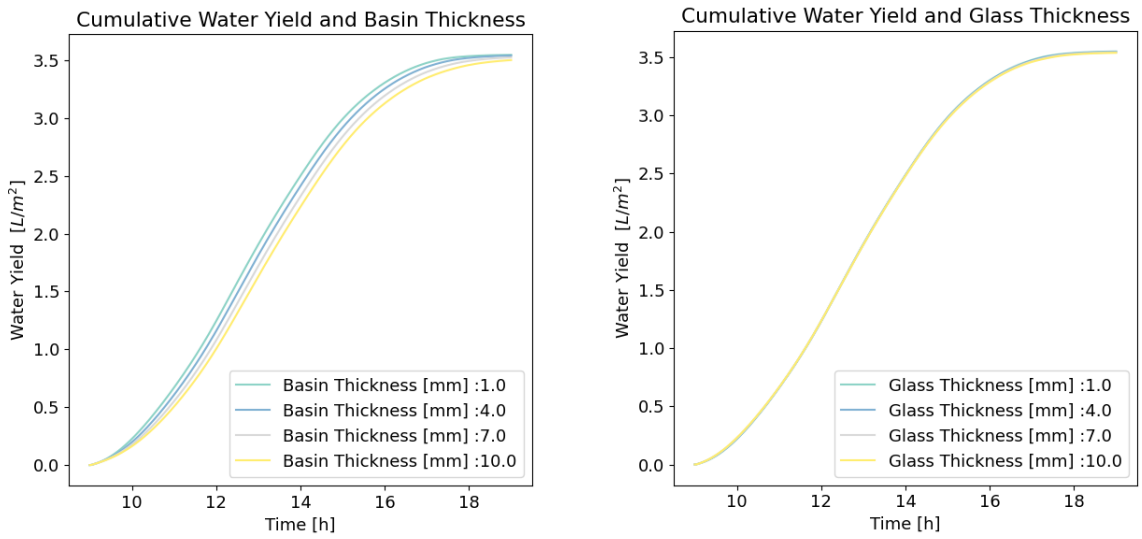

(a) Sensitive analysis to basin thickness (in mm)

(b) Sensitive analysis to glass thickness (in mm)

Figure 4.4: Sensitive analysis to thermal inertia of basin and glass.

Regarding the study of glass thickness, it should be mentioned that the values of transmissivity for the different thicknesses was kept the same, and only the thermal inertia effect was studied. However, with increasing glass thickness, transmissivity decreases. It should also be noted to the constructor that using a glass with a very small thickness to increase transmissivity, can turn this component into a fragile part of the system.

4.1.5 Basin and Walls Insulation

Insulation plays an important role, as it does not allow the heat inside the still to be lost. The worse the insulation, the less effective the performance of the solar still is. The ideal case would be to have the solar still perfectly insulated, however adding a large amount of insulation is not the solution, as the improvements tend to be small above a certain value. Moreover, the more insulation is used, the more expensive and heavy the still becomes.

Investigating the effect of insulation is important because it gives the constructor an insight into the insulation required to achieve satisfactory water productivity. In Fig. 4.5 it is possible to analyze the impact of changing the insulation thermal resistance (L_i/K_i) of walls and basin (blue line), varying the insulation of the walls for fixed insulation of basin, and vice-versa. The chosen L_i/K_i as the reference is the one of the experimental data ($L_i/K_i = 0.5$).

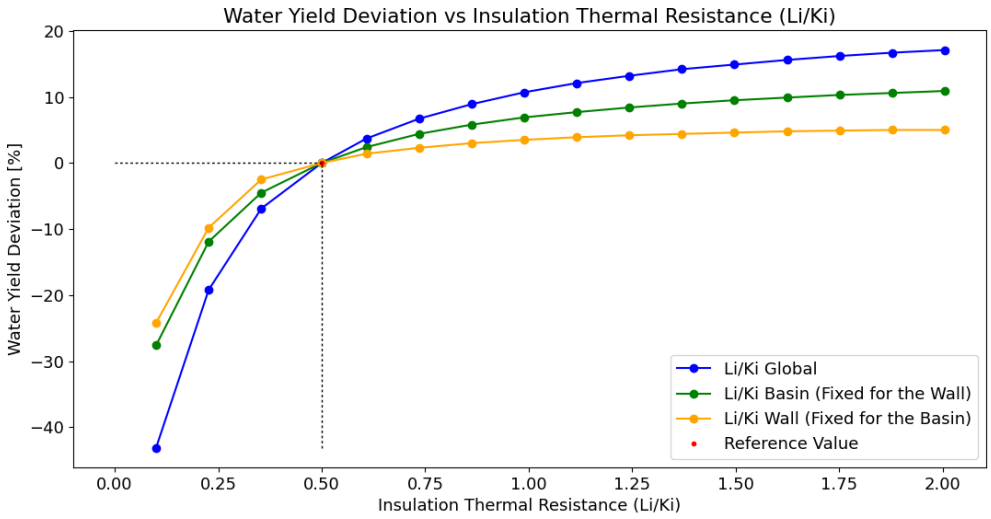

Figure 4.5: Sensitive analysis to water yield as function of L_i/K_i

L_i/K_i	0.25	**0.5**	1	2
L_i (m)	0.02	**0.04**	0.08	0.16
Weight (kg)	6.38	**12.6**	25.2	50.4
Insulation Cost (€)	1.1	**2.1**	4.3	8.56
Water Produced (L/m^2)	2.9	**3.55**	3.95	4.15

Table 4.1: Water yield and insulation thickness, wight and cost as function of L_i/Ki. Reference values are in bold. Sawdust properties: Ki=0.08 W/mK ; Cost=0.17€/kg

It is possible to infer that both basin and wall insulation is important for the still performance. If it is not possible to increase global insulation, it is preferred to add more insulation to the basin than to the walls. Table 4.1 highlights that more insulation will incur in more costs, a more complex structure since it will get heavier. Even though the aim of the solar still is to achieve maximum water yield it may not necessarily be advantageous to increase the insulation.

4.1.6 Feeding Water

Feeding Water Temperature

This subsection focus on the importance to renew the water evaporated with pre-heated water. Easily done by containing the water in a black reservoir, or using warm water from other sources, it can increase water production.

Table 4.2 demonstrates the water yield deviation for water renewal at different temperatures. The temperatures are assumed constant for the whole simulation, except on the last row. The last row is an ideal case, where the inlet water is at the same temperature as the one inside.

Inlet Water Temp.	35° C	40° C	50° C	Solar Still Water Temp.
Water yield deviation	+0,2%	+0,6%	+1,8%	+4,9 %

Table 4.2: Water yield deviation as function of inlet water temperature. Comparison with reference case in which water is provided at T_{out} (data in Appendix A.0.1).

Discrete or Continuous Water Feeding

Water can be introduced in the solar still, continuously or in a discrete way. In the first method, the water depth is kept constant throughout the day, whereas in the second, the depth diminishes until new water is introduced. The objective of this study is too observe if it compensates to only introduce the heat loss of introducing new water from time to time or continuously. Table 4.3 compares refilling water continuously, with 30 minute, 1h and 2h interval as well as no water renovation.

Feeding type	No Feeding	Discrete 30min	Discrete 1h	Discrete 2h
Water yield deviation	+1,6%	0%	+0,1%	+0,3 %

Table 4.3: Water yield deviation as function of water feeding type. Comparison with reference case in which water is continuously provided.

It has minimal effect the water feeding, thus feeding must be implemented in the less complex manner. In the study of El-Maghlany et al. [19], it is reported that discrete feeding increases more than the deviation predicted since, in their experimental work, the water in the reservoir had more time to increase temperature. It can be concluded that the reservoir should be exposed to the sun so that water yield increases.

4.1.7 Condensation

One of the problems of the solar still is that evaporation and condensation occur in the same physical space. Consequently, the condensation rate as shown in Fig. 3.2, will act as bottleneck of water evaporated. Moreover the mechanisms of heat and mass transfer are due to the natural convection pro-

moted by water-glass temperature difference. Increasing this temperature difference or the enhancing the convection inside the still will augment the water production.

A study was done by assuming walls temperatures the same as the air temperature, and a constant temperature for the basin. By varying the glass temperature for fixed basin temperatures, it is possible to confirm the enhancement of water production for increasing basin-glass temperatures difference, as presented in Fig. 4.6. From the figure, it is also possible to infer that is preferred higher temperature of all components for the same temperature difference. This is due to the fact that air can retain more water vapour and thus condense more.

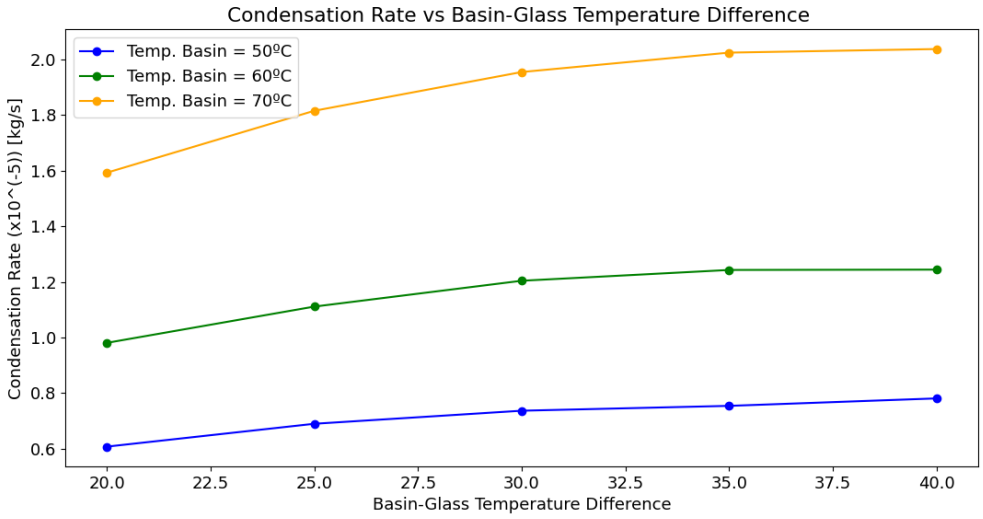

Figure 4.6: Sensitive analysis of condensation rate as function of $\Delta(T_b - T_g)$

Three major issues are identified that if optimized could increase water condensation:

1. Natural convection processes;
2. Water-glass temperature difference;
3. Evaporation and condensation in the same enclosure.

4.2 Approaches to Enhance Water Yield

The parametric study provided insight about key variables that, if optimized, can improve the performance of the solar still. Some examples were given along the parametric study such as, increasing the dimensions of the basin, small water depth, increasing the incident solar radiation, increasing the insulation, supplying renewal water as warm as possible, increasing the convection mechanisms inside the still, separating condensation and evaporation, or using a porous medium.

In this section, solutions are given based on the study carried out. Furthermore, the corrections that must be made in the thermal model to simulate these adjustments are provided.

4.2.1 Structure of the solar still

Modifying the structure of the solar still is an easy way to improve the water yield.Reducing wall height directly reduces heat loss because less wall area is in contact with the outside. The volume of air inside the solar still is smaller, which accelerates heat and mass transfer processes. In addition to these advantages, smaller walls mean less shading and therefore more incident solar radiation. To perform this study, the height of the front wall (lowest wall of the solar still) is attributed, and from this value, the other walls dimensions are computed.

The basin dimensions and the glass angle are kept as reported in the experiment. As can be seen in Fig. 4.7, by reducing the low wall height and consequently the remaining walls' height, an increase in water production can be achieved. The water yield enhancement can be up to 20 % in summer and up to 80% on a winter day.

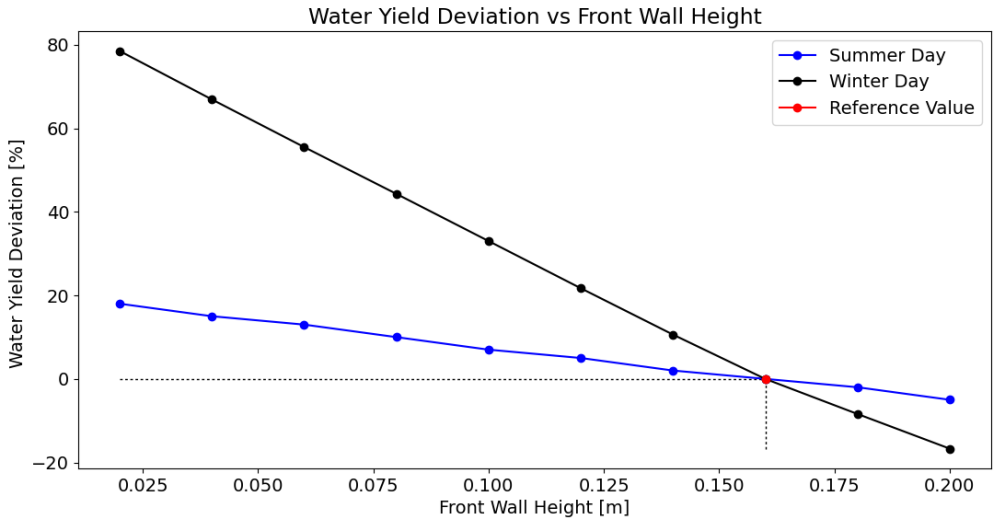

Figure 4.7: Water yield deviation as a function of low wall height, for a representative summer and winter day. This height influences the computing of the remaining walls and consequently the associated shadows.Reference summer day:3.55L/m^2; Reference winter day:0.61L/m^2

One similar option reported in the literature, is the use of the stepped solar still [14], which reduces even more the wall size and volume of the still (see Fig. 1.7). Moreover, for the same available ground space, the area of the basin is increased because of the use of steps.

4.2.2 Use of Mirrors/Refletors

Increasing the solar radiation on the basin can be achieved by using internal and/or external mirrors/refletors. One of the researchers that investigated this topic in more detail, both theoretically and experimentally, was Tanaka [44].

A conservative study is carried out by considering only the beam radiation reflected directly onto the basin. This means that for example, the radiation hitting the back wall and reflected onto the side mirror wall and finally onto the basin is not taken into account. Furthermore, the reflection is only taken into

account if the azimuth is between -90 ° and 90 ° .

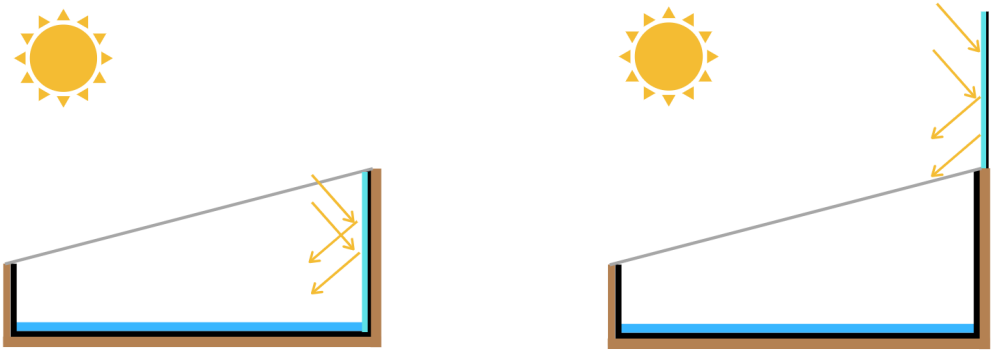

(a) Solar still with internal reflector. Lateral wall reflector not represented but considered.

(b) Solar still with external reflector

Figure 4.8: Representation of different type of reflectors

Inner reflectors

A detailed calculation of the reflected surface is performed, which is identical to the shadow computation. It can be seen that Fig. 4.9 resembles Fig. 2.7 and 2.8. The estimation of the reflected radiation areas is similar to the equations presented in subsection 2.2.3.

To compute the dimensions e, f, g and h in Fig. 4.9, Eq. 2.47 to 2.48 are used. The area reflected by the lateral walls (yellow area) is given by Eq. 2.53. The area reflected by the back wall (orange area), is given by Eq. 2.54. The overlap of the reflected areas must be summed to compute the correct total reflected area ($A_{Reflected}$).

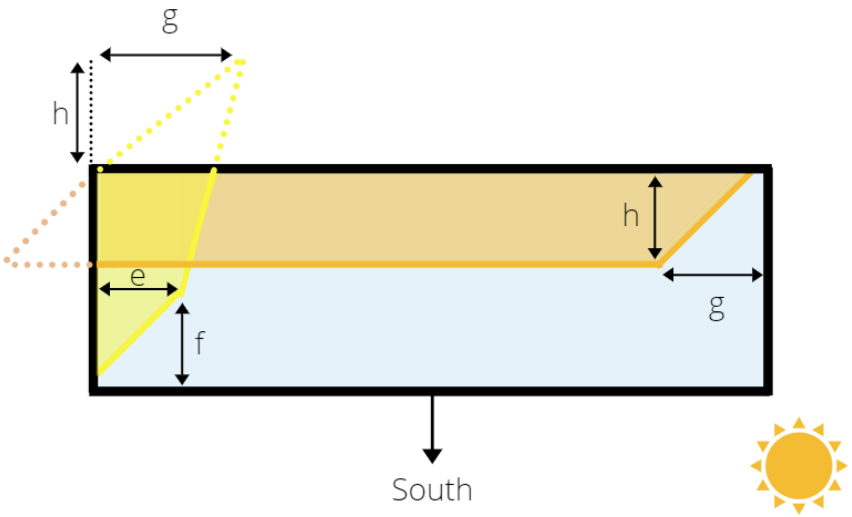

Figure 4.9: Representation of the solar still covered by back and lateral wall reflected area.

Similarly to subsection 2.2.3, it was also studied in this one if an average reflected area could be used, identical to that used in the shadow model, by using average reflected heights. Using identical

Eq. 2.59 to 2.62, it was found a water yield deviation around 3%.

Some adjustments have to be executed on the thermal model, because the black metallic walls are substituted by reflectors/mirrors. First, the radiative properties of the wall must be corrected, since mirrors are installed. A mirror reflects most of the solar radiation and has low absorption, so the following constant considerations are made: $\rho_{ref} = 0.75$ and $\alpha_{ref} = 0.25$.

The energy balance equation for the walls is kept the same as in Eq. 2.20. However, some terms have to be updated. The incident radiation absorbed by walls has to be corrected to,

$$Q_{sun,wall} = I_{dr,wall}(\tau_g)_{dr}\alpha_{ref}A_{exp,wall} + I_{dif}(\tau_g)_{dif}\alpha_{ref}A_{wall}F_{wall-g} \tag{4.1}$$

The basin will receive the reflected solar radiation, $Q_{ref,b}$, thus the energy balance must to be adjusted to,

$$(mc_p)_b\frac{\partial T_b}{\partial t} = Q_{sun,b} - Q_{c,b-w} - Q_{cond,b-out} + Q_{ref,b} \tag{4.2}$$

The reflected radiation reaching the basin, is both direct and diffuse. The reflected beam radiation is that which is accounted in the calculated reflected area. The additional diffuse radiation reaching the basin, is the sum of the reflected diffuse radiation from each wall to the basin, depending on the view factor.

$$Q_{ref,b} = A_{Reflected}I_{dr}(\tau_g\alpha_b)_{dr}\rho_{ref} + A_bI_{dif}\sum((\tau_g\alpha_b)_{dif}\rho_{ref}F_{b,wall}) \tag{4.3}$$

The study was performed for a summer day, however, in winter, due to the lower sun altitude, it is more significant the amount of solar radiation reflected to the basin. In summer, it has less influence, because the reflected radiation covers only a small percentage of the basin area. The left side of table 4.4 presents the water production for a summer and a winter day when using the experimental insulation for basin and walls. The results of using internal reflectors are in agreement with the literature [44].

One thing that is rarely taken into account is that the use of mirrors reduces the heat absorbed by the walls, which affects the solar still performance. The walls will not increase the temperature as much because the radiation absorption coefficient of the reflectors is very low in comparison with the common metallic materials painted black. It is therefore important to insulate the walls sufficiently to minimize heat loss from the mirrors. As can be seen from Table 4.4, the mirrors have a greater influence on the performance of the solar still when walls are properly insulated. For the summer day, perfectly insulating walls showed an improvement close to 8% (see Fig. 4.5), using mirrors with experiment insulation around 7%, and using both around 22%. For the winter day, water yield improvement increased from 79% to 125%.

	Exp. Insulation	No Wall Heat Losses
Summer Day	+7%	+22 %
Winter Day	+79%	+125%

Table 4.4: Water yield improvement on a summer (3.55 L/m^2) and winter (0.6 L/m^2) day when using internal mirrors. Walls perfectly insulated (no losses) or with the experiment insulation.

It is important to note that the use of internal mirrors and their improvement depends on the structure of the solar still. Lower walls have smaller mirrors and therefore less performance. This conclusion contrasts with the analysis made, in subsection 4.2.1, where it was seen that smaller walls increase water production. When building a solar still, the constructor must take into account the available materials and the environmental conditions of the location. According to the simulation results for the designed site, the most suitable structure must be implemented to obtain maximum yearly water yield.

Exterior reflector

Another option to increase solar radiation is to install an external reflector. The advantage of using an external reflector is that it is easy to install and remove, and because it can be adjusted according to the season, as shown in Fig. 4.10. Unlike the previous option, where the interior walls had less influence on the heating of the air, in this case, the interior walls remain unchanged. A disadvantage for some locations is the shadowing caused by the external reflector, which therefore has to be carefully analyzed for each specific situation.

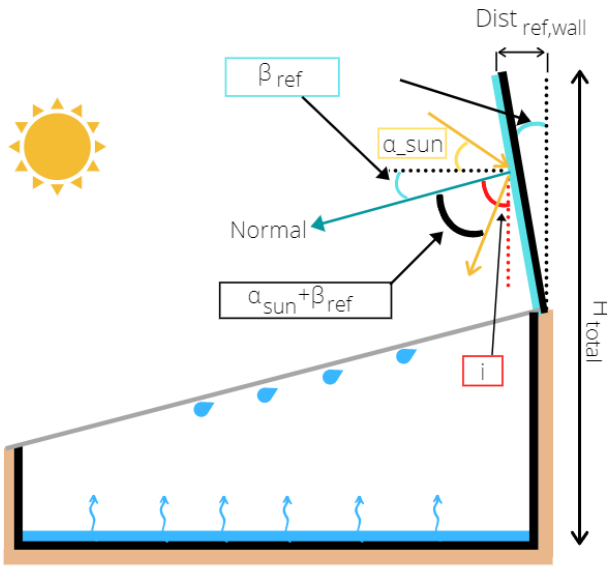

Figure 4.10: Representation of the solar still with a inclined external reflector

The reasoning presented below for the calculation of the reflected area applies to a range of external mirror tilting, which do not allow reflected radiation to the back wall. To clarify, the total angle of incidence ($\alpha_{sun} + \beta_{ref}$), will not exceed i. The value of angle i varies according to the exterior reflector angles, β_{ref}. To calculate i,

$$i = 180 - \beta_{ref} - 90 \tag{4.4}$$

It is only going to be considered the cases in which the total incidence angle is smaller than i,

$$\alpha_{sun} + \beta_{ref} \leq i \tag{4.5}$$

The maximum angle the reflector will be titled is computed with the maximum solar altitude of the studied day. After manipulating Eq. 4.4 and 4.5, it is possible to get,

$$\beta_{ref} \leq 45 - \frac{\alpha_{sun,max}}{2} \tag{4.6}$$

To compute the reflector total height, stated as H_{total}, and the distance of the tip of the mirror to the back wall, $Dist_{ref,wall}$,

$$H_{total} = H_{wall,back} + H_{ref} \cos(\beta_{ref}) \tag{4.7}$$

$$Dist_{ref,wall} = H_{ref} \sin(\beta_{ref}) \tag{4.8}$$

Following the same line of thinking as before, the surface reflected surface by the external reflector is calculated. Three situations can occur during the course of the day, as represented in Fig. 4.11 and Fig. 4.12.

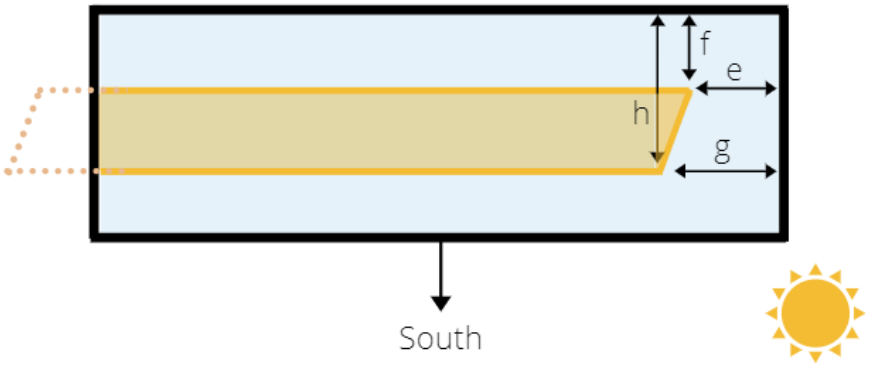

Figure 4.11: Representation of reflected area by the external reflector. View from above the solar still

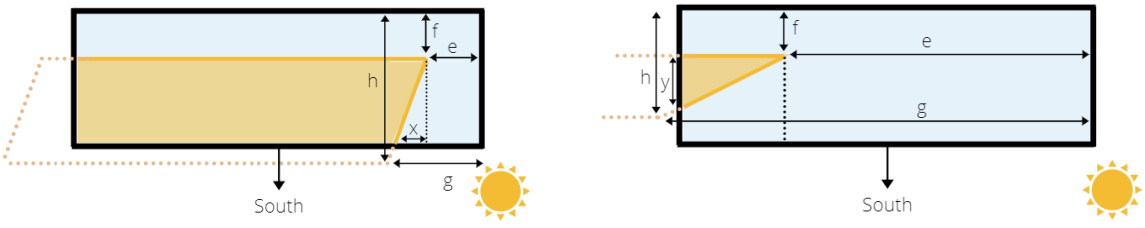

(a) Trapezoidal reflected area larger than the width and length of the basin

(b) Triangular reflected area

Figure 4.12: Representation of other possible reflected area by the external reflector. View from above the solar still

Starting by the computation of area in Fig. 4.11. The dimensions h and f, are given by,

$$h = \frac{H_{total}}{\tan(90 - (i - (\alpha_{sun} + \beta_{ref})))} \cos(\gamma_{sun}) + Dist_{ref,wall} \tag{4.9}$$

$$f = \frac{H_{wall,back}}{\tan(\alpha_{sun})} \cos(\gamma_{sun}) \tag{4.10}$$

For the calculation of e and g in Fig. 4.12, Eq. 2.47 is used, with back wall height and total reflector height respectively. The area reflected will be,

$$A_{Reflected} = \frac{(C - e) + (C - g)}{2} \times (h - f) \tag{4.11}$$

To compute the reflected area presented Fig. 4.12.(a), it is needed to do a linear regression as done in subsection 2.2.3. To compute x, a linear regression is done.

$$y = ax \tag{4.12}$$

It is possible to find a,

$$a = \frac{g - e}{h - f} \tag{4.13}$$

and, by manipulating Eq. 4.12 and setting the height, $y = l - f$,

$$x = \frac{l - f}{a} \tag{4.14}$$

The base of the trapezoidal reflected area is computed as, C subtracted by e, and the height is the width of the basin, L, subtracted by f.

$$A_{Reflected} = \frac{(C - e) + (C - x - e)}{2} \times (l - f) \tag{4.15}$$

Lastly, the area of Fig. 4.12.(b), a similar linear regression has to be done, however, this time y is calculated,

$$y = a \times (c - e) \tag{4.16}$$

$$A_{Reflected} = \frac{(c - e)}{2} y \tag{4.17}$$

The basin energy balance has to be adjusted, since the solar radiation reflected by the external mirror will be absorbed,

$$(mc_p)_b \frac{\partial T_b}{\partial t} = Q_{sun,b} - Q_{c,b-w} - Q_{cond,b-out} + Q_{ref,b} \tag{4.18}$$

Where the reflected solar radiation is given by,

$$Q_{ref,b} = A_{Reflected} I_{dr} (\tau_g \alpha_b)_{dr} \rho_{ref} + A_b I_{dif} (\tau_g \alpha_b)_{dif} \rho_{ref} F_{b,ref} \tag{4.19}$$

Figure 4.13 presents an analysis for a summer and a winter day to observe the effect of adding the external reflector. In the summer, mounting the reflector, automatically increases the water yield, however, increasing the reflector angle does not bring any benefits. In winter, the sun is at lower altitude, and because the external reflector is mounted above the back wall, no reflected solar radiation reaches the basin unless the reflector is tilted. In this season, it is necessary to tilt the external reflector to obtain water yield improvement, as show in the figure.

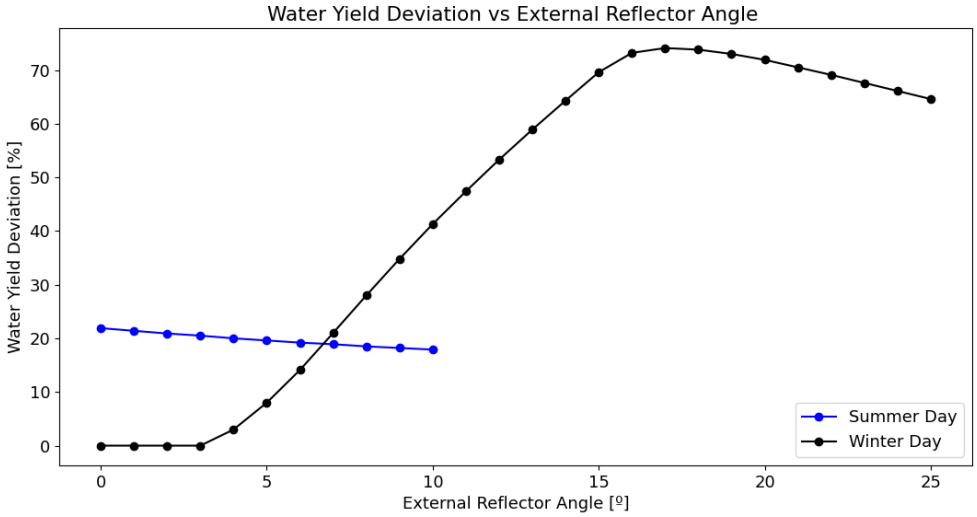

Figure 4.13: Water yield deviation as a function of external reflector angle, for a representative summer and winter day. Mirror is tilted until the angle computed by Eq. 4.6. The external reflector dimensions are assumed to be equal to the back wall.

Implementing the external reflector seems to be a great option to improve water yield, particularly if the mirror is tilted according to the time of the year. It is needed to highlight that it was considered a mirror with the same dimensions as the back wall. Water yield improvements will vary according to the mirror dimensions, which directly influence the solar radiation input (the more radiation is reflected, the larger the improvements, as seen in Fig. 4.2).

4.2.3 Convection Enhancement

The aim of the study presented here is to analyze the effect of increasing the heat transfer coefficient. To increase mass transfer, a small fan can be used. To model the use of a fan inside the still, the main adjustment to be done is modifying the heat transfer coefficients computation. Depending on the fan velocity, the convection coefficient will be in a regime of natural, forced or in combined convection regime.

Equations 4.20 and 4.21 present the laminar and turbulent correlations for forced convection, respectively. It was assumed a transition Reynolds number of 5×10^5.

$$Nu_L = 0.664 Re_L^{1/2} Pr^{1/3} \qquad (Re_L < 5 \times 10^5) \tag{4.20}$$

$$Nu_L = (0.037Re_L^{4/5} - A)Pr^{1/3} \qquad (A = 871\ for\ Re_L = 5 \times 10^5) \tag{4.21}$$

It is possible to know the convection regime by computing the Richardson number,

$$Ri = \frac{Gr}{Re^2} \tag{4.22}$$

In the literature it is seen that, free convection is negligible if (Gr/Re^2) << 1 and that forced convection is negligible if (Gr/Re^2) >> 1 [45], meaning that combined convection will lie between those values. To compute the combined heat transfer coefficient, the correlation in Eq. 4.23 is used. Nusselt number for forced convection (Nu_{forced}) are given by Eqs. 4.20 and 4.21, and for natural convection ($Nu_{natural}$) in section 2.3. The exponent,3, as been demonstrated to best suit data [45].

$$Nu^3 = (Nu_{forced})^3 + (Nu_{natural})^3 \tag{4.23}$$

A study was carried out to predict the water yield as a function of the fan velocity. The heat and mass transfer analogy used until now was applied to calculate condensed and evaporated water. The fan was assumed to have the same impact on the walls, the cover, and the basin, being all subject to the same fan velocity. To note that under realistic conditions, the fan may not affect all components in the same way, mainly depending on the size of the still and the placement of the fan.

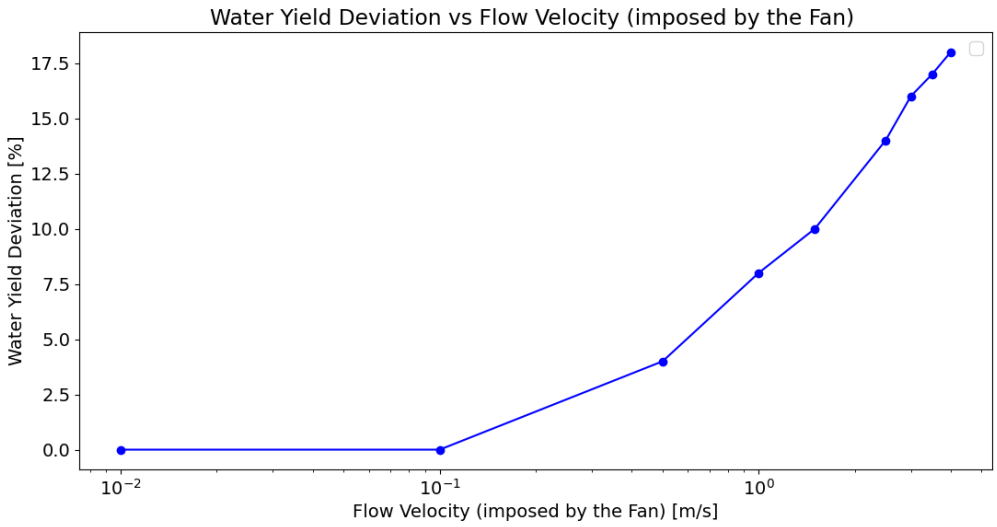

Figure 4.14: Water yield deviation as a function of the fan velocity.

From Fig. 4.14, is possible to conclude that for very low speeds, convection is similar to natural convection and therefore the water yield is approximately the same. An increase in the fan speed improves the yield considerably. It is important to note that despite the productivity improvement, adding this component increases cost and complexity, along with the need for an external power source to keep the fan working.

4.2.4 Reducing Glass Temperature

A modification frequently found in the literature is the use of a fan or a water film to cool the glass cover of the solar still. The aim of this modification is to remove the latent heat from the condensation on the glass and thus increase the temperature difference between water and glass, so that the heat and mass transfer increases.

Before the necessary modifications in the thermal model are discussed in detail, a prior analysis is necessary to further understand the results. After making the correct adjustments to the proposed model, reducing the glass temperature to the experimental data used so far caused almost no production deviation or in some cases decrease in water yield.

This experiment has a small water quantity, the water depth is about 5 mm and therefore has a low thermal inertia. The simulation of the cooled cover, presented negligible or negatively effects. Since the same energy input is given, but the losses increase at a huge rate and the water mass cannot reach as higher temperatures as before. Cooling the cover glass revealed to be advantageous when it was simulated for a larger mass of water. Due to the greater thermal inertia of the water, its temperature drops more slowly along the day, which increases the temperature difference to the glass, thus increasing mass transfer. This is consistent with experimental procedures from the literature [21, 30].

It should be noted that in subsection 4.1.3 it was examined that an increase in water quantity lead to a decrease in water production. It is preferred to use minimum water depth, which will not benefit from the reduction of the glass temperature. As mentioned before, when using the solar still it can be complicated to maintain such small water depths, and therefore a larger depth is used.

Due to all this, a study is done on the experiment for 3 different water depths: 5 mm (used in the experiment), 2 cm and 5 cm.

Fan Over the Cover

In this section, the influence of different wind speeds on the water yield is analyzed, which is achieved by placing a fan above the cover. Instead of comparing the deviations of the water yield with the experimental wind speed, this analysis compares the deviation of the water yield in the absence of external speed on the cover, v=0m/s, with increasing wind speed, as shown in Fig. 4.15.

To note that Fig. 4.15 may give the false impression that greater water production is achieved for the bigger water depth. This is not the case, the greatest percentage improvement in water yield will be in the 5 cm, but when comparing the yield values themselves, it can be seen that a lower water depth is preferred, as shown in Table 4.5.

Water Depth	**v = 0 m/s**	v = 7.5 m/s	Yield Deviation
0.5 cm	**3.56**	3.53	-0.9%
2 cm	**3.24**	3.42	+5.4%
5 cm	**2.34**	2.9	+24.2%

Table 4.5: Water yield (L/m^2) and water yield deviation for different water depths and glass wind velocities. In bold a reference case with no glass wind velocity.

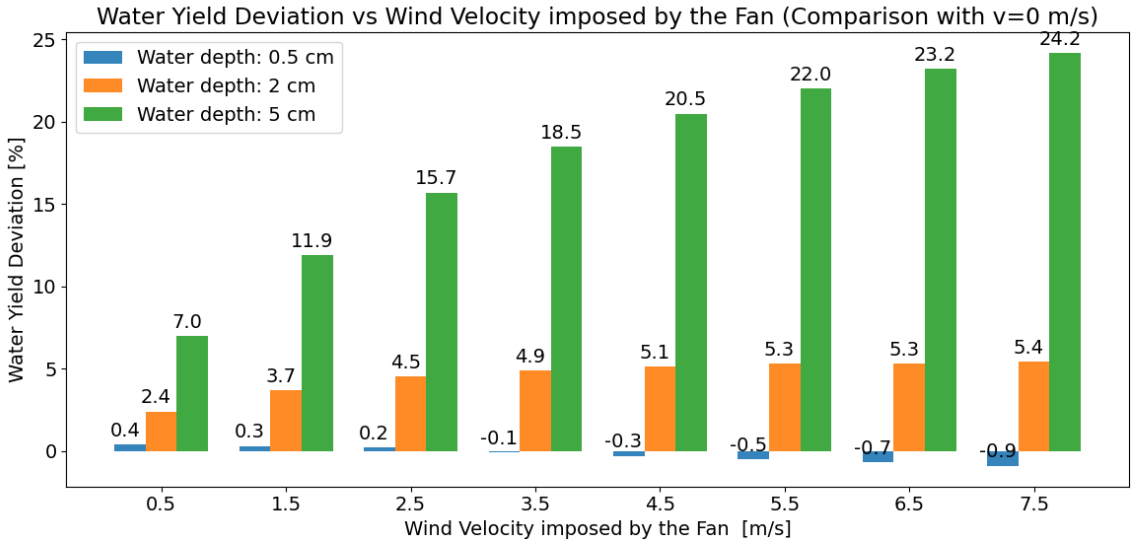

Figure 4.15: Water yield deviation for three water depths, as function of the glass cover wind velocity. Results are compared to no wind velocity on the glass cover.

Water Film Cooling

A similar result occurs when the glass temperature is reduced with a film of water over the glass cover. The advantage of cooling the glass with this technique is that it is a process that requires almost no additional equipment, as in the previous study, where an external fan was required. If water already needs to be pumped to the solar still, a simple modification is required by creating an additional channel to cool the cover.

An adjustment had to be made to the energy balance on the glass cover and an additional energy balance for the water film (subscript $film$) is created. The following adjustments are in concordance with ones seen in the literature [52]. The energy balance for glass is as follows,

$$(mc_p)_g \frac{\partial T_g}{\partial t} = Q_{sun,g} + Q_{cond} + Q_{r,g} + Q_{c,a-g} - Q_{c,film-g} \tag{4.24}$$

An energy balance is done to the water film,

$$(mc_p)_{film} \frac{\partial T_{film}}{\partial t} = Q_{c,film-g} - Q_{r,film-sky} - Q_{c,film-out} - Q_{evap,film} \tag{4.25}$$

The heat lost by convection from the glass to the film (Q_{film}) and the rate of evaporation of the water film to ambient air ($Q_{evap,film}$) are respectively given by,

$$Q_{c,film-g} = A_g h_{film} (T_g - T_{film}) \tag{4.26}$$

$$Q_{evap,film} = 0.013 h_{c,film-out} (p_{film} - \phi p_{out}) \quad (from\ [52]) \tag{4.27}$$

Where h_{film} is computed with the forced convection coefficient in Eqs. 4.20 and 4.21, and $h_{c,film-out}$

is computed with Eq. 2.99.

Three different water depths are investigated (0.5, 2 and 5 cm). The mass flow rate of the cooling film is varied considering a constant film thickness of 5 mm. As performed in the previous study, the water yield is presented and compared for different water depths, with no wind speed on the glass cover as shown in Fig. 4.16. In addition, the actual values are presented in Table 4.6.

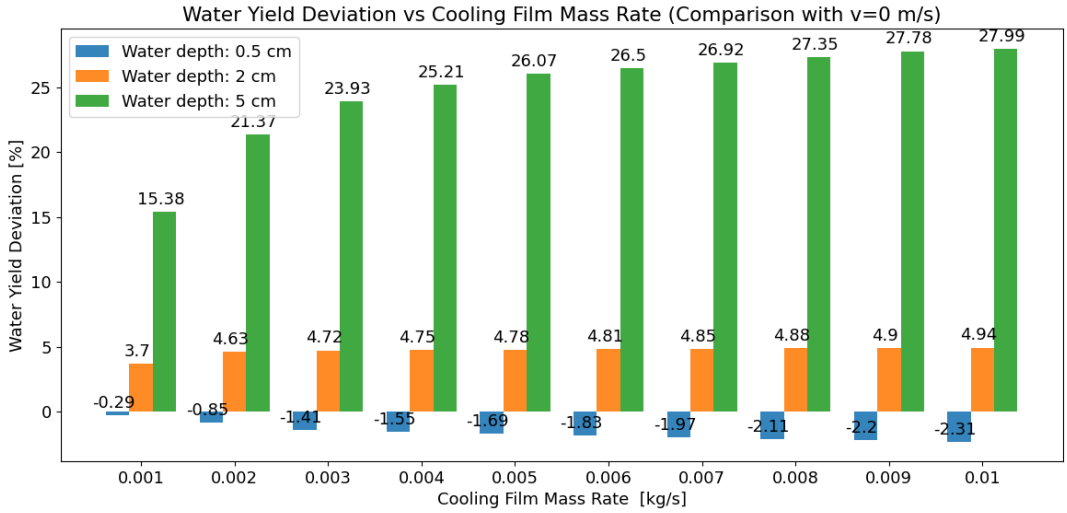

Figure 4.16: Water yield deviation for three water depths, as function of the film cooling rate over the glass. Results are compared to no wind velocity on the glass cover.

Water Depth	**v = 0 m/s**	$\dot{m}_{film}$ = 0.001 kg/s	$\dot{m}_{film}$ = 0.01 kg/s
0.5 cm	**3.56**	3.55 (-0.29%)	3.47 (-2.31%)
2 cm	**3.24**	3.36 (+3.7%)	3.40 (+4.94%)
5 cm	**2.34**	2.70 (+15.38%)	2.99 (+27.99%)

Table 4.6: Water yield (L/m^2) and yield deviation for different water depth and cooling mass rates (cooling film thickness is set constant, 5 mm). In bold a reference case with no glass wind velocity.

Reducing glass temperature with water flow also reveals a greater improvement when a large mass of water is present in the solar still. As mentioned before, depending on the situation, this may be an option that should be considered to increase productivity. It should be emphasized that the comparisons are all made without wind speed over the glass cover so that the influence of cooling is characterized. However, depending on the location, the solar still will have wind velocity varying along the day.

4.2.5 Porous Medium

Porous surfaces have been increasingly used on the solar still. The development of new materials such as carbon foam has made it possible to create an extremely porous material with a high capillary flow, and that absorbs almost all of the incident radiation. An advantage of using these structures is that it can be set above the water mass. In the conventional solar still, some solar radiation is reflected by the

seawater and does not reach the basin (which has the function of heating the seawater). By placing the porous medium above the water, it is maximized the solar radiation which is absorbed.

Porous Medium Model

Based on the experiment carried out by Canbazoglu et al. [51], a simple thermal model was created to understand if the reasoned equations in this work would give reasonable results that could follow and simulate the use of a porous medium.

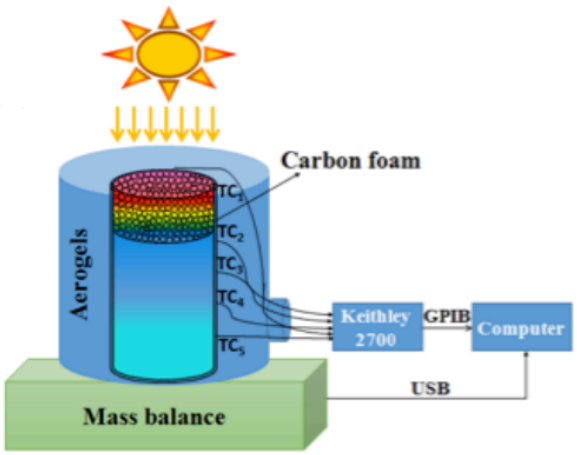

Figure 4.17: Representation of the experimental setup by Canbazoglu et al. [51].

It is possible to observe the experimental setup in Fig. 4.17, where water was poured into an aerogel container and covered by a carbon foam. The experiment gives little information about the ambient conditions, therefore the values for the ambient temperature and the relative humidity were set constant during the whole simulation (described in the Appendix A.0.5). Consequently, these approximations will cause the simulation to obtain more conservative values. The experiment was performed with foams of different porosities.

To compute the mass of the foam ($foam$) and the respective water in the foam ($w, foam$), as well as the combination of both (mix),

$$m_{foam} = \rho_{foam} A_{foam} H_{foam} (1 - \Phi_{foam}) \tag{4.28}$$

$$m_{w,foam} = \rho_{w} A_{foam} H_{foam} \Phi_{foam} \tag{4.29}$$

$$m_{mix} = m_{foam} + m_{w,foam} \tag{4.30}$$

where, Φ_{foam} is the foam porosity.

Due to the fact that the carbon foam has a high porosity, the thermo-physical properties are computed as a combination of water and foam properties. The porous fraction x,

$$x = \frac{m_{foam}}{m_{mix}} \tag{4.31}$$

and,

$$c_{p,mix} = x c_{p,foam} + (1-x) c_{p,w} \tag{4.32}$$

Macroscopic energy balances were done to the carbon foam saturated with water, and to the water under the foam. It was assumed that the setup was perfectly insulated due to the small lateral area and the well insulating material used.

1. **Porous Medium Energy Balance**

   The energy balance equation for the porous medium saturated with water (notation used is mix) is the following,

   $$(mc_p)_{mix} \frac{\partial T_{mix}}{\partial t} = Q_{sun,mix} - Q_{c,mix-out} - Q_{evap} - Q_{c,mix-w} - Q_{r,mix-out} - \dot{m}_{evap} c_{p,w} (T_{mix} - T_w) \tag{4.33}$$

   where $Q_{sun,mix}$ represents the input energy absorbed (product of input power and absorption of the porous medium), $Q_{c,mix-out}$ represents the heat lost by the saturated porous medium to the outside by convection (similar to Eq.2.9), $Q_{r,mix-out}$ represents the heat lost to the outside by radiation (similar to Eq.2.96), and the last term represents the energy lost by the porous medium to heat the water that renews the evaporating water (porous medium considered always saturated).

2. **Water under Porous Medium Energy Balance**

   The energy balance equation for the water under porous medium is the following,

   $$(mc_p)_w \frac{\partial T_w}{\partial t} = Q_{c,mix-w} \tag{4.34}$$

   The heat gained by water due to convection with the foam is,

   $$Q_{c,mix-w} = A_b h_{c,mix-w} (T_{mix} - T_w) \tag{4.35}$$

The heat transfer convection coefficient $h_{c,mix-w}$, is given by

$$Nu_L = 0.27 Ra_L^{1/4} \qquad (10^7 < Ra_L < 10^{11}) \tag{4.36}$$

The result of the simulation is compared with the available experimental data. Starting with the analysis of Fig. 4.18, where it is possible to evaluate the temperature variation and observe that the theoretical results can capture reasonably well the values of the experimental data. The theoretical temperatures indicate the average temperature of the porous saturated medium and the water under the foam. The thermocouple of the foam is located on top of it (TC_1), thus it has a steep temperature rise at the beginning compared to the theoretical values. The theoretical water temperature values lie between the upper TC_2 and lower TC_5 water thermocouple.

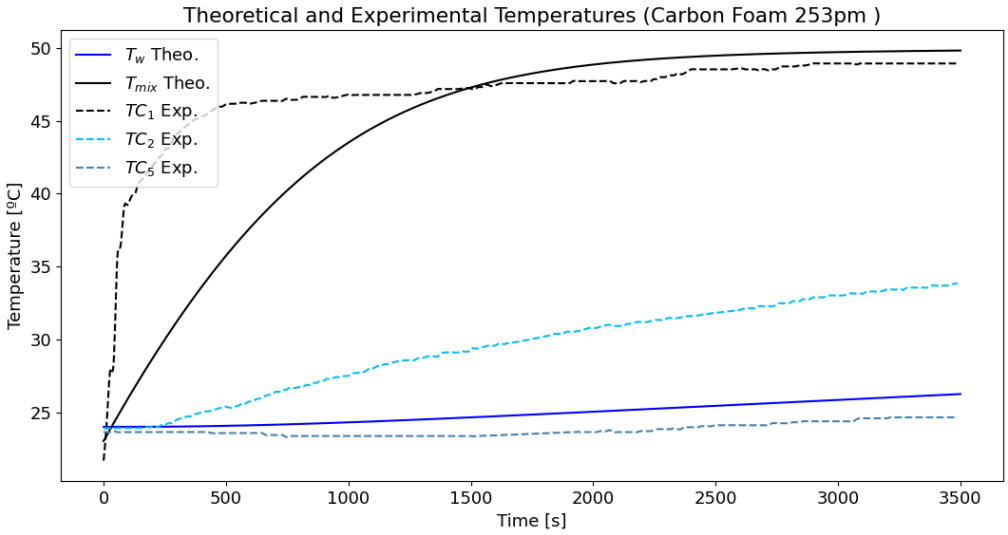

Figure 4.18: Comparison between experimental data [51] measured temperatures and the theoretical foam and water temperatures. Legend: TC_1 - measured porous medium temperature; TC_2 and TC_5 - measured water temperatures. Thermocouples placement represented in Fig. 4.17.

Examining in more detail Fig. 4.19 which shows the rate of evaporation of water as a function of time. Unlike the simulation, where the evaporation rate increases and stabilizes, the experimental evaporation rate starts immediately and then decreases until it stabilizes. Under real conditions, the temperature in the upper part of the foam rises rapidly, as shown in Fig. 4.18 with thermocouple TC_1. Therefore, the water in the upper part of the carbon foam evaporates immediately and then decreases as TC_1 does not vary significantly, resulting in a constant evaporation rate. In the theoretical simulation, the average saturated foam temperature T_{mix} is used, on which the evaporation depends. Initially, T_{mix} slowly increases, which slowly increases the evaporation. Thus, the experimental and theoretical data initially show qualitatively different results. When the equilibrium condition is reached, the evaporation rate is slightly larger than the experimental data because the ambient conditions were considered constant.

The initial discrepancy in the cumulative evaporated water represented in Fig. 4.20, is due to the situation that was reported about the immediate evaporation in real conditions. As already mentioned, the relative humidity and air temperature values were kept the same throughout the simulation, which necessarily does not reproduce accurately the real situation.

Nonetheless is possible to say that this model follows the physical process quite well and that the results also show agreement with the experimental data.

Implementation on the thermal model

To implement a porous surface on the basin, the equations Eqs. 4.33 and 4.38 are applied. Fig. 4.21 shows a representation of the still with a porous medium without and with insulation. If a porous insulation is used under the porous medium, the heat losses to the water below are reduced.

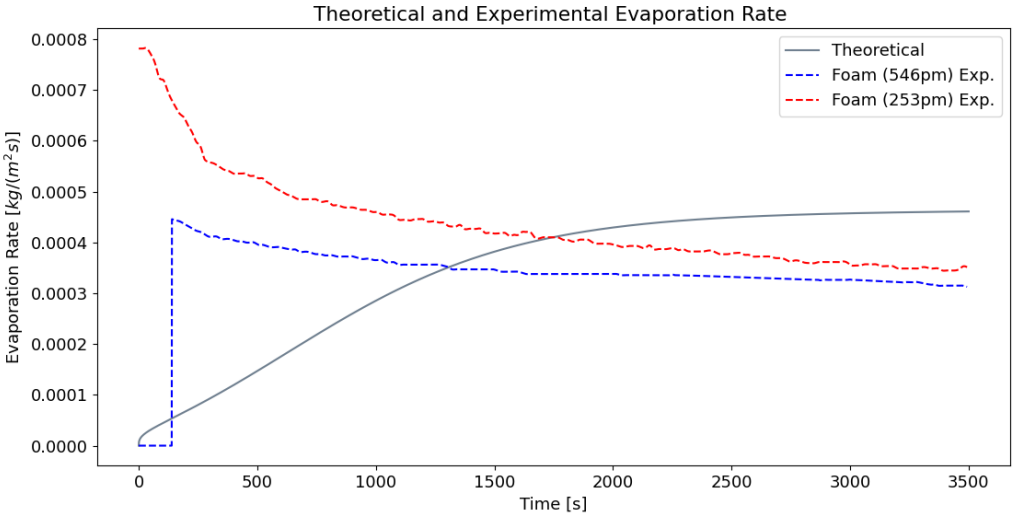

Figure 4.19: Comparison between experimental data [51] evaporation rate for carbon foam with different porosity, and the theoretical computation

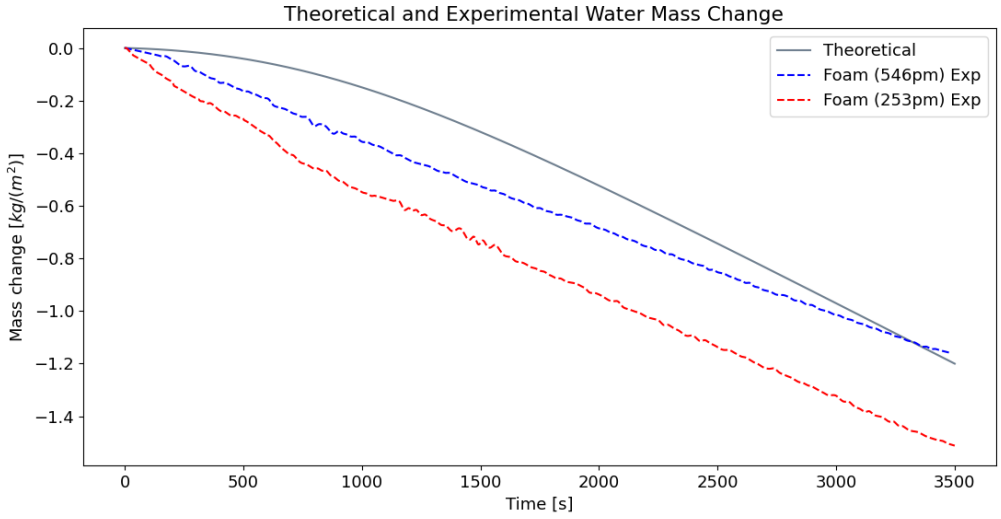

Figure 4.20: Comparison between experimental data [51] water mass change when using carbon foams with different porosity, and the theoretical computation.

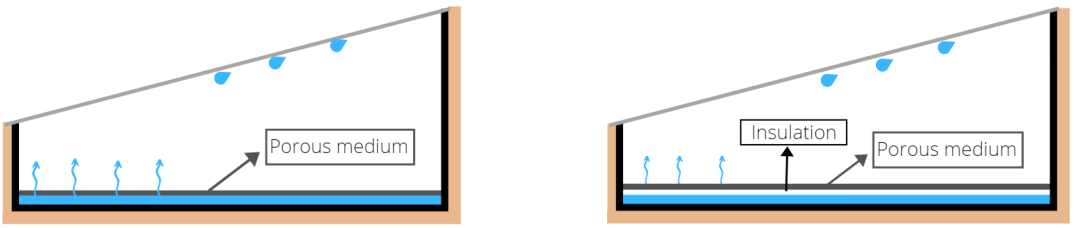

(a) Porous medium without insulation.

(b) Porous medium with porous insulation under.

Figure 4.21: Representation of the solar still with a porous medium.

The energy balances for Fig. 4.21 have to be adjusted. The energy balances used for a basin with water over it, must be updated to a porous medium with water below. The energy balances for glass and wall remain the same as in Eqs. 2.1 and 2.20.

The general equation for the porous medium saturated, and for the water below, are respectively,

$$(mc_p)_{mix}\frac{\partial T_{mix}}{\partial t} = Q_{sun,mix} - Q_{c,mix-a} - Q_{evap} - Q_{loss,mix} - Q_{r,mix} - \dot{m}_{evap}c_{p,w}(T_{mix} - T_w) \quad (4.37)$$

$$(mc_p)_w\frac{\partial T_w}{\partial t} = Q_{loss,mix} - Q_{cond,w-out} - \dot{m}_{evap}(T_w - T_{out})c_{p,w} \quad (4.38)$$

In the case shown in Fig. 4.21(a), the heat lost by the porous medium to the water is given by Eq. 4.39, and it's heat coefficient by Eq. 4.36

$$Q_{loss,mix} = A_b h_{c,mix-w}(T_{mix} - T_w) \quad (4.39)$$

In the case shown in Fig. 4.21(b), the heat exchange between porous medium and the water under the insulation depends on the thermal conductivity, and the thickness, of the insulation material.

$$Q_{loss,mix} = A_b\frac{K_i}{L_i}(T_{mix} - T_w) \quad (4.40)$$

Fig. 4.22 shows the effect of using a porous medium with two thicknesses. To clarify, the blue line is the conventional solar still case, without the porous medium. The remaining graphic lines represent when a porous medium is used above the water, as represented in Fig. 4.21(a). It is assumed that by adding a foam, of for example of 1 mm, absorbs the corresponding water quantity ($\approx$ 0.97 kg/m^2) from the water present in the solar still. The remaining water is assumed to be under the porous medium. The green line starts at 10 kg/m^2, because smaller amounts of water in the solar still would not saturate the porous medium (10 mm porous medium needs $\approx$ 9.7 kg/m^2 of water to saturate).

As mentioned before, increasing water mass, increases thermal inertia and consequently reduces water yield. If a porous medium is added, the effect of thermal inertia of the water is minimized. Since the porous medium is set above the water, the thermal inertia has less influence on the overall water yield. An optimal situation would be using the thinnest saturated foam, with minimum water mass under it, to minimize losses.

Fig. 4.23, analyzes the advantage of increasing insulation thickness under the porous medium (porous medium 1mm thick), to reduce heat losses. The study presents the water yield deviation for different insulation thicknesses and compares it with the case where no porous medium is used. It were considered larger quantities of water in the solar still, since, for example, it is not feasible to implement a porous medium with 2cm insulation, when there is only 5 kg/m^2 of water (equivalent to 5mm of water depth in 1m^2 basin). It is possible to establish that the water yield is independent of the increasing water mass under the insulated porous medium. Moreover the better the insulation, the larger the water yield.

When looking at the actual values of water yield for the porous medium with insulation of 2cm (green

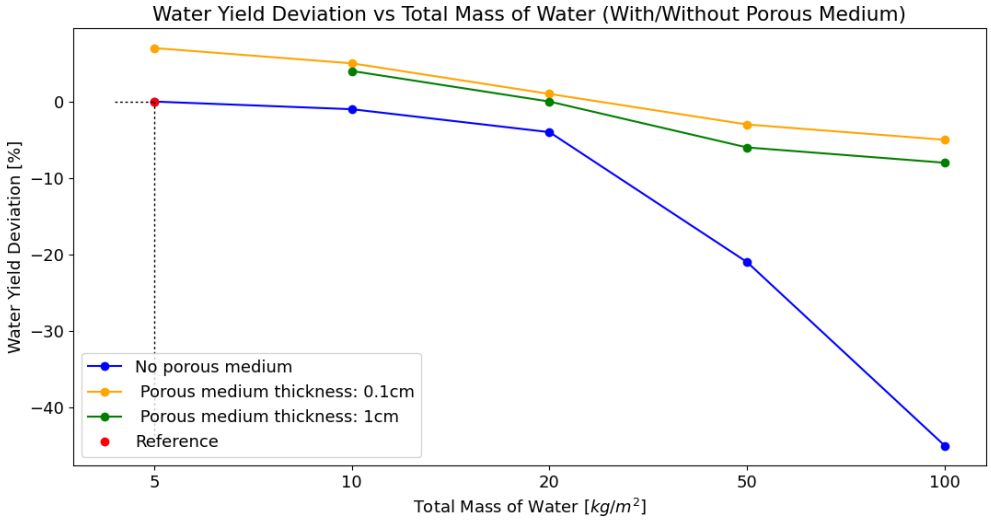

Figure 4.22: Water yield deviation as a function of the total water mass in the solar still, with/without porous medium. Green line only starts at 10 kg/m^2, before that value there is not enough water to saturate the porous medium. Reference value: 3.55 L/m^2

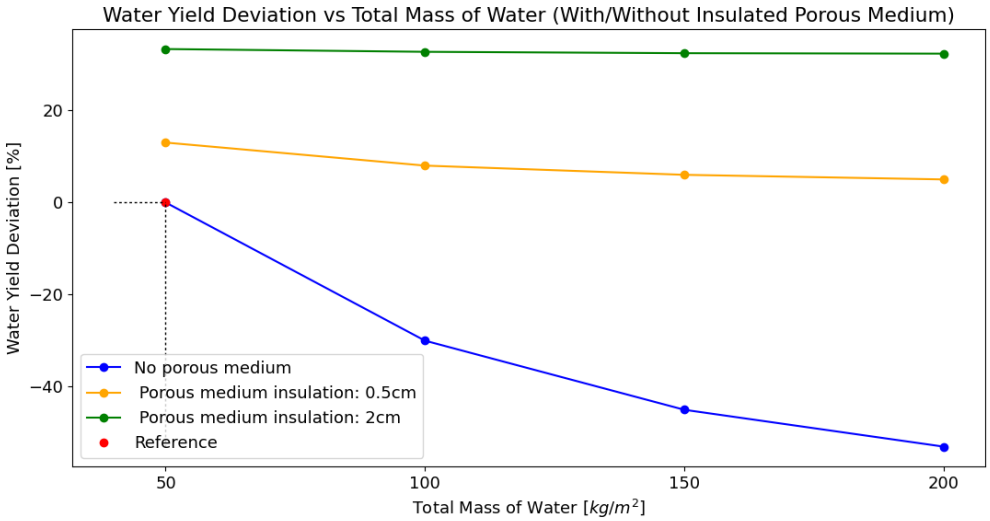

pp

Figure 4.23: Water yield deviation as a function of total water mass in the solar still, for porous medium 1mm thick with/without insulation. Larger quantities of water are considered than in Fig .4.22 for practical reasons. Reference value: 2.85 L/m^2.

line in Fig 4.23, reference value of 2.85 L/m^2 and improvement around 33%) and the porous medium with 0.1cm set in the minimum depth water (yellow line for 5 kg/m^2 total mass of water in Fig 4.22, reference value of 3.55 L/m^2 and improvement around 7%), the same water yield is achieved. The advantage of using a porous medium insulated, is that it can be used for large water quantities in the solar still, yet obtaining the same water yield results as using low mass of water considered. This can be an advantage for the constructor since it is not needed to build a complex system to renew the water on the basin constantly, since a large water quantity can be left on the device to evaporate.

It is important to highlight that a simple and preliminary analysis was carried out. Since the thermal model presented in the beginning of this section showed reasonable results, it was implemented in the solar still. Nonetheless more complex evaporation capillary effects were not modeled and should be considered in future work for a more detailed analysis.

4.2.6 Separate Evaporation and Condensation

The separation of condensation and evaporation processes enables greater evaporation of the basin water, as it is no longer restricted by the condensation. This is represented in Fig. 3.2(b), which presents an initial high evaporation rate that quickly decreases (air becomes saturated), and for the rest of day follows the condensation rate. According to Hammadi [53] the water yield can be enhanced when this technique is implemented. The theoretical analysis is similar to the one of Hammadi [53], however, a more humid site is considered and a deeper study is presented.

A preliminary study is carried out on a simple structure shown in Fig. 4.24 to understand when this option can be beneficial. The evaporator is similar to the solar still, has a metal basin, water, and a glass cover. In this preliminary study, the wall effect was neglected, meaning that not shading is considered, and it is assumed that the water does not condense on the glass cover. The only change made to the still structure was the choice of water depth (in the experiment was 5 mm), which was considered to be 10 cm. This change was made because the study will include the water yield as a function of the evaporator length, and in a real construction with a 20 m long evaporator maintaining 5 mm water depth is not reasonable. The condenser was modeled as a large surface with a fixed temperature of 20° C to replicate a long tube in the ocean or underground. The effects of a variation of the reservoir temperature are later are investigated. It was chosen not to consider shadows, as the structures of this device and that of the conventional solar still are different. By not taking shadows into account, the devices can be fairly compared. Nevertheless, the shadow should be considered in a detailed analysis.

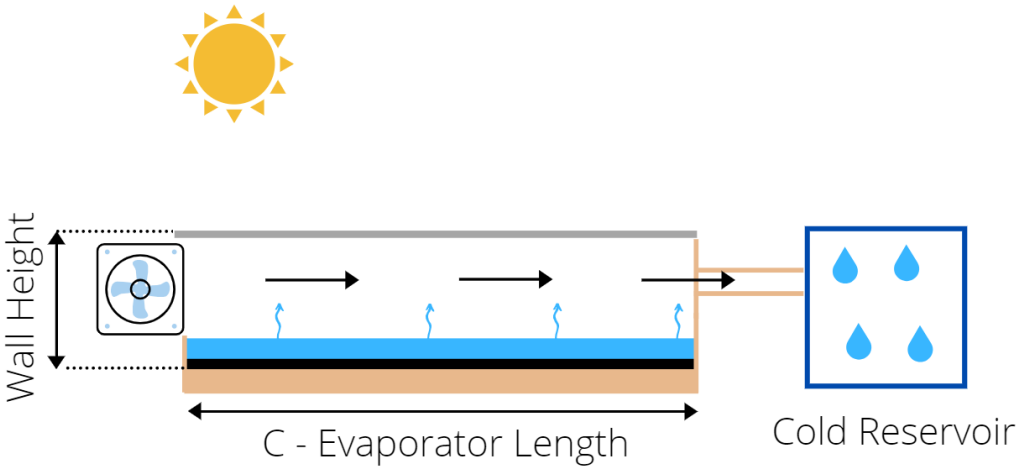

Figure 4.24: Representation of the simple structure with separate evaporation and condensation

An insight is given by performing a simple model with the experimental environmental data, solar

radiation, outdoor temperature, and wind speed used so far. It was considered that the glass cover transmitted the same amount of solar radiation as the conventional solar still to make a fair comparison. However, if a horizontal cover glass as shown in Fig. 4.24 is used, in a detailed study the transmissivity must be corrected to the glass angle. To model these processes, it must be taken into account that a pump or fan is needed to move air from the evaporator to the condenser, causing forced convection. It is possible to determine the heat transfer coefficients between air and glass and air and water, as shown in Eqs. 4.20 and 4.21.

A simple mass balance to the system must be made to compute the water that will be carried by the moving air. The subscript in refers to the air entering the evaporator, and out the air leaving the evaporator.

$$\dot{m}_{w,out} = \dot{m}_{w,in} + \dot{m}_{evap} \tag{4.41}$$

$$\dot{m}_{evap} = \dot{m}_a \Delta w_a \tag{4.42}$$

As reported in Eq. 2.89, the evaporation rate is given by,

$$\dot{m}_a \Delta w_a = \frac{h_c}{c_{p,a}} (w_w - w_a) L \Delta x \tag{4.43}$$

Integrating this equation using inlet boundary, that when $C = 0$, $w = w_{a,in}$,

$$\frac{w_{a,out} - w_w}{w_{a,in} - w_w} = \exp\left(-\frac{h_c L}{\dot{m}_a c_{p,a}} C\right) \tag{4.44}$$

The energy balance of the glass in Eq. 2.1 has to be changed, because it is assumed that no condensation occurs in the evaporator, thus the glass does not receive condensation heat.

$$(mc_p)_g \frac{\partial T_g}{\partial t} = Q_{sun,g} + Q_{r,g} + Q_{c,a-g} - Q_{r,g-sky} - Q_{c,g-out} \tag{4.45}$$

It is performed a steady energy balance to the air flow.

$$(mc_p)_a \frac{\partial T_a}{\partial t} = Q_{c,w-a} - Q_{c,a-g} \tag{4.46}$$

At the end of each time step an average air temperature is computed to compute heat transfer convection coefficient and air properties for the next time step.

$$T_a = \frac{T_{a,in} + T_{a,out}}{2} \tag{4.47}$$

The basin and the water energy balance are similar to the ones of Eqs. 2.17 and 2.10, respectively.

It is assumed that all water present in the humid air condensates until it reaches cold reservoir temperature. The lower the reservoir temperature, the more condensation will occur. To calculate the water condensed in each time step, the following equation was established,

$$\dot{m}_{cond} = \dot{m}_a (w_{a,out} - w_{res}) \tag{4.48}$$

The four most important parameters to analyze in this technique are: solar still length, initial air humidity, air mass flow and velocity of the air flow. Figs. 4.25 and 4.26 the water yield as a function of the solar still length for two different relative humidities of the air discharged in the still and for different air flow velocities. Comparing the two figures, it becomes clear that a lower inlet humidity reduces the water production.

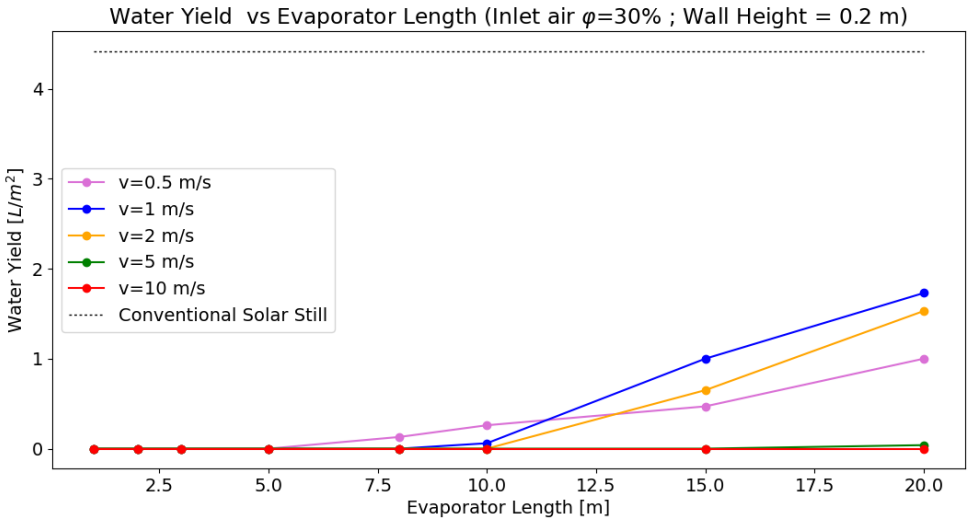

Figure 4.25: Water yield as a function of evaporator length, for different velocities. Intake air with 30% relative humidity, and wall height of 0.2m. Conventional solar still yield: 4.42 L/m^2

Lower speeds are advantageous in shorter evaporators, because air has a larger residence time and can retain more water that at higher speed. At low speed, the water production converges with increasing length of the still (see pink line on Fig. 4.26), as the water productivity does not increase proportionally to the evaporator area. With increasing area, the absorbed solar radiation increases, but also the amount of water mass. Since evaporation is not proportional to the length of the still, productivity may even decrease with increasing length, as shown in Fig. 4.26. Higher velocities, mean a shorter residence time in the evaporator but also a higher mass transfer. It can be also inferred that higher velocities show a better result for longer evaporators.

The non-linearity of water production as a function of evaporator length and air flow velocity is due to the convection regime. For example, in Fig. 4.26, for $v = 0.5\ m/s$ (represented by the pink line), there is a slight convergence in water production until 15m of still length. A longer length increases water productivity because the air enters in a turbulent regime. This leads to more evaporation and therefore makes the air more humid. The air flow reaches the cold reservoir more humid and consequently more condensation occurs.

If we compare the results of this technique simulation with the theoretical computed yield from the conventional solar still, it can be seen that this technique shows no improvement.

This technique needs to be optimized, thus the effect of decreasing inlet area is analyzed in Fig 4.27. Reducing inlet area means lower air mass flow for the same evaporator area. For this study the wall

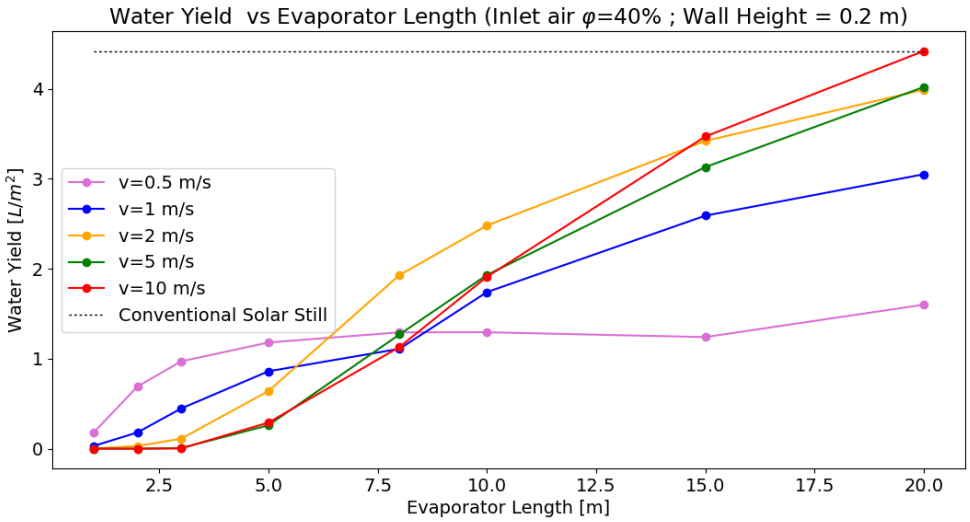

Figure 4.26: Water yield as a function of evaporator length, for different velocities. Intake air with 40% relative humidity and wall height of 0,2 m. Conventional solar still yield: 4.42 L/m^2.

height, represented in Fig. 4.24, was reduced to 0.1 m. By comparing Fig. 4.26 and Fig. 4.27 it is possible to infer that reducing inlet area increases water production for all velocities, and that the technique can even exceed the conventional still water yield. The study was also investigated for a air supply with $\varphi = 30\%$, however, it did not exceed the conventional solar still productivity. The choice of the appropriate air mass flow rate is of great importance for this technique. When comparing to the conventional solar still, separating evaporation and condensation has almost doubled productivity when using the longer evaporator and higher velocity.

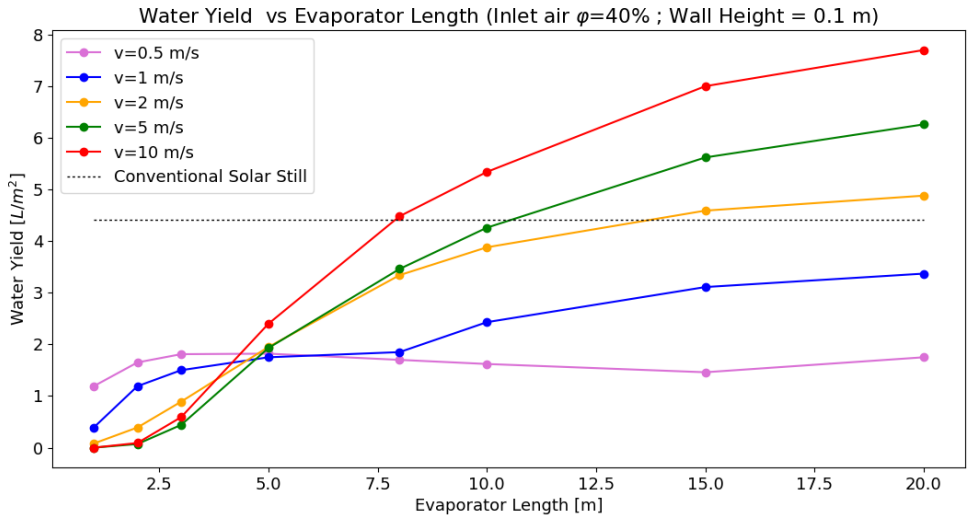

Figure 4.27: Water yield as a function of evaporator length, for different velocities. Intake air with 40% relative humidity, and wall height of 0,1m. Conventional solar still yield: 4.42 L/m^2

An analysis was carried out on the increase in solar radiation as done in subsection 4.1.2. In Fig. 4.28

the effect of the increasing incident solar radiation by 50% in an evaporator with a wall height of 0.1m is analyzed, and compared with the conventional solar still for the same condition. This study shows that productivity is still greater than the conventional solar still at higher speeds and evaporator lengths. However, the improvements are by a smaller amount than presented in Fig. 4.27.

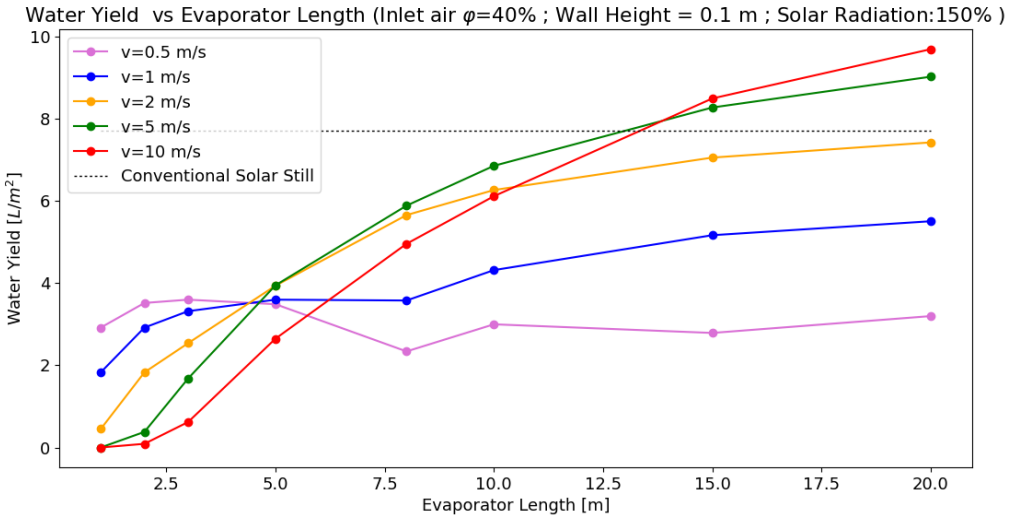

Figure 4.28: Water yield as a function of evaporator length, for different velocities. Intake air with 40% relative humidity, wall height of 0.1m, and solar radiation increased in 150%. Conventional solar still yield: 7.72 L/m^2

The last parameter analyzed was the temperature of the cold reservoir. It is evident that if a colder reservoir temperature is used, the larger will be the water condensed. It can be seen in Fig. 4.29 and 4.30 that a change of 1° C in the reservoir temperature alone, has a significant influence in water yield. This is more noticeable at higher speeds, where the increase or decrease of water yield is up to 26%, as can be seen in Fig. 4.30.

In summary, this option requires very specific parameters to be competitive with the conventional solar still. It showed to be more effective for a large evaporator and with smaller air mass flow. This option is highly dependent on the location, environmental conditions, and cold reservoir temperature. It is expected to be more productive in locations where the relative humidity of the ambient air is already high, when a large scale construction is possible, and a low cold reservoir temperature is present. The design of the evaporator is of greater importance, as the air must leave the evaporator with maximum water vapor. This technique can further increase water production if all parameters are optimized.

It is important to recall that this preliminary study did not take shadows into account and used the same amount of solar radiation as a conventional still so that they could be compared fairly. Other parameters that were not studied in detail must be analyzed, such as water depth or cover glass inclination.

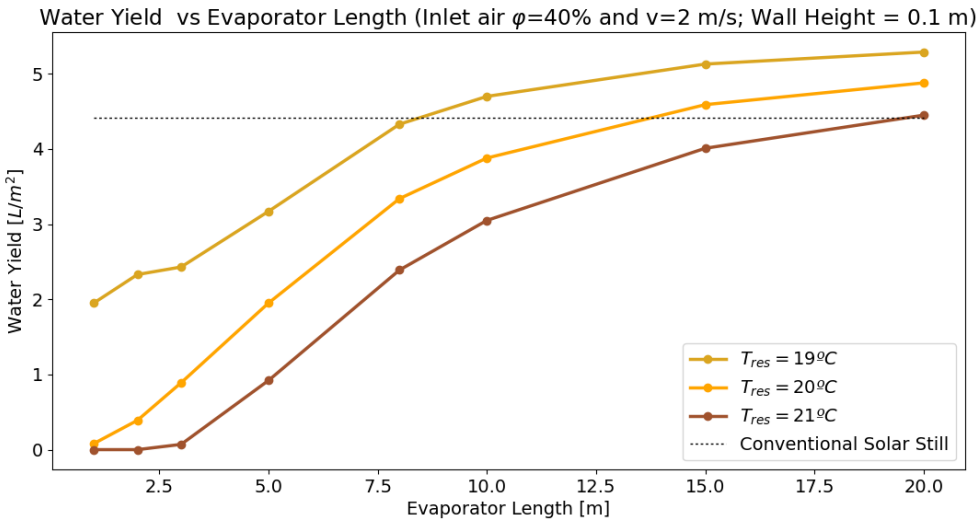

Figure 4.29: Water yield as a function of evaporator length, for v=2m/s and different cold reservoir temperatures (T_{res}). Intake air with 40% relative humidity, and wall height of 0.1m. Conventional solar still yield: 4.42 L/m^2

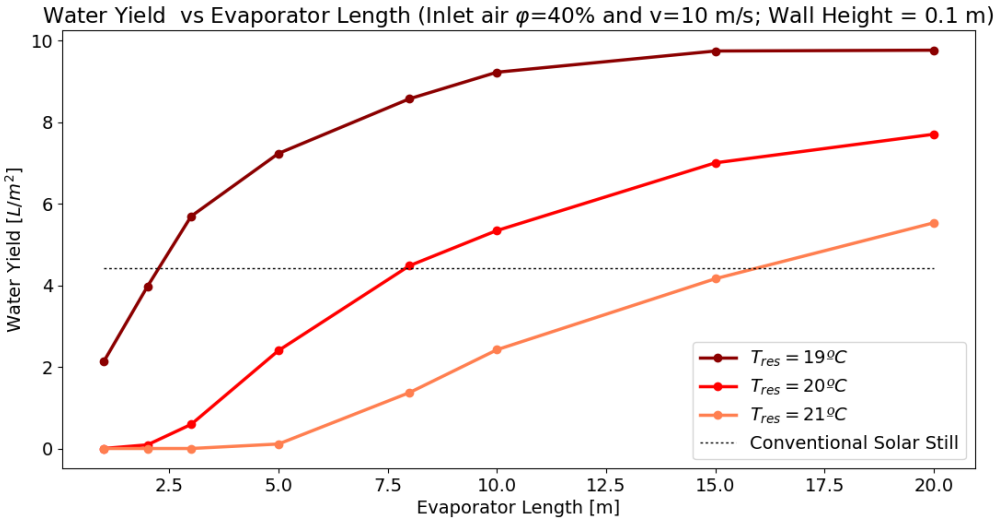

Figure 4.30: Water yield as a function of evaporator length, for v=10m/s and different cold reservoir temperatures (T_{res}). Intake air with 40% relative humidity, and wall height of 0.1m. Conventional solar still yield: 4.42 L/m^2

Chapter 5

Conclusions

5.1 Achievements

The work presented, focused on elaborating a thermal model capable of predicting the performance of the solar still. The model was successfully applied to various locations, ambient conditions, and solar still structures, exhibiting acceptable water yield values deviations from the experimental data. As it is mentioned in this work, it is important to establish a reliable model, so that it can be analyzed, without the resource of experimental procedures, the implementation of a solar still on a specific site. Essential aspects have been highlighted, such as taking into account shadowing, separate beam and diffuse radiation components, the angle dependency of the radiative properties, or the influence of walls.

Comparing Dunkle's model with the one proposed, it can be inferred that to achieve good results with Dunkle, the pre-processing data had to be done, as well as the radiative properties dependency of the angle of incidence and the shadow model. The refined model showed good results however, it was neglected the influence of walls (heat and loss gains), which as studied in this work have an important role. The provided model is more intuitive to understand since all the thermodynamic processes are modeled in detail. Another advantage of the model provided is that it allows to investigate in depth which solar still parameters can be optimized to increase the water yield.

A detailed analysis was provided, to identify possible parameters that can improve the water productivity. Moreover, practical and realistic implementations based on the parametric study were given, modeled, and evaluated. The advantages and drawbacks of each option are mentioned so that according to the location and available material, the optimum solar still is constructed. All improvements studied should be taken into account when constructing the still. The options considered easier to be implemented and that theoretically estimated larger water productivity, where reducing the height of the walls, reducing water depth, installing reflectors, and increasing insulation. More complex solutions were provided, such as installing a fan inside or cooling the glass. Preliminary studies, on the use of a porous surface and separate evaporation/condensation, also showed satisfactory results.

An important point to note is that some adjustments only improved productivity when other variables of the solar still were changed (see section 4.2.4). This is important to point out, that the literature is

commonly reports improvements in water yield for some adjustments that may not be equal or even exist for solar stills which possess different design parameters, locations and/or ambient conditions.

5.2 Future Work

Some simplifications were done in the thermal model of this work, thus it would be interesting to investigate this issue further. Firstly, the radiation model, to compute beam and diffuse components, that was taken into account, even though it gave reasonable values, it is fairly simple and can be more detailed. Furthermore, an average monthly clearness index is applied and assumed constant throughout the days of the experiments. A more detailed shadow model for the walls should be studied, since an approximation was done for easier computation. A better approach can be provided to model the air, which was considered in this work a unique and homogeneous body. A final remark is that, CFD could be used to obtain heat convection correlations for specific geometries and flow regimes, to validate and improve the applied ones (section 2.3).

Though the thermal model has shown coherent results with various experiments from the literature, it is important to apply the thermal model to more experimental procedures to guarantee its quality, and if possible perform experimental work. Other suggestions is to, through the use of detailed CFD simulations validate the simplified macroscopic model presented. The enhancement solutions should also be tested, to make sure that the adjustments done in the model are reliable. It is important that when implementing any kind of optimization to the solar still, different reference cases are evaluated (e.g.for different water depths). Analyzing only one reference case does not give sufficient confidence.

In section 4, both parametric study and solutions provided to enhance water production were simulated for the experiment day or/and the winter representative day. For a profound understanding of the water yield improvement, a simulation should be done for different locations and throughout a whole year. It is not possible to get a yearly representation of total water yield production by these two days.

In subsection 4.2.5, a preliminary study was also done on the porous mediums. It is advised to look deeper into this subject, especially capillary evaporation and condensation, which were not taken into account in the thermal model. Special attention to capillary condensation, which is condensation occurring below the saturation vapor pressure, because of the porous material structure. A capillary condenser is a very interesting option to model and implement in all the options presented since it can produce more condensate. A more detailed study should also be done on the separate evaporator and condenser, which seems to be a suitable option for large-scale implementation. A thorough study should be done on which locations and ambient conditions this is a feasible and productive option.

Finally, it is suggested to analyze all possible combinations between enhancement solutions. The majority of the presented solutions were only investigated individually, and by combining the suggested approaches the overall yield productivity can be even more enhanced. Adding to this a cost analysis, on the construction and maintenance of the different structures should also be conducted. Even though the main goal is to produce as much water as possible, the complexity of the structure, maintenance and the cost of the solar still must not be neglected.

Bibliography

[1] USGS. Where is earth's water? Retrieved July 3, 2020 from www.usgs.gov/.

[2] M. M. Mekonnen and A. Y. Hoekstra. Four billion people facing severe water scarcity. *Science Advances*, 2, Feb. 2016. doi:10.1126/sciadv.15003234.

[3] W. S. Atlas. Global population living in water scarcity. Retrieved July 5, 2020, from https://waterscarcityatlas.org/?fbclid=IwAR3y9rQhqyeLDDt5yZkqoEowZRiNmP2Acvoodg-suZyXkzJHxGzLqYTEtDA.

[4] U. Nations. Sustainable development goals. Retrieved September 9, 2020 from https://www.un.org/sustainabledevelopment/sustainable-development-goals/.

[5] G. Tiwari and L. Sahota. *Advanced Solar-DistillationSystems*, pages 21–36. Springer, 2017.

[6] A.Karaghoul and L. L.Kazmerski. Energy consumption and water production cost of conventional and renewable-energy-powered desalination processes. *Renewable and Sustainable Energy Reviews*, 24:343–356, Aug. 2013. doi:10.1016/j.rser.2012.12.064.

[7] I. C. Karagiannis and P.G.Soldatos. Water desalination cost literature: review and assessment. *Desalination*, 223(9-10):448–456, Mar. 2008. doi:10.1016/j.desal.2007.02.071.

[8] Waterpedia. Multi effect distillation adsorption desalination. Retrieved September 10, 2020, from https://www.youtube.com/watch?v=wpTUay98YcIt=1sab_channel=Waterpedia.

[9] R. Castelnuovo. Multi-stage flash distillation. Retrieved September 10, 2020, from https://en.wikipedia.org/wiki/Multi-stage_flash_distillation.

[10] C. Shono, M. Nong, N. Arboleda, C. Simons, R.Chuang, and I. Martin. Vapor compression desalination proposal. Retrieved September 10, 2020, from https://docplayer.net/30068875-Vapor-compression-desalination-proposal.html.

[11] J. Duffie and W. A. Beckman. *Solar Engineering of Thermal Processes*, volume 3, pages 640–650. Wiley, 2007.

[12] G. Tiwari, V. Dimri, and A. Chel. Parametric study of an active and passive solar distillation system: Energy and exergy analysis. *Desalination*, 242:1–18, Mar. 2009. doi:10.1016/j.desal.200.0.08327.

[13] L.Mu, X.Xub, T.William, C. Debrou, R. Gomez, Y. Park, H. Wang, K. Kota, P. Xub, and S. Kuravia. Enhancing the performance of a single-basin single-slope solar still by using fresnel lens: Experimental study. *Journal of Cleaner Production*, 239, Dec. 2019. doi:10.1016/j.jclepro.2019.118094.

[14] Z.M.Omara, A.E.Kabeel, and M.M.Younesa. Enhancing the stepped solar still performance using internal reflectors. *Desalination*, 314, Apr. 2013. doi:10.1016/j.desal.2013.01.007.

[15] Z.M.Omara, A. Kabeel, and M. Younes. Enhancing the stepped solar still performance using internal and external reflectors. *Energy Conversion and Management*, 78:876–881, 2014. doi:10.1016/j.enconman.2013.07.092.

[16] H. Tanaka. Experimental study of a basin type solar still with internal and external reflectors in winter. *Desalination*, 249:130–134, 2009. doi:10.1016/j.desal.2009.02.057.

[17] A. Khalifa. On the effect of cover tilt angle of the simple solar still on its productivity in different seasons and latitudes. *Energy Conversion and Management*, 52:431–436, Jan. 2011. doi:10.1016/j.enconman.2010.07.018.

[18] J. A. Jones and L. W. L. . K. E. Lindsay. Effects of wind and choice of cover material on the yield of a passive solar still. *Desalination and Water Treatment*, 52:48–56, Apr. 2014. DOI:10.1080/19443994.2013.784715.

[19] W. M. El-Maghlany, A. Abdelaziz, A. Hanafy, and A. Kabeel. Effect of continuous and discrete makeup water on the productivity of conventional solar still. *Journal of Energy Storage*, 28, Apr. 2020. doi:10.1016/j.est.2020.101223.

[20] P. Vishwanath, K. O. K. Anil, P. Ajay, and K. Kaviti. Solar stills system design: A review. *Renewable and Sustainable Energy Reviews*, 51:153–181, June 2015. doi:10.1016/j.rser.2015.04.103.

[21] Z.M.Omaraa, A.Abdullah, A.E.Kabeelb, and F.A.Essaa. The cooling techniques of the solar stills' glass covers – a review. *Renewable and Sustainable Energy Reviews*, 78:176–193, Oct. 2017. doi:10.1016/j.rser.2017.04.085.

[22] A.E.Kabeel, A.Khalil, M.Omara, and M.M.Younes. Theoretical and experimental parametric study of modified stepped solar still. *Desalination*, 289:12–20, 2012. doi:10.1016/j.desal.2011.12.023.

[23] T.Elango and K. Murugavel. The effect of the water depth on the productivity for single and double basin double slope glass solar stills. *Desalination*, 359:82—-91, 2015. doi:10.1016/j.desal.2014.12.036.

[24] F. Tabrizi and A.Z.Sharak. Experimental study of an integrated basin solar still with a sandy heat reservoir. *Desalination*, 253:195–199, Apr. 2010. doi:10.1016/j.desal.2009.10.003.

[25] A.E.Kabeel and M.Abdelgaied. Improving the performance of solar still by using pcm as a thermal storage medium under egyptian conditions. *Desalination*, 383:22–28, Apr. 2016. doi:10.1016/j.desal.2016.01.006.

[26] O. Mahian and A. Kianifar. Mathematical modelling and experimental study of a solar distillation system. *Journal of Mechanical Engineering Science*, 225:1203–1212, Apr. 2011. doi:10.1177/2041298310392648.

[27] K. Murugavel and K.Sritharb. Performance study on basin type double slope solar still with different wick materials and minimum mass of water. *Renewable Energy*, 36:612–620, Feb. 2011. doi:10.1016/j.renene.2010.08.009.

[28] S. Abdallah, M. M.Abu-Khader, and O. Badran. Effect of various absorbing materials on the thermal performance of solar stills. *Desalination*, 242:128–137, June 2009. doi:10.1016/j.desal.2008.03.036.

[29] A. Bilal, B. Jamil, N. U. Haque, and M. A. Ansari. Investigating the effect of pumice stones sensible heat storage on the performance of a solar still. *Groundwater for Sustainable Development*, 9, Oct. 2019. doi:10.1016/j.gsd.2019.100228.

[30] O. Badran. Experimental study of the enhancement parameters on a single slope solar still productivity. *Desalination*, 209:136–143, Apr. 2007. doi:10.1016/j.desal.2007.04.022.

[31] A.A.El-Sebaii. Effect of wind speed on some designs of solar stills. *Energy Conversion and Management*, 41:523–538, Apr. 2000. doi:10.1016/S0196-8904(99)00119-3.

[32] A. Z. Al-Garni. Productivity enhancement of solar still using water heater and cooling fan. *Journal of Solar Energy Engineering*, 134, Aug. 2012. doi:10.1115/1.4005760.

[33] E. Chiavazzo, M. Morciano, F. Viglino, M. Fasano, and P. Asinari. Passive solar high-yield seawater desalination by modular and low-cost distillation. *Nature Sustainability*, 1:763–772, Dec. 2018. doi:10.1038/s41893-018-0186-x.

[34] Z.Xu, L. Zhang, L.Zhao, B.Li, B.Bhatia, C.Wang, K.L.Wilke, Y.Song, O.Labban, J.H.Lienhard, R.Wang, and E. N. Wang. Ultrahigh-efficiency desalination via a thermally-localized multistage solar still. *Energy Environmental Science*, 13:830–839, Jan. 2020. doi:10.1039/C9EE04122B.

[35] C. Elango, N. Gunasekaran, and K. Sampathkumar. Thermal models of solar still—a comprehensive review. *Renewable and Sustainable Energy Reviews*, 47:856–911, July 2015. doi:10.1016/j.rser.2015.03.054.

[36] R. Dunkle. Solar water distillation, the roof type still and multiple effect diffusion still. Proceedings of the International Heat Transfer Conference, Part V—International Developments in Heat Transfer, 1961. p. 895–902.

[37] M.Jakob. *Heat transfer. Vol. 1*. Wiley.

[38] P. Pal and R. Dev. Thermal modeling, experimental validation, and comparative analysis of modified solar stills. *Journal of Solar Energy Engineering*, 141:061013, 2019. doi:10.1115/1.4043955.

[39] J. Clark. The steady-state performance of a solar still. *Journal Solar Energy*, 44:43–49, 1990. doi:10.1016/0038-092X(90)90025-8.

[40] R. S. Adhikari, A. Kumar, and A. Kumar. Estimation of mass-transfer rates in solar stills. *International Journal of Energy Research*, 14:737–744, 1990. doi:10.1002/er.4440140705.

[41] S. Kumar and G. Tiwari. Estimation of convective mass transfer in solar distillation systems. *Journal Solar Energy*, 57:459, 1996. doi:10.1016/S0038-092X(96)00122-35.

[42] P.T.Tsilingiris. The influence of binary mixture thermophysical properties in the analysis of heat and mass transfer processes in solar distillation systems. *International Journal Solar Energy*, 81: 1482–1491, 2007. doi:10.1016/j.solener.2007.02.005.

[43] M. Modest. *Radiative Heat Transfer*, volume 3, pages 96–99. Academic Press, 2013.

[44] H. Tanaka and Y.Nakatake. Theoretical analysis of a basin type solar still with internal and external reflectors. *Desalination*, 197:205–216, 2006. doi:10.1016/j.desal.2006.01.017.

[45] T. Bergman, F. Incropera, D. DeWitt, and A. Lavine. *Fundamentals of Heat and Mass Transfer*, volume 6, pages 560–618. Wiley, 2007.

[46] T. Fuji and H. Imura. Natural-convection heat transfer from a plate with arbitrary inclination. *Journal of Heat and Mass Transfer*, 15:755–764, 1979. doi:10.1016/0017-9310(72)90118-4.

[47] G. Vliet. Natural convection local heat transfer on constant-heat-flux inclined surfaces. *Journal of Heat Transfer*, 91:511–516, 1969. doi:10.1115/1.3580235.

[48] M. Örvös, V. Szabó, and T. Poós. Rate of evaporation from the free surface of a heated liquid. *Journal of Applied Mechanics and Technical Physics*, 57:1108—-1117, 2016. doi:10.1134/S0021894418010248.

[49] J. Watmuff, W. Charters, and D. Proctor. Solar and wind induced external coefficients solar collectors. Technical report, Revue International d'Helio- technique,, 1977.

[50] P. Roache. *Verification and Validation of Computational Fluid Dynamics Simulations*. NM, 1998.

[51] F. M. Canbazoglu, B. Fan, A. Kargar, K. Vemuri, , and P. Bandaru. Enhanced solar evaporation of water from porous media, through capillary mediated forces and surface treatment. *AIP Adv.*, 6: 85218, 2016. doi:10.1063/1.4961945.

[52] B.Abu-Hijleh and H. A.Mousa. Water film cooling over the glass cover of a solar still including evaporation effects. *Energy*, 22:43–48, 1997. doi:10.1016/S0360-5442(96)00088-6.

[53] S. H.Hammadi. Integrated solar still with an underground heat exchanger for clean water productions. *Journal of King Saud University - Engineering Sciences*, 32:339–345, 2020. doi:10.1016/j.jksues.2019.04.004.

[54] JRC. Photovoltaic geographical information system. Retrieved August 15, 2020, from https://re.jrc.ec.europa.eu/pvg_tools/en/tools.html.

Appendix A

Experimental Data

A.0.1 Experiments conducted by Omara et al. [14] and Kabeel et al. [22]

These experiments are conducted with the same solar still structure, being the main differences, the day the experiment occurs and the environment conditions.

Property	**Value**	**Units**
Structure		
Solar Still Length - C	2	m
Solar Still Width - L	0.5	m
Basin/Wall Thickness	1.5	mm
Basin/Wall Density	7874	kg/m^3
Basin/Wall Specific Heat Capacity - $c_{p,b}$	473	J/kg.K
Basin/Wall Insulation Thickness - L_i	0.04	cm
Basin/Wall Insulation Thermal Conductivity - K_i	1.5	W/(m.K)
Glass Angle - β_g	30	º
Glass Height	0.58	m
Glass Thickness	3	mm
Glass Density	2700	kg/m^3
Glass Specific Heat Capacity - $c_{p,g}$	840	J/(kg.K)
Water depth	5	mm
Water density	1000	kg/m^3
Back wall height	0.45	m
Front wall height	0.16	m
Day and location		
Day number	240[14]; 221 [22]	
Latitude	31.07	º
Clearness index factor (*)	0.66	
Wind velocity (*)	3	m/s

Table A.1: Experimental data from the experiments conducted by Omara et al. [14] and Kabeel et al. [22].

Property	Value	Units
View Factors		
View factor water to lateral wall - $F_{w,Lateral}$	0.03	
View factor water to front wall - $F_{w,Front}$	0.12	
View factor water to back wall - $F_{w,Back}$	0.25	
View factor water to glass - $F_{w,g}$	0.57	
View factor lateral wall to glass - $F_{Lateral,g}$	0.29	
View factor front wall to glass - $F_{Front,g}$	0.18	
View factor back wall to glass - $F_{Back,g}$	0.5	

Table A.2: Experimental data from the experiments conducted by Omara et al. [14] and Kabeel et al. [22].Values with (*) were assumed based on the data given.View factors were computed.

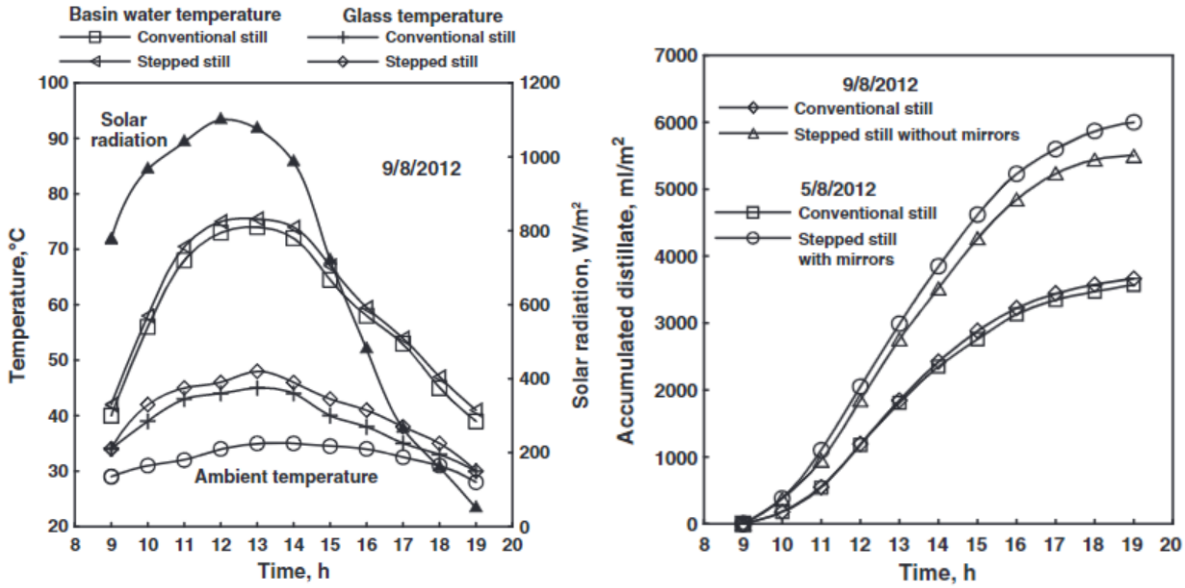

(a) Solar Radiation and hourly temperature variation. The data used was from 9/8/2012 for the conventional solar still.

(b) Cumulative water yield.The data used was from 9/8/2012 for the conventional solar still.data

Figure A.1: Experimental data from the experiment carried out by Omara et al. [14]

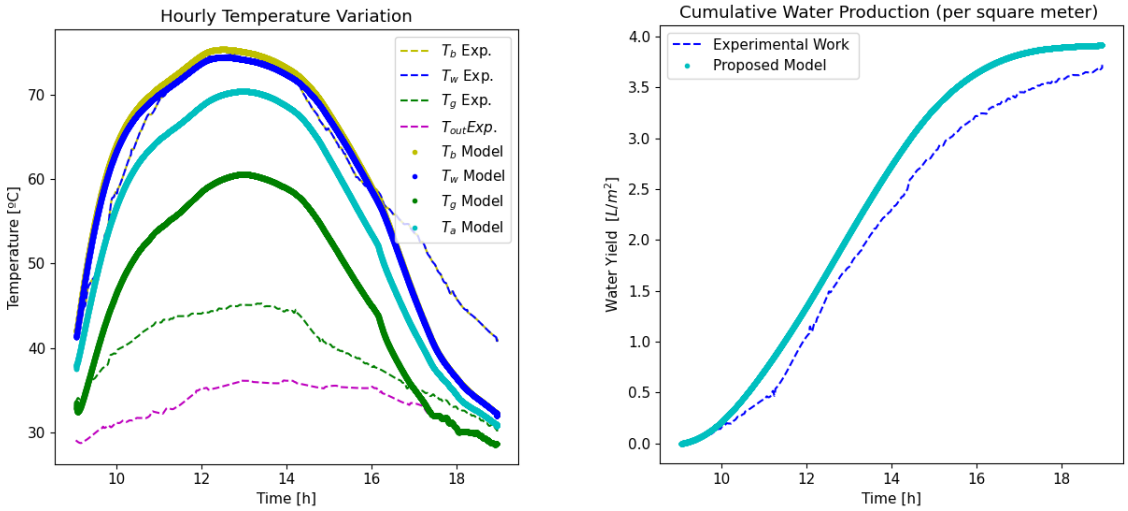

(a) Hourly temperature variation for the proposed model, as well as the experimental data

(b) Cumulative water yield for the proposed model, as well as the experimental data

Figure A.2: Hourly temperature variations and cumulative water yield of the thermal model when applied to the data from the experiment conducted by Omara et al. [14]

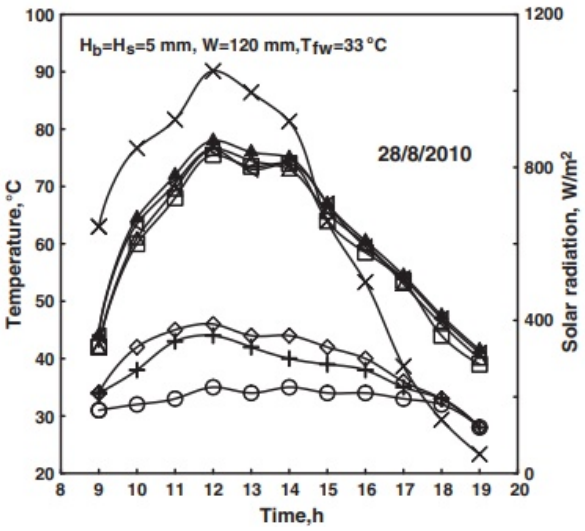

(a) Solar Radiation and hourly temperature variation.

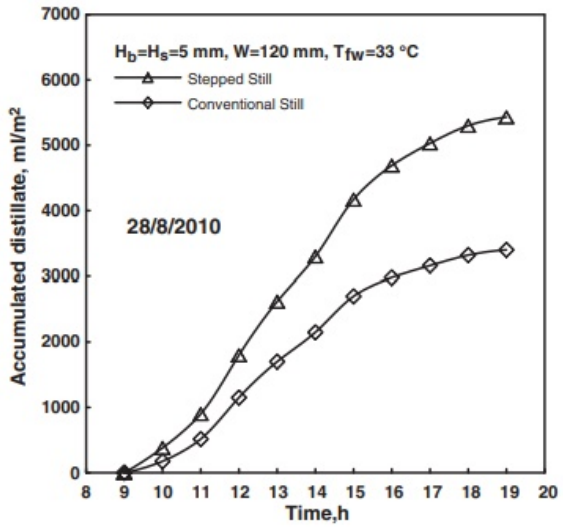

(b) Cumulative water yield.The data used was the one of the conventional solar still.

Figure A.3: Experimental data from the experiment carried out by Kabeel et al. [22]

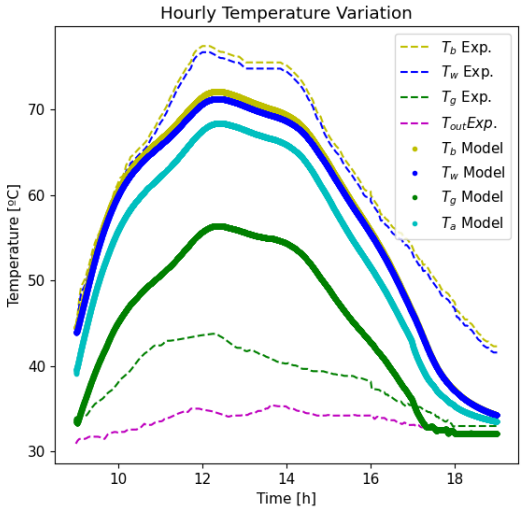

(a) Hourly temperature variation for the proposed model, as well as the experimental data

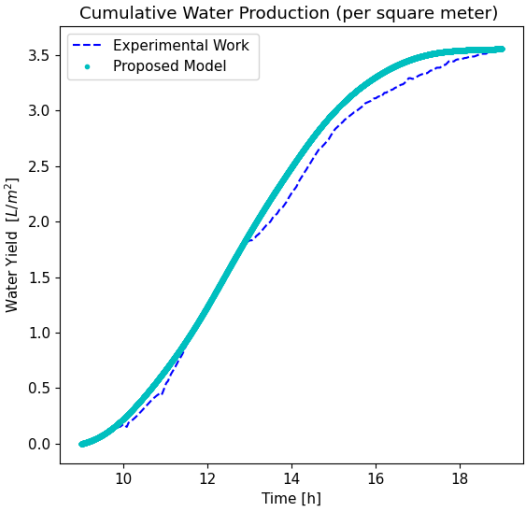

(b) Cumulative water yield for the proposed model, as well as the experimental data

Figure A.4: Hourly temperature variations and cumulative water yield of the thermal model when applied to the data from the experiment carried out by Kabeel et al. [22]

It is mentioned in subsection 4 that it was studied a representative winter day.All data provided below refers to January 1st for the location of these experiments (Tanta, Egypt).The input solar radiation and ambient temperature, given in Fig. A.5(a) and A.5(b), were obtained from JRC data [54].The sky clearness index (k_t), based on day chosen, is around 0.55. The outputs of the thermal model are given in Fig. A.6 .

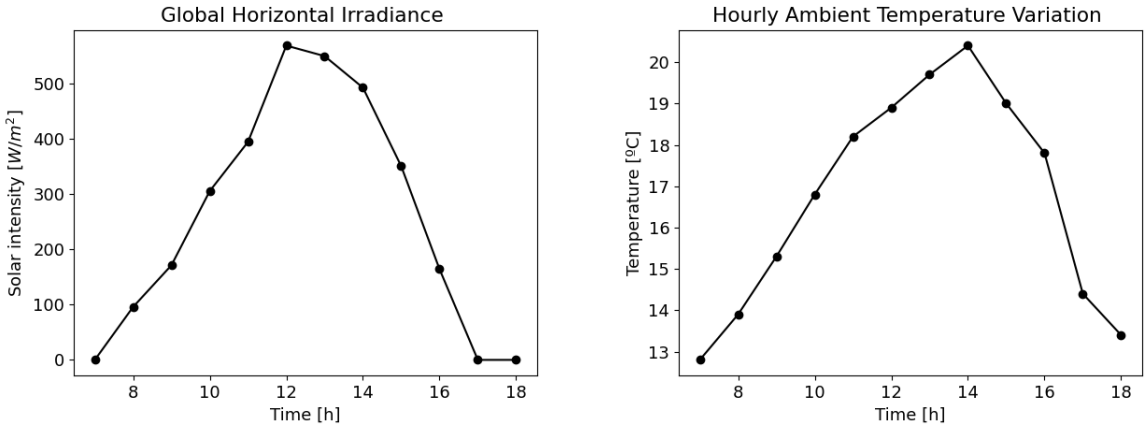

(a) Solar radiation (b) Ambient temperature

Figure A.5: Solar radiation and ambient temperature of a winter representative day for the location of experiments (data obtained from [54])

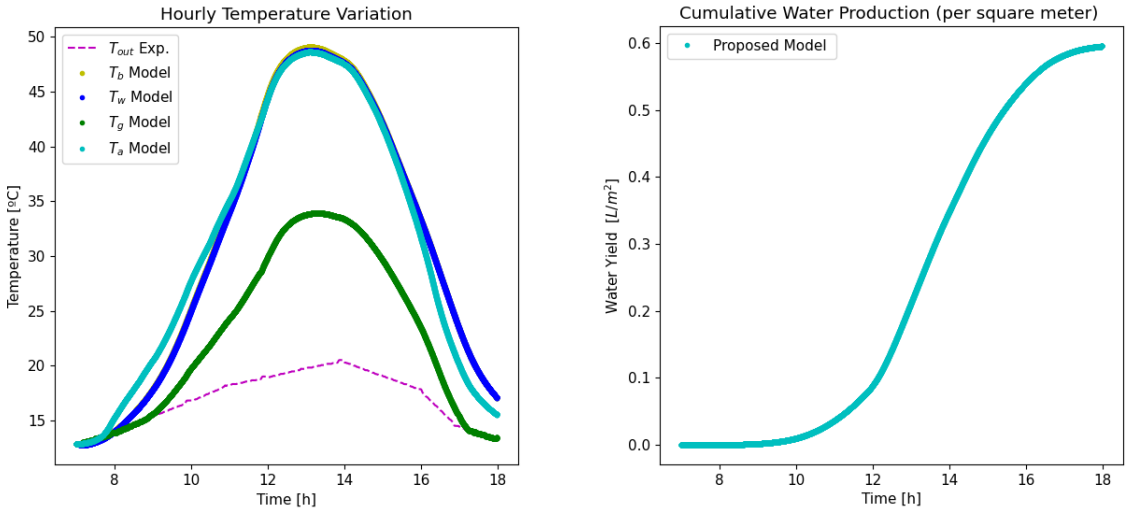

(a) Hourly temperature variation for the proposed model. (b) Cumulative water yield for the proposed model

Figure A.6: Hourly temperature variations and cumulative water yield of the thermal model when applied to the representative winter day, with solar still structure from the experiment carried out by Kabeel et al.[22]

A.0.2 Experiments conducted by Kabeel et al. [25] (a and b)

These experiments are conducted with the same solar still structure, being the main differences, the day the experiment occurs and the environment conditions.

Property	**Value**	**Units**
Structure		
Solar Still Length - C	1.2	m
Solar Still Width - L	0.6	m
Basin/Wall Thickness	1.5	mm
Basin/Wall Density	7874	kg/m^3
Basin/Wall Specific Heat Capacity - $c_{p,b}$	473	J/kg.K
Basin/Wall Insulation Thickness - L_i	0.05	cm
Basin/Wall Insulation Thermal Conductivity - K_i	0.033	W/(m.K)
Glass Angle - β_g	30.47	º
Glass Height	0.69	m
Glass Thickness	3	mm
Glass Density	2700	kg/m^3
Glass Specific Heat Capacity - $c_{p,g}$	840	J/(kg.K)
Water depth	2	cm
Water density	1000	kg/m^3
Back wall height	0.47	m
Front wall height	0.12	m
Day and location		
Day number	173 (a); 203 (b)	
Latitude	31.07	º
Clearness index factor	0.68 (a), 0.67(b)	(*)
Wind velocity (*)	3	m/s
Property	**Value**	**Units**
View Factors		
View factor water to lateral wall - $F_{w,Lateral}$	0.07	
View factor water to front wall - $F_{w,Front}$	0.07	
View factor water to back wall - $F_{w,Back}$	0.21	
View factor water to glass - $F_{w,g}$	0.58	
View factor lateral wall to glass - $F_{lateral,g}$	0.36	
View factor front wall to glass - $F_{Front,g}$	0.21	
View factor back wall to glass - $F_{Back,g}$	0.51	

Table A.3: Experimental data from the experiments conducted by Kabeel et al. [25] (a and b).Values with (*) were assumed based on the data given.View factors were computed.

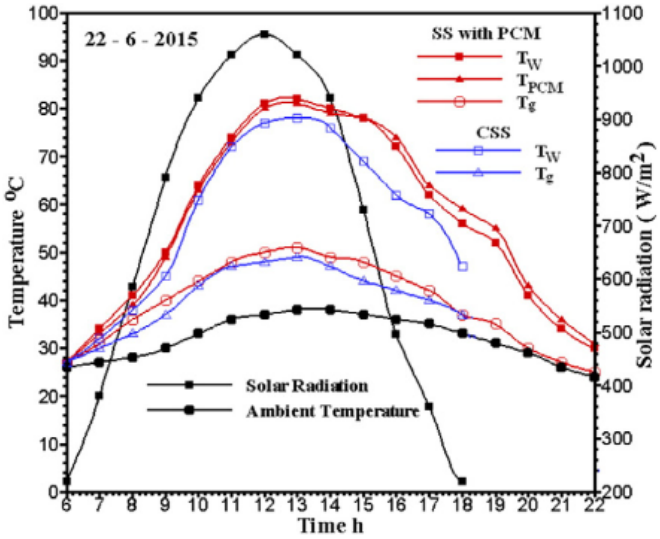

Figure A.7: Experimental data, more specifically solar radiation and hourly temperature variation, from the experiment conducted by Kabeel et al.[25](a)

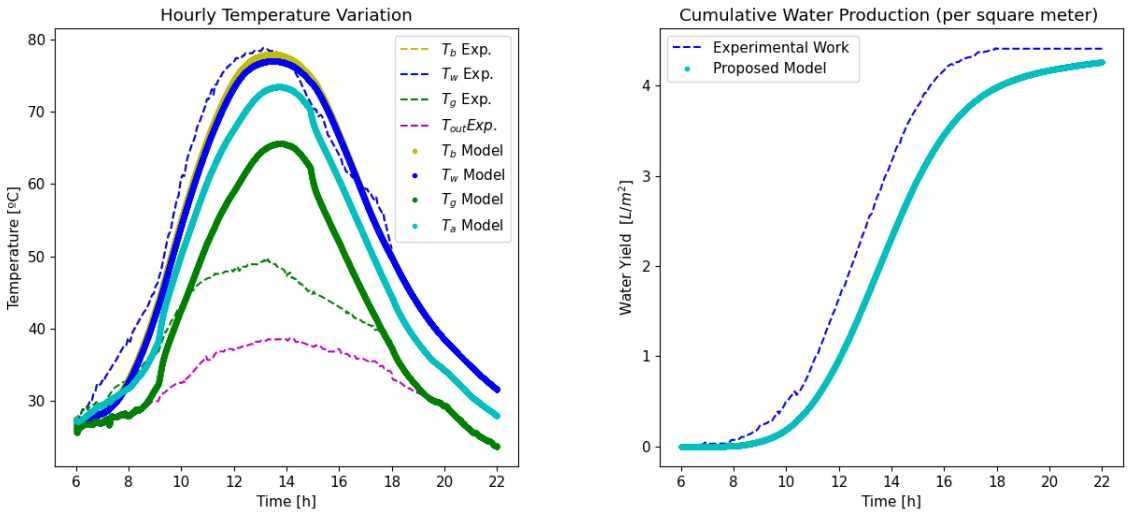

(a) Hourly temperature variation for the proposed model, as well as the experimental data

(b) Cumulative water yield for the proposed model, as well as the experimental data

Figure A.8: Hourly temperature variations and cumulative water yield of the thermal model when applied to the data from the experiment conducted by Kabeel et al. [25](a)

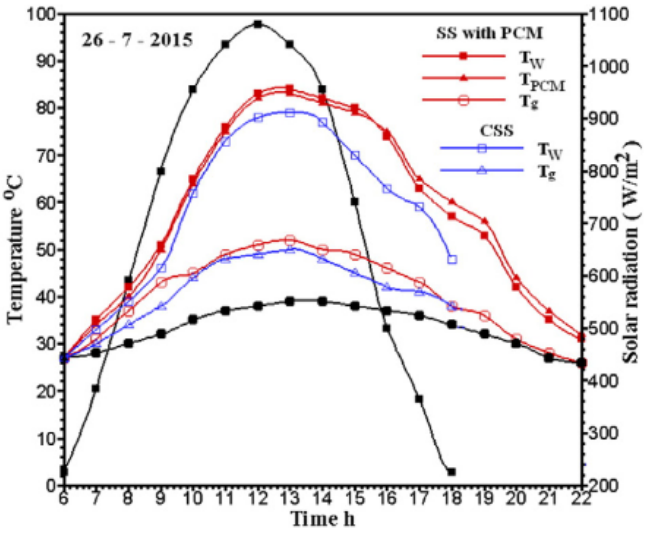

Figure A.9: Experimental data, more specifically solar radiation and hourly temperature variation, from the experiment conducted by Kabeel et al. [25](b)

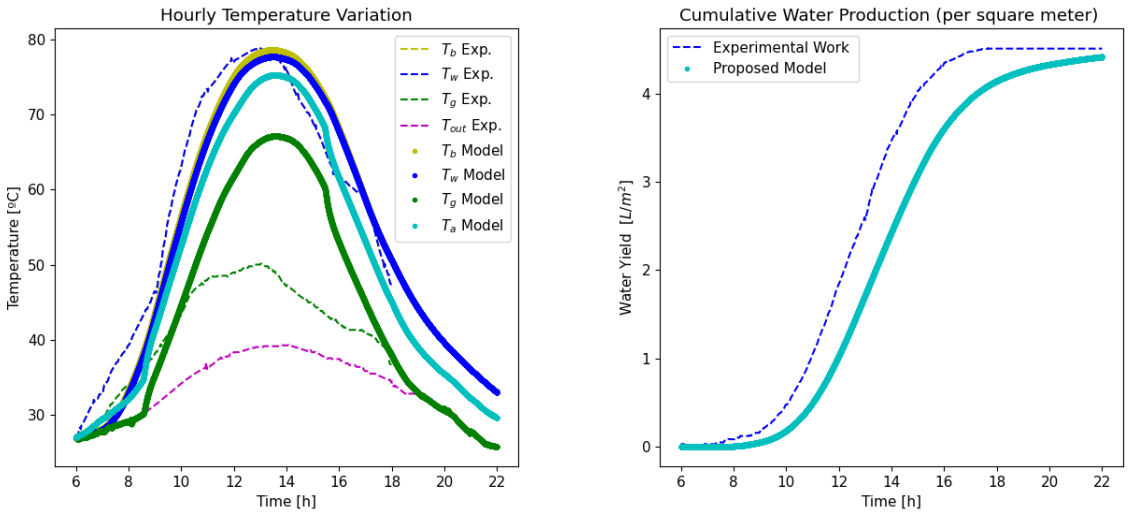

(a) Hourly temperature variation for the proposed model, as well as the experimental data

(b) Cumulative water yield for the proposed model, as well as the experimental data

Figure A.10: Hourly temperature variations and cumulative water yield of the thermal model when applied to the data from the experiment conducted by Kabeel et al. [25](b)

A.0.3 Experiments conducted by Elango et al. [23]

This experiments differentiate from the others because, it is a double slope solar still.All components were modeled, the two glasses included, with the reasoning presented in this work.

It is important to take into account that one glass faces south and the other north.This is relevant for the shadows computations of the walls.It was assumed the foe the triangular shape walls, an average height to ease the computations.Nonetheless for a more better computation, an appropriate detailed shadow model should be made.

In Fig.A.11 it is possible to see the air temperature suddenly increasing, around 7.5h, and decreasing, around 17.5h, because of the strict restrictions imposed.When the sun is moving form east to west, one inner wall receives radiation.However, when the sun is at a low altitude, the wall receiving solar radiation is shaded by the opposite wall.It was assumed that if the shadow height imposed by the wall was larger than the width of the solar still, no solar radiation would reach the other inner wall.The same for the case in which the shadow is shorter than the width, and thus the inner wall receives solar radiation.

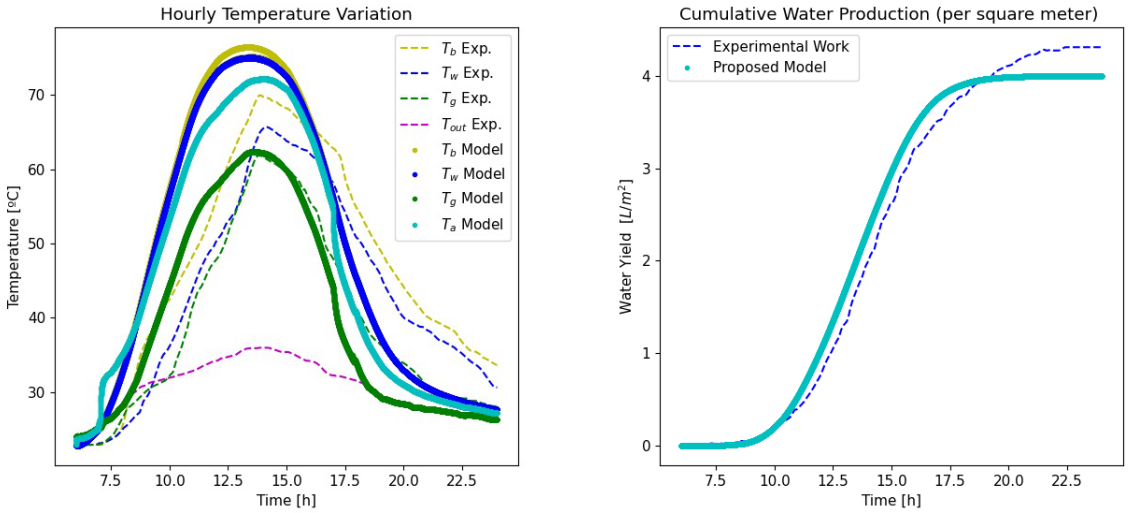

(a) Hourly temperature variation for the proposed model, as well as the experimental data

(b) Cumulative water yield for the proposed model, as well as the experimental data

Figure A.11: Hourly temperature variations and cumulative water yield of the thermal model when applied to the data from the experiment conducted by Elango et al. [23]

Property	Value	Units
Structure		
Solar Still Length - C	0.9	m
Solar Still Width - L	0.9	m
Basin/Wall Thickness	8	mm
Basin/Wall Density	2700	kg/m^3
Basin/Wall Specific Heat Capacity - $c_{p,b}$	840	J/kg.K
Basin/Wall Insulation Thickness - L_i	12.7	cm
Basin/Wall Insulation Thermal Conductivity - K_i	0.035	W/(m.K)
Glass Angle - β_g	30	º
Glass Height (both glass)	0.52	m
Glass Thickness	5	mm
Glass Density	2700	kg/m^3
Glass Specific Heat Capacity - $c_{p.g}$	840	J/(kg.K)
Water depth	1	cm
Water density	1000	kg/m^3
Back/Front Wall Height (smaller walls)	0.1	m
Lateral Wall Height (triangular walls)	0.36	m
Day and location		
Day number	66	
Latitude	9.11	º
Clearness index factor (*)	0.65	
Property	**Value**	**Units**
View Factors		
View factor water to lateral wall - $F_{w,Lateral}$	0.1	
View factor water to back/front wall - $F_{w,Back/Front}$	0.0.05	
View factor water to glass - $F_{w,g}$	0.7	
View factor lateral wall to glass - $F_{lateral,g}$	0.58	
View factor back/front wall to glass - $F_{Back/Front,g}$	0.62	

Table A.4: Experimental data from the experiments conducted by Elango et al. [23].Values with (*) were assumed based on the data given.View factors were computed.

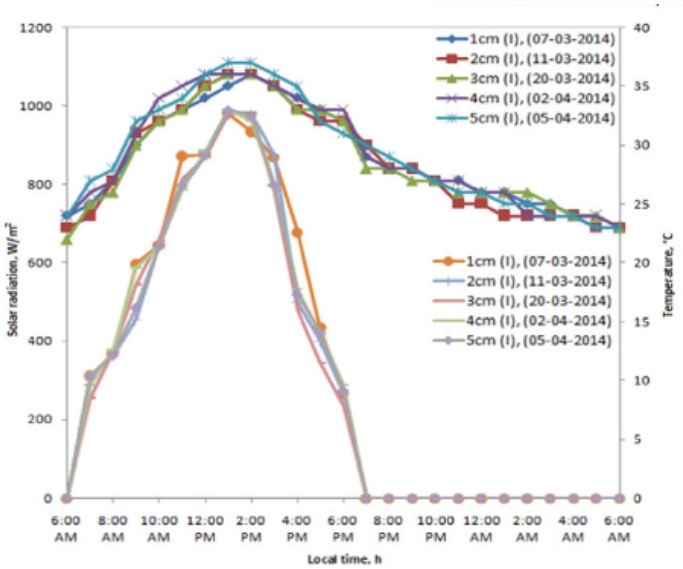

Figure A.12: Experimental data, more specifically solar radiation and hourly ambient temperature variation, from the experiment conducted by Elango et al. [23].The data used was the one of the 1cm water depth.

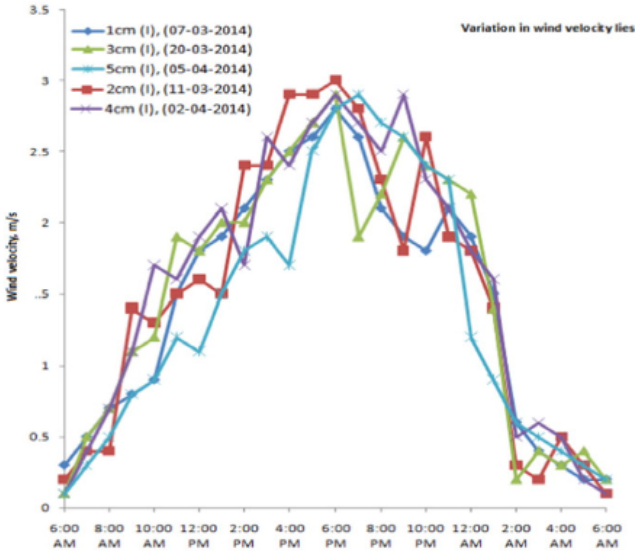

Figure A.13: Experimental data, more specifically wind hourly variation, from the experiment conducted by Elango et al. [23]. The data used was the one of the 1 cm water depth.

A.0.4 Experiments conducted by Tabrizi et al. [24]

This experiment was conducted in a particular structure, because instead of opaque walls painted black, it possesses walls made of glass.Condensation will occur not only in the top glass, but also on the walls.There is also a reservoir of sand under the basin, which also needs to be modeled.

Some modifications have to be made in energy balance equations in order to predict this solar still structure performance.

1. **Wall Energy Balance**

   Starting by the equations for the walls, which are made of glass, and are not insulated.These walls are in direct contact with the exterior and inner solar still air.Moreover condensation occurs not only on the top glass, but also on the lateral glass wall, thus it is needed to compute the respective Q_{cond}.

$$(mc_p)_{wall}\frac{\partial T_{wall}}{\partial t} = Q_{sun,wall} + Q_{r,w-wall} - Q_{r,wall-g} - Q_{c,a-wall} - Q_{lost,wall} + Q_{cond} \tag{A.1}$$

   Condensation was modeled according to subsection 2.4 , using the respective convection coefficient for each wall.It was computed the condensed water in each wall, and that water quantity was subtracted to the air humidity before computing condensation for the remaining walls.

   Another terms that must be updated is , the lost heat to the exterior,

$$Q_{lost,wall} = A_{wall}h_{c,wall-out}(T_{wall} - T_{out}) \tag{A.2}$$

   where, $h_{c,wall-out}$ is given by Eq. 2.99

   Evidently it is necessary to update the properties of the walls with radiant, thermal and physical properties of the glass.

2. **Basin Energy Balance**

   Firstly, it is important to look at the energy balance equation.

$$(mc_p)_b\frac{\partial T_b}{\partial t} = Q_{sun,b} - Q_{c,b-w} - Q_{lost,b} \tag{A.3}$$

   Analysing in more detail the radiation that reaches the basin.The shadows computation, by following subsection 2.2.3, mus take into consideration that the wall that makes shadow, has the same height from all sides, and therefore must be updated in the thermal model.Moreover, due to the particular solar still structure, when computing the diffuse radiation that reaches the basin, it can be considered that the view factor of the basin to the sky is approximately of 1.

   The basin looses by conductivity to the sand reservoir below.Thus, $Q_{lost,b}$ must be updated to,

$$Q_{lost,b} = A_b U_b (T_b - T_{res}) \tag{A.4}$$

where, T_{res} is the reservoir temperature and U can be computed as,

$$U = \frac{K_i}{L_i} \tag{A.5}$$

where, K_i and L_i, represent the thermal conductivity of sand and half of the sand reservoir height, respectively.

3. **Sand Heat Reservoir Energy Balance**

The energy balance of the sand reservoir, includes the absorption of heat that the basin above looses ($Q_{lost,b}$), and the loss of heat laterally to the outside ($Q_{lost,res}$).

$$(mc_p)_{res} \frac{\partial T_{res}}{\partial t} = Q_{lost,b} - Q_{lost,res} \tag{A.6}$$

The sand reservoir heat losses are due to the heat loss to the exterior,

$$Q_{lost,res} = A_{res,Lateral} U_{res} (T_{res} - T_{out}) \tag{A.7}$$

where, $A_{res,Lateral}$ is the sum of all the lateral are of the reservoir, and U_{res} is ,

$$U_{res} = \left(\frac{L_i}{K_i} + \frac{1}{h_{c,res-out}} \right) \tag{A.8}$$

where, $h_{c,res-out}$ is given by Eq. 2.99.

It is possible to see in Fig. A.14 that the reservoir temperature does not follow rigorously the experimental temperature.It is needed to take into account that the modeled temperature is an average temperature of the whole reservoir, and it is not certain were the experimental temperature was measured (if closer to the basin or further).

Property	**Value**	**Units**
Structure		
Solar Still Length - C	0.74	m
Solar Still Width - L	0.55	m
Basin/Wall Thickness	3	mm
Basin/Wall Density	7874	kg/m^3
Basin/Wall Specific Heat Capacity - $c_{p,b}$	473	J/kg.K
Top Glass Angle - β_g	45	º
Top Glass Height	0.78	m
Back Glass Height	0.55	m
Glass Thickness	5	mm
Glass Density	2700	kg/m^3
Glass Specific Heat Capacity - $c_{p,g}$	840	J/(kg.K)
Water depth	4	cm
Water density	1000	kg/m^3
Wall height	0.08	m
Reservoir Height	0.12	m
Reservoir Lateral Area ($A_{res,Lateral}$)	0.31	m^2
Reservoir Insulation Thickness - L_i	0.04	cm
Reservoir Insulation Thermal Conductivity - K_i	0.03	W/(mK)
Day and location		
Day number	85	
Latitude	29.49	º
Clearness index factor	0.6	
Property	**Value**	**Units**
View Factors		
View factor water to lateral glass - $F_{w,Lateral}$	0.1	
View factor water to back glass - $F_{w,Back}$	0.21	
View factor water to top glass - $F_{w,g}$	0.57	
View factor lateral glass to top glass - $F_{lateral,g}$	0.4	
View factor back glass to top glass - $F_{Back,g}$	0.5	

Table A.5: Experimental data from the experiments conducted by Tabrizi et al. [24]

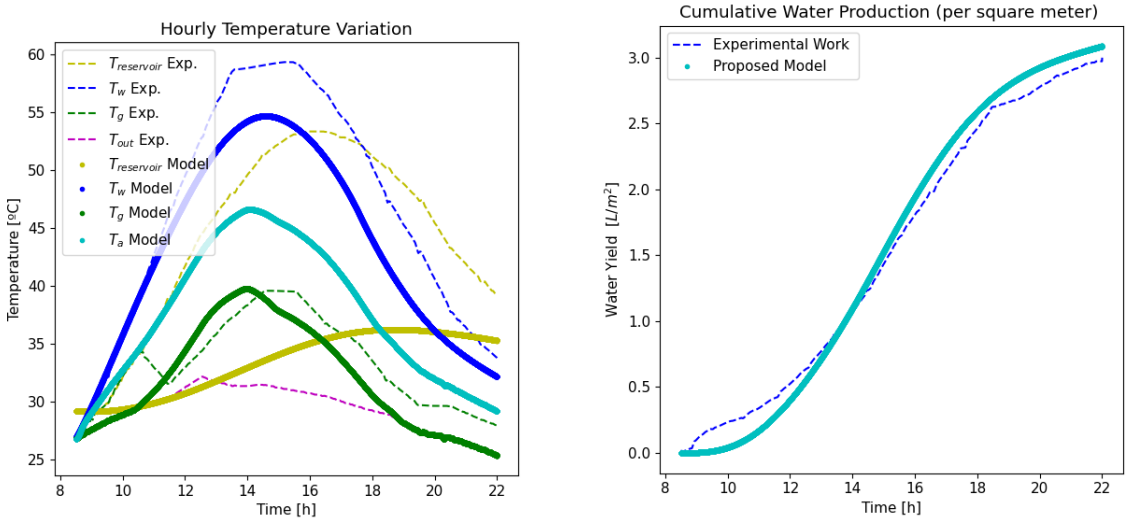

(a) Hourly temperature variation for the proposed model, as well as the experimental data

(b) Cumulative water yield for the proposed model, as well as the experimental data

Figure A.14: Hourly temperature variations and cumulative water yield of the thermal model when applied to the data from the experiment conducted by Tabrizi et al. [24]

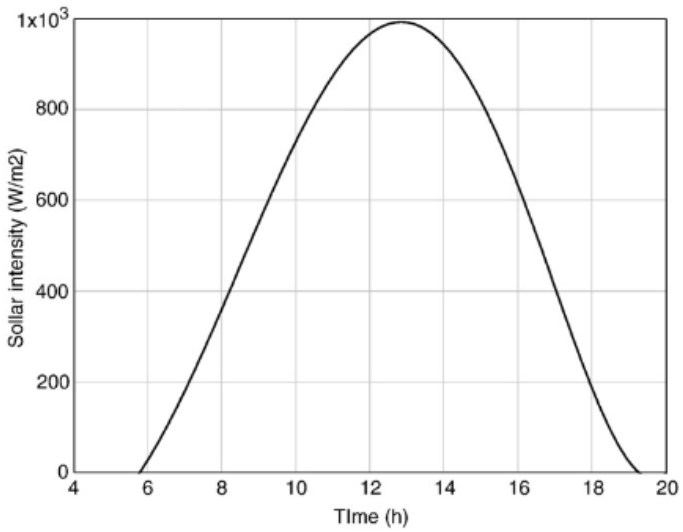

Figure A.15: Experimental data, more specifically solar radiation variation, from the experiment conducted by Tabrizi et al. [24]

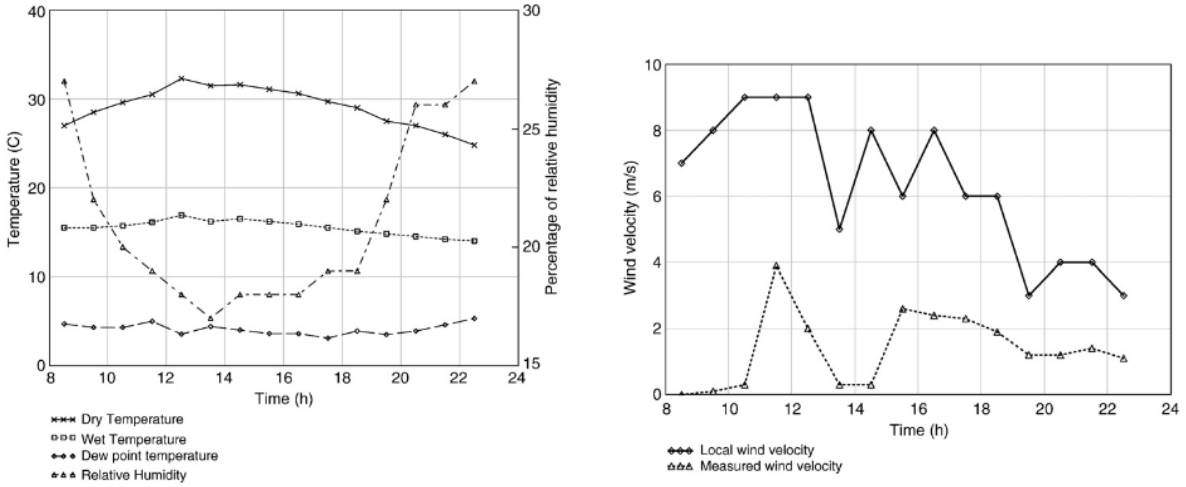

(a) Hourly temperature variation for the proposed model, as well as the experimental data

(b) Cumulative water yield for the proposed model, as well as the experimental data

Figure A.16: Experimental data, more specifically ambient temperature and wind variation, from the experiment conducted by Tabrizi et al. [24]

A.0.5 Experiment conducted by Canbazoglu et al. [51]

Property	**Value**	**Units**
Carbon foam diameter	3.6	cm
Carbon foam height	1.2	cm
Energy input	1700	W/m^2
Carbon foam density - ρ_{foam} (*)	2260	kg/m^3
Carbon foam thermal conductivity - K_i (*)	120	W/(mK)
Carbon foam porosity - Φ_{foam} (*)	97%	
Carbon foam absorption - α_{foam} (*)	0.95	
Water under the foam height (*)	3.6	cm
Ambient air relative humidity - φ (*)	30%	
Ambient air temperature - T_a (*)	23	ºC

Table A.6: Experimental data from the experiment conducted by Canbazoglu et al. [51].Values with (*) were attributed, since they are not specified.